

Proteomic analysis of synaptic dysfunction in the hippocampus of late-stage Parkinson´s Disease

Dissertation

for the award of the degree

“Doctor rerum naturalium” (Dr.rer.nat.)

of the Georg-August-Universität Göttingen

within the doctoral program

“Cellular and Molecular Physiology of the Brain”

of the Georg-August University School of Science (GAUSS)

submitted by

Carmina Carelia Warth Pérez Arias

born in Mexico City, México

Göttingen, August 2021

Thesis Committee

Prof. Dr. Paul Lingor (Dept.of Neurology–Translational Neurodegeneration Laboratory, Rechts der Isar Hospital of the Technical University Munich)

Prof. Dr. Silvio Rizzoli (Dept.of Neuro-and Sensory Physiology, University Medical Center Göttingen)

Prof. Dr. Tiago Fleming Outeiro (Dept. of Experimental Neurodegeneration, University Medical Center Göttingen)

Members of the Examination Board

1st Referee: **Prof. Dr. Paul Lingor** (Dept.of Neurology–Translational Neurodegeneration Laboratory, Rechts der Isar Hospital of the Technical University Munich)

2nd Referee: **Prof. Dr. Silvio Rizzoli** (Dept.of Neuro-and Sensory Physiology, University Medical Center Göttingen)

Further members of the Examination Board

Prof. Dr. Tiago Fleming Outeiro (Dept. of Experimental Neurodegeneration, University Medical Center Göttingen)

Prof. Dr. Carolin Wichmann (Institute for Auditory Neuroscience & InnerEarLab, University Medical Center Göttingen)

Prof. Dr. Christine Stadelmann-Nessler (Institute of Neuropathology, University Medical Center Göttingen)

Prof. Dr. André Fischer (Dept. Epigenetics and Systems Medicine in Neurodegenerative Diseases, DZNE Göttingen, University Medical Center Göttingen)

Date of oral examination: 16.09.2021

Declaration

I, Carmina Carelia Warth Pérez Arias, hereby declare that the doctoral thesis entitled
“Proteomic analysis of synaptic dysfunction in the hippocampus of late-stage Parkinson’s
Disease”
has been written independently and with no other sources and aids than quoted.

Göttingen, August 2021

Carmina Carelia Warth Pérez Arias

Preface

A manuscript has been prepared which resembles parts of this doctoral thesis in form and content of the description and discussion of the results, as well as in methods. Figures were modified for this thesis. Preliminary information on the title and authors of the manuscript: Warth Perez Arias C., Silbern I., Lenz C., Wartmann H., Dambeck V., Barski L., Caldi Gomes L., Bähr M., Outeiro T., Bonn S., Rizzoli S., Urlaub H., Lingor P. Proteomic analysis of human hippocampus identifies neuronal pentraxin 1 (NPTX1) as synapto-axonal target in late-stage Parkinson's disease.

Disclosure

The work conducted as part of this thesis was supported with funding from the German Research Foundation (DFG) via the Collaborative research Centre SFB 1286 "Quantitative Synaptology" through project B09.

Dedicated to my younger self: We did it!

Table of contents

List of abbreviations	iii
List of figures	vii
List of tables.....	viii
Chapter 1: Introduction	1
1.1 Introduction to the study	1
1.2 Parkinson´s disease.....	2
1.2.1 History and phenotype of Parkinson´s disease.....	2
1.2.2 Disease progression and symptoms	4
1.2.3 The hippocampus of PD and cognitive dysfunction.....	5
1.2.4 Pathogenesis of PD	9
1.3 Pentraxins.....	12
1.3.1 Short pentraxins.....	14
1.3.2 Long pentraxins	14
1.3.3 Involvement of pentraxins in neurodegenerative diseases.....	17
1.4 Aims of the present study.....	19
Chapter 2: Materials and Methods	21
Chapter 3: Results.....	35
3.1 Differential abundance of proteins in whole tissue lysate samples retrieved from human hippocampal PD samples.....	35
3.1.1 Aims.....	35
3.1.2 Results	35
3.2 Differential abundance of proteins in synaptosomal fractions retrieved from human hippocampal PD samples	63
3.2.1 Aims.....	63
3.2.2 Results	63
3.3 Changes in synaptic morphology induced by dysregulation of NPTX1 in primary cell cultures	82
3.3.1 Aims.....	82
3.3.2 Results	82
3.4 Summary of Results	87
Chapter 4: Discussion	90
4.1 Differences in the hippocampus of Parkinson´s disease	90

4.2 Biological relevance and biological processes impacted by dysregulation of hippocampal proteins in PD	94
4.3 Changes in synaptic morphology caused by modulation of NPTX1 in primary mouse cultures	100
Chapter 5: Concluding remarks	101
Chapter 6: Summary	103
7. References	105
8. Acknowledgments	119
9. Curriculum Vitae	Error! Bookmark not defined.

List of abbreviations

6-OHDA: 6-hydroxydopamine-lesion

A β : Amyloid- β

AGC: Automatic gain control

AGRN: Agrin

AD: Alzheimer's disease

aSyn: Alpha-synuclein

ATP6V1B2: V-type proton ATPase subunit B

ATP6V1H: V-type proton ATPase subunit H

BASP1: Brain acid soluble protein 1

BH: Benjamini-Hochberg

bRP: Basic reversed-phase

BSA: Bovine serum albumin

CAMK2A: Calcium/calmodulin-dependent protein kinase type II subunit alpha

CGN: Cerebellar granule neurons

CNS: Central nervous system

CPLX2: Complexin-2

CRP: C reactive protein

CSF: Cerebrospinal fluid

CTR: Control

DE: Differential expression

DLB: Dementia with Lewy bodies

FCS: Fetal calf serum

FDR: False discovery rate

FWHM: Full width half maximum

GAP43: Growth associated protein 43

GAPDH: Glyceraldehyde-3-phosphate dehydrogenase

GO: Gene ontology

GPI: Internal globus pallidus

HBSS: Hanks balanced salt solution

HI: Hypoxia-ischemia

HSPA1B: Heat shock 70kDa protein 1B

HSPH1: Heat shock protein 105kDa

IHC: Immunohistochemistry

iTRAQ: Isobaric tagging for relative and absolute quantification

L-DOPA: Levodopa

LB: Lewy body

LID: L-DOPA-induced dyskinesia

MAPK1: Mitogen-activated protein kinase 1

MAPK3: Mitogen-activated protein kinase 3

MARCKS: Myristoylated alanine-rich C-kinase substrate

MBP: Myelin basic protein

MCI: Mild cognitive impairment

MOBP: Myelin-associated oligodendrocyte basic protein

MPTP: 1-methyl-4-phenyl-1,2,3,6-tetrahydropyridine

MRM: Multiple reaction monitoring

nbM: Nucleus basalis of Meynert

NCE: Normalized collision energy

NDUFS7: Complex I subunit NADH dehydrogenase iron-sulfur protein 7

NMS: Non-motor symptoms

NPTX1: Neuronal pentraxin 1

NPTX2: Neuronal pentraxin 2

NPTX1AS: Antisense oxyribonucleotides against NPTX1 mRNA

NPTXR: Neuronal pentraxin receptor

OGD: Oxygen glucose deprivation

PBS: Phosphate buffered saline

PEA15: Astrocytic phosphoprotein PEA-15

PD: Parkinson's disease

PDD: Parkinson's disease with dementia

PFA: Paraformaldehyde

PMI: Post mortem interval

PPI: Protein-protein interaction

PPP3R1: calcineurin subunit B type 1

RAB1B: Ras-related protein Rab-1B

RAB6A: Ras-related protein Rab-6A

RBD: REM-sleep behaviour disorder

REM: Rapid eye movement

RHOT1: Mitochondrial Rho GTPase 1

ROCK2: Rho-associated protein kinase 2

ROS: Reactive oxygen species

RPL4: 60S ribosomal protein L4

RPL11: 60S ribosomal protein L11

RPS9: 40S ribosomal protein S9

RPS16: 40S ribosomal protein S16

RPS21: 40S ribosomal protein S21

RT: Room temperature

SAP: Serum amyloid P

SDS: Sodium dodecyl sulphate polyacrylamide gel electrophoresis

SNAP25: synaptosomal-associated protein, 25kDa

SNpc: Substantia nigra pars compacta

snRNPs: Small nuclear ribonucleoproteins

SYN1: Synapsin 1

SYP: Synaptophysin

SWATH-MS: Sequential window acquisition of all theoretical mass spectra

ULCH1: Ubiquitin carboxyl-terminal hydrolase isozyme L1

UPS: Ubiquitin-proteasome system

YWHAE: 14-3-3 protein epsilon

YWHAH: 14-3-3 protein eta

YWHAQ: 14-3-3 protein theta

WB: Western blot

WGCNA: Weighted correlation network analysis

WT: Wild type

List of figures

Figure 1. Structure of neuronal pentraxin family members	13
Figure 2. Workflow for sample collection of whole tissue lysate samples.....	36
Figure 3. Cell type specific markers mapped onto proteins from whole tissue samples	37
Figure 4. Differential expression analysis of proteins from whole tissue lysate samples.....	38
Figure 5. Cell type specific markers mapped onto DE proteins from whole tissue samples...	41
Figure 6. Protein-protein interaction (PPI) networks of differentially expressed proteins	43
Figure 7. Functional annotation of 55 DE proteins.....	44
Figure 8. Network analysis based on co-expression of all 2089 identified proteins from the whole tissue lysates.....	48
Figure 9. Location of the 55 DE proteins of the whole tissue sample cohort in the individual WGCNA modules.....	49
Figure 10 Summarized biological relevance of individual modules of the whole tissue lysate reduced data set.....	52
Figure 11. Synaptic module W03 overview.....	54
Figure 12. Whole tissue lysate validation of NPTX1 differential expression via western blot.	56
Figure 13. Differential expression analysis of proteins from hippocampus of A53T mice.....	58
Figure 14. Differential expression analysis of proteins from cerebellum of A53T mice	59
Figure 15. Overview of overlaps of proteomic data sets of A53T mice and whole tissue lysate samples.....	61
Figure 16. Longitudinal progression of DE in hippocampal and cerebellar proteins in A53T mice	62
Figure 17. Workflow for sample collection and enrichment of synaptosomal fractions	64
Figure 18. Synaptosomal fraction quality control.....	66
Figure 19. Overview of overlaps in proteomic data sets of human synaptosomal fractions and human whole tissue lysate samples.....	67
Figure 20. Heat map of Z-scores of top 55 DE proteins of the synaptosomal fraction	68
Figure 21 Differential expression analysis of proteins from synaptosomal fractions.....	69
Figure 22. Protein-protein interaction network of DE proteins from synaptosomal fractions	70
Figure 23. Protein-protein interaction network sub-clusters of DE proteins from synaptosomal fractions	72
Figure 24. Network analysis based on co-expression of all 2413 identified proteins from the synaptosomal fraction	75
Figure 25. Summary of modules from both whole tissue lysates and synaptosomal fractions assigned to one of twelve umbrella terms.....	79
Figure 26. Synaptic module S01 overview	80
Figure 27. Endogenous NPTX1 expression in mouse hippocampal primary cell cultures.....	83
Figure 28. Treatment scheme for daily NPTX1 dosages on primary hippocampal cell cultures.....	84
Figure 29. Characterization of morphological changes of the neuronal synapse treated with NPTX1	85
Figure 30. Quantification of morphological changes of synapses from neurons treated with NPTX1	86

List of tables

Table 1. Human sample clinical and demographic information.	21
Table 2. List of used equipment.	25
Table 3. List of used software.	25
Table 4. List of all proteins with differential abundance in PD vs. CTR sorted by pValue	40
Table 5. Functional annotation of the top 10 biological process of DE proteins from whole tissue lysate samples, divided into data sets of higher and lower abundance in PD.	45
Table 6. Functional annotation of top 10 molecular functions of DE proteins from whole tissue lysate samples, divided into data sets of higher and lower abundance in PD.	46
Table 7. Functional annotation of top 10 cellular compartments of DE proteins from whole tissue lysate samples, divided into data sets of higher abundance in PD.	46
Table 8. Functional annotation of biological processes for each module of co-expressed proteins from the whole tissue lysate sample.	50
Table 9. Functional annotation of molecular function for each module of co-expressed proteins from the whole tissue lysate sample.	51
Table 10. Functional annotation of cellular component for each module of co-expressed proteins from the whole tissue lysate sample.	51
Table 11. Functional annotation of top 10 biological processes of DE proteins from synaptosomal fraction samples.	73
Table 12. Functional annotation of top 10 molecular functions of DE proteins from synaptosomal fraction samples.	73
Table 13. Functional annotation of top 10 cellular components of DE proteins from synaptosomal fraction samples.	74
Table 14. Functional annotation of biological processes for each module of co-expressed proteins from the synaptosomal fractions.	76
Table 15. Functional annotation of molecular function for each module of co-expressed proteins from the whole tissue lysate sample.	76
Table 16. Functional annotation of cellular compartments for each module of co-expressed proteins from the whole tissue lysate sample.	77
Table 17. Break down of biological processes assigned to the different umbrella terms created for comparison of functional annotation of both whole tissue lysates and synaptosomal fractions.	78
Table 18. All DE proteins contained in the synaptic module S01 from synaptosomal fractions. .	81

Chapter 1: Introduction

1.1 Introduction to the study

Parkinson's disease (PD) is a common progressive neurodegenerative disease. It presents a heterogeneous symptomatology arising from a pathology that affects extensive regions of the nervous system. Amongst the symptoms accompanying the progression of the disease, motor dysfunction is considered a hallmark of PD. In terms of pathology, the onset of the motor symptoms has been linked with a prominent loss of dopaminergic neurons in the nigrostriatal pathway. However, PD is further associated with numerous non-motor symptoms (NMS) both preceding and following the onset of motor dysfunction.

The mechanisms that have been implicated in disease's progression are multifactorial and wide-ranged, including protein misfolding and aggregation, mitochondrial dysregulation and synaptic dysfunction (Bredesen et al. 2006; Skovronsky et al. 2006). Furthermore, evidence hints towards a heterogeneity in disease mechanisms and progression amongst patients. As a result, the exact pathomechanisms for PD remain unclear, hindering the advances of a curative therapy. The treatments available to date mostly address the symptoms arising from the dopaminergic loss. However, re-balancing the dopamine dysregulation is not sufficient to fully address the complexity of PD, often leaving late-stage complications uncontrolled. As a consequence, cognitive impairment and dementia, dysfunctions unavoidable for the vast majority of patients, remain a key aspect contributing to the severe socioeconomic burden of this disease. The exact mechanisms contributing to dementia in PD remain unclear. However, the important role of the hippocampus in memory paired with evidence suggesting a strong degeneration in PD, postulate it as a region of special interest.

In order to expand our understanding of this neurodegenerative disease, the present study focussed on assessing changes in the hippocampus as a result of late-stage PD. Human post-mortem hippocampal samples were used to address these changes, quantifying significant alterations in protein abundance in PD versus controls. Proteomic data sets were gathered from whole tissue lysates as well as enriched synaptosomal fractions and characterized by means of protein-protein interaction networks, functional annotation analyses and network analyses of protein expression. In addition, the broad proteomic data sets were narrowed down to a single protein of interest, integrating the

1. Introduction

proteomic characterisation with known literature, placing special interest on the involvement in neurodegenerative diseases and synaptic dysfunction.

In summary, this study was able to identify changes in protein expression levels in the hippocampus of PD patients, characterize the functional interactions and biological relevance of these dysregulated proteins and address in further detail the implication of the dysregulation of a selected protein of interest in a neuronal network.

1.2 Parkinson's disease

1.2.1 History and phenotype of Parkinson's disease

The first recorded description of Parkinson's disease was published over two centuries ago by James Parkinson. In his "Essay on the Shaking Palsy", Parkinson described several clinical features of PD, such as resting tremor and gait disorder, as well as addressing some NMS including sleep disturbance and impaired bowel function (Parkinson, 1817). The resting tremor described by Parkinson is nowadays incorporated to the Movement Disorder Society clinical diagnosis criteria for PD, with the core motor parkinsonism being defined as bradykinesia accompanied by rest tremor or rigidity (Postuma et al., 2015).

A hundred years later, in 1919, Tretiakoff analysed 54 brain samples, amongst which were six samples of patients with paralysis agitans and three samples presenting postencephalic Parkinsonism. In these samples, he described a prevalent loss of dopaminergic neurons in the substantia nigra pars compacta (SNpc) (Tretiakoff, 1919, Lees, 2007). He furthermore noted the presence of inclusion bodies in some surviving nigral cells, which he termed "corps de Lewy" in recognition of the description first provided by Frederic Lewy in 1912 (Lees, 2007). These inclusion bodies, now pivotal in PD pathology, were characterized 85 years later, finding aggregated alpha-synuclein (aSyn) as the main component (Spillantini et al., 1997).

Continuous research over the next 100 years contributed vastly to new insights on PD. In terms of pathogenic mechanisms, only 5% of the PD cases were linked to genetic mutations. Familial cases of PD have to date been linked to mutations in 23 genes (Blauwendraat et al., 2019), with 10 genes showing recessive inheritance and 13 genes showing dominant inheritance (Puschmann, 2013; Singleton and Hardy, 2016; Singleton and Hardy 2019; Sudhama et al., 2016; Quadri et al., 2018;

Blauwendraat et al., 2019). The more common cases of PD, idiopathic or sporadic PD, occur sporadically without an identifiable cause but show similarities to some mechanisms underlying familial PD, including oxidative stress, mitochondrial dysfunction, neuroinflammation, and dysfunctional protein handling (De Lau and Breteler, 2013; Dexter and Jenner, 2013; Johnson et al., 2019; Hirsch and Hunot, 2009).

In terms of clinical diagnosis, PD is determined by the occurrence of motor symptoms, which arise at intermediate stages of the pathophysiological disease progression. The motor symptoms of PD include rigidity, postural instability, bradykinesia, resting tremor, flexed posture, freezing, mask-like facial expression and problems to speak and swallow (Jankovic 2008). However, continuous research has found a much more complex composition of symptoms accompanying the progression of PD. In addition to both dopamine-dependent as well as non-dopamine-dependent motor symptoms, PD features a wide range of NMS such as autonomic dysfunctions, sleep disturbance, mood disorders, cognitive decline and dementia (Agid, 1991; Lim et al., 2009).

The complexity of possible mechanisms involved in the progression of PD and the broad range of their effects on the nervous system, coupled with the involvement of both environmental and genetic risk factors (Dexter and Jenner, 2013; Schapira and Jenner, 2011), have hindered the precise description of a uniform pathogenesis for PD. Consequently, while multiple treatments for PD are available, all are aimed at alleviating symptoms, with most treatment focusing on the pharmacological replenishment of dopamine. As such, the dopamine precursor L-3,4-dihydroxyphenylalanine, also known as levodopa (L-DOPA), is administered either orally or directly to the gastrointestinal tract to increase its brain levels in PD patients. The treatment is effective in diminishing motor symptoms, helping to increase life quality for the patients on a medium-term. However, in spite of the the motor improvement provided by the treatment, long term complications are unavoidable. As such, L-DOPA dependent drug-induced dyskinesia as well as treatment independent complications such as progressive cognitive defects, depression and other psychiatric disorders are commonly seen in late-stage PD (Conolly and Lang, 2014; Marsden, 1994; Nutt et al., 1994).

As an age-related disease, the occurrence of PD has increased significantly alongside the constant rise in life expectancy, positioning it as the second most prevalent neurodegenerative disease worldwide (de Lau and Breteler, 2006). With an estimated global population of 9.4 million affected people in 2020 (Maserejian et al., 2020) and a projection of expected growth surpassing 12 million by 2040 (GBD 2016 Neurology Collaborators, 2019; Dorsey et al., 2018) the impact of PD on the

1. Introduction

society, public health and economy is undeniable, supporting the need for novel therapeutic strategies for PD.

1.2.2 Disease progression and symptoms

Parkinson's disease is a systemic disease, affecting a broad range of areas of the central nervous system (CNS). An example of this systemic nature can be seen in the localization of Lewy bodies (LB). These inclusions, primarily consisting of the synaptic protein α -synuclein (aSyn), can be found mostly in axons and presynaptic boutons, with aSyn spreading throughout the entire brain of affected patients (Braak et al., 2003; Spillantini et al., 1997). The effect of LB remain unclear, with a debate between a protective mechanism or a direct cause of cell death (Braak et al., 2003; Dexter and Jenner, 2013; Lu et al., 2005; Olanow et al., 2004). However, in terms of their involvement in the progression of PD, a stereotyped temporal and spatial progression has been proposed for the LB pathology in the brain. This progression describes the spread of aggregated alpha-synuclein throughout the nervous system, starting from the peripheral nervous system and advancing to the CNS in a caudal-to-rostral direction. In early stages, the intraneuronal pathology starts in the medulla oblongata, spreading at intermediate stages over the brain stem and basal ganglia, reaching the neocortex in late stages of the disease (Braak et al., 2003).

Early stages of PD, also known as pre-motor phases, have been linked to a number of NMS such as constipation, hyposmia and, REM-sleep behaviour disorder (RBD) (Gonera et al., 1997; Schenck et al., 2002; Abbott et al., 2001; Katzenschlager and Lees, 2004). Furthermore, these NMS have been shown to precede the onset of classical motor symptoms, often occurring several years prior (Schenck et al., 1996). Neuroanatomically, constipation might be associated with early degeneration of the dorsal nucleus of the vagus (Braak et al., 2006) as well as the accumulation of aSyn in the mesenteric nervous system (Beach et al., 2010), while premotor RBD could be linked to the early involvement of the pedunculopontine nucleus and the locus subcoeruleus (Tolosa and Pont-Sunyer, 2011).

The advance towards the midbrain in intermediate stages of the disease accompanies the widely studied involvement of dopaminergic neurons in the SNpc and their proneness to neurodegeneration, insults which are linked to the progressive motor symptoms characteristic for PD. It is interesting to underline at this stage, that by the time motor symptoms manifest, the loss of

dopaminergic cell bodies is less pronounced than the loss of striatal projections. This observation hints towards a degeneration starting at the synaptic terminals, which then leads to axonal degeneration and a consequent progression to cell body loss (Burke and O'Malley, 2013; Tönges et al., 2012).

The dopaminergic neurons of the SNpc regulate voluntary movements as part of the basal ganglia, projecting long unmyelinated axons into the striatum and modulating the activity of spiny striatal neurons by targeting dopamine receptors D1 and D2 (Kandel et al., 2000). The depletion of striatal dopamine resulting from the strong loss of dopaminergic neurons in PD, heavily impacts the complex basal ganglia circuitry, increasing the activation of the internal globus pallidus (GPi) and in turn decreasing the activity of the thalamus and motor cortex, giving rise to the hallmark motor symptoms of PD (Obeso et al., 2000; Smith et al., 2012).

In addition to the strong loss of dopamine, other neurotransmitter systems such as cholinergic, noradrenergic, and serotonergic systems are affected by PD (Schapira et al., 2006; Brooks et al., 2007). Late stages of the disease introduce NMS such as dementia, depression, pain, sleep disorders and, dysautonomia. All of these symptoms increase in frequency and severity with the progression of PD (Tolosa et al., 2006), turning into the major source of disability for the patient (Chapuis et al., 2005; Goetz, 2003; Schrag et al., 2007). Interestingly, in these late stages of PD, the LB pathology has most convincingly been linked to cognitive decline, with non-motor complications such as dementia having been correlated by several studies to the severity of LB pathology (Selikhova et al., 2009; Kempster et al., 2010; Irwin et al., 2012).

1.2.3 The hippocampus of PD and cognitive dysfunction

As previously stated, the life quality of PD patients is not solely impacted by motor symptoms, with NMS representing an especially strong burden in late stages of the disease (Chaudhuri et al., 2006; Docherty and Burn, 2010). In this regard, cognitive decline is especially prevalent, with a vast majority of patients progressing to Parkinson's disease with dementia (PDD) (Hely et al., 2008). Characteristic for late-stage cognitive decline are disorders such as severe attention deficits, impaired executive and visuospatial function, as well as a significant decline in retrieval memory (Emre et al., 2007). Despite extensive studies the neuropathology responsible for this cognitive decline in PD remains however unclear. Amongst the research conducted to investigate the cognitive decline in PD,

1. Introduction

a connection has been found between the severity of aSyn pathology in form of cortical LB and the severity of cognitive decline in PD cases (Mattila et al., 2000; Kövari et al., 2003). Furthermore, the involvement of the hippocampus, a brain area crucial for memory formation and retrieval, represents a potential target for addressing dementia in PD, with a critical involvement having already been established in other forms of dementia (Fox et al., 1996; Seeley et al., 2009; Darby et al., 2019).

The hippocampus of PD patients with dementia presents a higher density of LB pathology compared to non-demented patients (Harding and Halliday, 2001; Hall et al., 2014), and shows a progressive atrophy with the progression of the disease (Aybeck et al., 2009; Weintraub et al., 2012; Mihaescu et al., 2018). Further, while neuroimaging studies of dementia in PD present a high heterogeneity (Lanskey et al., 2018), the individual reports of insult can be linked back to a common affected region. As such, a meta-analysis by Weil et al., 2019 linked various studies reporting abnormalities in PD dementia, to a common neuroanatomical substrate, which localized to the hippocampus. The analysis gathered 11 studies reporting neuroimaging findings for PD dementia, which comprised a total of 385 patients (n = 175 PD with dementia vs n = 210 PD without cognitive impairment). By means of a coordinate-based network mapping approach, the study linked the diverse abnormalities reported in the 11 studies to a common brain network centred on the hippocampus. This lesion network mapping technique was further shown to be symptom and stage specific. A second meta-analysis based on the same network mapping technique, showed a distinctly different mapping for the meta-analysis of reported lesions of PD patients with hallucinations. The lesion reports gathered from 9 studies (n = 168 PD with hallucinations vs n = 234 PD without hallucinations), localized to the lateral geniculate nuclei in the thalamus. Similarly, the network mapping of 15 studies reporting atrophy in PD with mild cognitive impairment (MCI) (n = 355) and PD with no cognitive impairment (n = 489) showed a localization of the reported lesions to the lateral temporal cortex (Weil et al., 2019).

Further insights to the cognitive decline in PD can be gathered from a neurotransmitter point of view. While dopamine replacement treatment in PD patients successfully addresses motor impairment, there is limited effect on the cognitive decline. In a study of 20 patients with short term levodopa treatment (22 months or less), 20 patients with long term levodopa treatment (40 months or more) and a control group consisting of the patient's spouses, it was shown that no memory measurements correlated with dosage levels. Furthermore, while initial improvements in cognition had been seen at the start of L-DOPA treatment these were not permanently sustained, with memory having a subtle regression to pre-levodopa levels starting at 2 years of treatment (Halgin et al., 1977).

In line with this, the limited effect that dopamine therapy has on counteracting cognitive decline, points towards additional neurochemical deficits besides dopamine dysfunction leading to PDD. Based on its important role in cognition (Bartus et al., 1982), acetylcholine is an important neurotransmitter to be considered.

Interestingly, research has shown a significant loss of acetylcholine-producing cells in the nucleus basalis of Meynert (nbM) in PD, leading to a cholinergic dysfunction in patients (Perry et al., 1985). Furthermore, the decrease in cholinergic activity in PD has been associated with increase in aSyn pathology in the CA2 region of the hippocampus. A study addressing aSyn pathology in the midbrain, basal forebrain, and the hippocampus of PD patients with and without dementia (n = 5 and n = 6, respectively) as well as age-matched individuals without neurological diseases (n = 5), showed a significant reduction in hippocampal cholinergic activity with a significant increase in aSyn pathology severity in the basal forebrain and hippocampus (Hall et al., 2014). Furthermore, while most PD patients shared a loss of pigmented A9 dopaminergic neurons, PD patients with dementia had additional loss of the lateral part of A10 dopaminergic neurons as well as Ch4 nucleus basalis neurons. This was consistent with cortical cholinergic reduction in all PD patients, with a differentiated cholinergic reduction in the hippocampus present solely in PD patients with dementia (Hall et al., 2014).

Furthermore, while Lewy pathology burden functions as a clear differentiator of PD cases with and without dementia, loss of cholinergic fibres in the CA2 was shown to be a more sensible marker, being able to differentiate between PD cases with MCI and cases without cognitive deficits (Liu et al., 2019). The study explored the burden of LB pathology in the CA2 subsector of PD patients (n = 67), PD patients with mild cognitive impairment (n = 34) and PD patients with dementia (n = 96), showing that the significant increase in LB pathology was found only in patients with dementia, while mild cognitive impairment showed an evident depletion of cholinergic fibres which correlated with the loss of cholinergic neurons in Ch2 (Liu et al., 2019).

Lastly, there is an important connection between dopamine transmission and the synaptic plasticity of the hippocampus (Wittmann et al., 2005; Adcock et al., 2006; Pessiglione et al., 2006). Several pathophysiological mechanisms of NMS and neuropsychiatric manifestations in PD have been proposed to be potentially related to an altered dopamine reward system, a dysfunction caused by the dopamine imbalance affecting the interplay between the hippocampus and the ventral striatum (Lisman and Grace, 2005; Chaudhuri and Schapira, 2009; Voon et al., 2009; Kehagia et al., 2010; Shohamy and Adcock, 2010; Svenningsson et al., 2012). Furthermore, dopamine has been shown to

1. Introduction

have the ability to modulate membrane properties and synaptic transmission in the hippocampus (Hammad and Wagner, 2006; Noriyama et al., 2006; Kobayashi and Suzuki, 2007), possibly impacting hippocampus-dependent memory as well as having behavioural implications (Lisman et al., 2011, Lisman and Grace, 2005; Shohamy and Adcock, 2010).

Moreover, in terms of cognition, both learning and motivation might be directly influenced by dopamine imbalances and consequent hippocampal activation. The functional loop connecting dopaminergic neurons of the ventral tegmental area to the hippocampus enables phasic bursts of dopamine to increase hippocampal activity via D1-like receptors, while also silencing prefrontal cortex activity (Lisman and Grace, 2005). Increases in dopamine induced by rewards, contribute to the hippocampus exerting a stronger input on the nucleus accumbens compared to the input from the prefrontal cortex, helping to maintain the behaviour that initially led to a reward (Calabresi et al., 2013). Inversely, decreased dopamine in the absence of a reward, increases the prefrontal input over the hippocampal input, boosting the flexibility for alternate behaviours in search of a more favourable outcome (Grace et al., 2007).

The correct functioning of the dopamine reward system might in turn be hindered in PD, with patients that are not receiving a pharmacological substitution of dopamine facing a decreased learning ability based on the overall dopamine deficiency. Inversely, dips in dopamine caused by negative stimulus are masked in treated patients with a surplus of dopamine availability, thus hindering learning (Frank et al., 2004).

Additionally, complications linked to the dopamine treatment may arise in some patients, including impulsive-compulsive behaviours as well as punding, a hyperdopaminergic syndrome (Voon et al., 2011.1; Voon et al., 2011.2). From a functional point of view, hyperdopaminergic states in the ventral tegmental loop would increase hippocampal activity, strongly facilitating a particular behaviour over other options, possibly explaining the compulsive behaviours (Calabresi et al., 2013). Further, some neuropsychiatric symptoms such as anxiety, depression and apathy, a hypodopaminergic syndrome, are directly related to a dopaminergic deficit. In this case, the hypodopaminergic states would reduce the hippocampal activation, thus reducing also motivation (Calabresi et al., 2013).

1.2.4 Pathogenesis of PD

A variety of factors have been shown to contribute to idiopathic PD, involving genetic predisposition as well as environmental risk factors (Schapira and Jenner, 2011). Similarly, a broad range of underlying cellular mechanisms have been proposed, mostly focused on protein mishandling and aggregation, mitochondrial dysfunction, and oxidative stress, as well as other mechanisms such as synaptic dysfunction (Bredesen et al. 2006; Skovronsky et al. 2006).

1.2.4.1 Protein mishandling and aggregation

A pivotal mechanism contributing to PD are cytoplasmic inclusions consisting largely of aggregated aSyn, as well as neurofilaments and ubiquitin (Spillantini et al., 1997). These inclusions are known as LB and they can be found throughout the entire brain in PD patients (Braak et al., 2003). The pathogenic role of LB remains unclear, with a debate between a protective mechanism based on sequestering toxic material or a direct cause of cell death (Braak et al., 2003; Dexter and Jenner, 2013; Lu et al., 2005; Olanow et al., 2004). Interestingly, both idiopathic and familial PD show LB formation. In familial PD, 6 point mutations of the alpha-synuclein gene SNCA are known (Krüger et al., 1998; Zarranz et al., 2004; Ki et al., 2007; Appel-Cresswell et al., 2013; Lesage et al., 2013; Pasanen et al., 2014), all found to cause a biophysical change by amino acid substitution. These mutations, combined with SNCA polymorphisms lead to oligomerization, fibril formation and aggregation of aSyn (Lázaro et al., 2014). In idiopathic PD no mutations are present in the aSyn gene, however aggregation of aSyn and LB formation point towards an additional malfunction of protein degradation pathways, on top of the possible involvement of excess protein seen in familial PD (Moore et al., 2003).

In terms of degradation pathways, several studies have shown a malfunction of the ubiquitin-proteasome system (UPS), a major contributor to protein degradation via ubiquitin targeting of proteins for proteolysis. In familial PD, mutations in *parkin*, the gene encoding E3 ligase Parkin, interfere with substrate recruitment (Kitada et al., 1998), while idiopathic PD shows deficits in the 20/26s proteasome, a protein complex crucial for protein degradation after ubiquitin tagging (McNaught et al., 2002; McNaught et al., 2003).

1.2.4.2 Mitochondrial dysfunction and oxidative stress

In addition to the impact of protein mishandling and aggregation in PD, imbalances in mitochondrial function and energy supply can severely affect neurons, leading to degeneration. The high metabolic activity of neurons requires a high amount of energy, which additionally has to be efficiently distributed to active areas such as synapses. Accordingly, the correct function of neurons relies heavily on unhindered mitochondrial function and transport systems (Exner et al., 2012). In 1980, the discovery of 1-methyl-4-phenyl-1,2,3,6-tetrahydropyridine (MPTP), a contaminant of the illegal synthesis of the opioid analgesic drug desmethylprodine (MPPP), first introduced mitochondrial dysfunction as a possible mechanism involved in idiopathic PD. MPTP is metabolized in glia cells after crossing the blood-brain-barrier, producing MPP⁺, which in turn is transported into dopaminergic neurons via the dopamine transporter. Once present in the dopaminergic neurons, it inhibits the complex I of the mitochondrial respiratory chain (Gerlach et al., 1991; Przedborski and Jackson-Lewis 1998). In turn, the hindered functionality of the complex I was shown to strongly contribute to the parkinsonian syndrome observed in connection to MPTP.

Further studies support the involvement of mitochondrial dysfunction in PD, showing a strong reduction of complex I activity in the SNpc of PD patients. In a study analysing respiratory-chain enzyme proteins in post-mortem tissue of the SN (n = 9 PD and n = 9 CTRs), NADH-ubiquinone reductase (complex I) and NADH cytochrome c reductase activity levels were found to be significantly reduced in PD, while cytochrome c reductase activity remained normal. Together, these findings hinted towards a specific defect of complex I activity in the SN in PD (Schapira et al., 1990). Similarly, both a study addressing iron-dependent aconitase activity in post-mortem SNpc tissue (n = 7 PD and n = 7 CTRs) as well as a study measuring iron and ferritin levels in post-mortem SNpc samples (n = 18 PD and n = 22 CTRs), showed significant decrease in complex I activity in PD (Mann et al., 1994; Janetzky et al., 1994).

The dysregulation of the complex I activity in PD might in turn have widespread implications. For instance, a reduction in complex I activity directly reduces energy availability due to decreases in ATP, hindering the normal function of high-energy demanding processes such as synaptic transmission. On the other hand, reduced complex I activity contributes to increased production of reactive oxygen species (ROS) and thus contributes to higher levels of oxidative stress. In combination with the inherent high oxidative burden of dopaminergic cells caused by the H₂O₂ produced during dopamine recycling (Sidhu et al., 2004), abnormally increased levels of oxidative

stress make dopaminergic cells highly susceptible, possibly contributing to a prevalent neurodegeneration.

1.2.4.3 Synaptic dysfunction

While mechanisms related to the increase of oxidative stress hint towards an increase in neurodegeneration likely triggering cell death mechanisms, also crucial changes to the synaptic functionality of neurons have been addressed in PD, often preceding the degeneration of the cell bodies. Altered synaptic transmission can be seen in animal models used to study both familial and idiopathic PD, including pathogenic models like the 6-hydroxydopamine-lesion (6-OHDA) and MPTP intoxication. (Schirinzi et al., 2016). Studies from the aforementioned models have indicated a complex homeostatic rearrangement of the nigrostriatal circuitry in response to a striatal dysregulation of dopamine, significantly affecting synaptic transmission in early and late stages of PD (Schirinzi et al., 2016).

Ample work has also established the important role in synaptic regulation of several genes implicated in familiar PD, including SNCA and LRRK2 (Plowey and Chu, 2010). Genetic animal models of aSyn overexpression show neuronal dysfunction even without complete cell loss, resulting in motor defects, electrophysiological changes to the basal ganglia, and variations in the release of dopamine (Tan et al., 2000). In addition, these studies also highlight early alterations of proteins involved in synaptic vesicle exocytosis, changes mostly preceding the loss of cell bodies (Chung et al., 2009). Furthermore, in normal rodents, extracellular aSyn has been shown to impair hippocampal LTP expression as well as increasing basal synaptic transmission of AMPA receptors (Diógenes et al., 2012).

Similarly, genetic models of LRRK2 have shown disrupted vesicle cycling by impaired endocytosis as well as reduced ability of repeated synaptic release (Lee et al., 2010; Matta et al., 2012), with synaptic abnormalities having been demonstrated even in the absence of overt neurodegeneration or significant abnormalities in striatal dopamine function (Walker et al., 2014).

In sum, ample experimental evidence supports a link between dopaminergic dysfunction and corticostriatal synaptopathy, with early imbalances in synaptic plasticity often occurring prior to neuronal cell death and the progression of the synaptopathy linked to the increase in biochemical damage of the nigral neurons (Schirinzi et al., 2016).

1.3 Pentraxins

Pentraxins are members of an evolutionary conserved superfamily of proteins, which present an amino acid domain of 200 amino acids in the C-terminus with an eight amino acid structural motif, the pentraxin signature (Garlanda et al., 2005). They are involved in acute immunological responses (Gewurz et al., 1995), with some members exerting their protective role in the periphery by activating the complement cascade and triggering an immune response (Hicks et al., 1992; Ying et al., 1992). Two subtypes of pentraxins are known, short and long pentraxins. The small pentraxins include proteins such as C reactive protein (CRP) and serum amyloid P (SAP), while long pentraxins comprise amongst others neuronal pentraxins 1 and 2 as well as the neuronal pentraxin receptor (**Figure 1**).

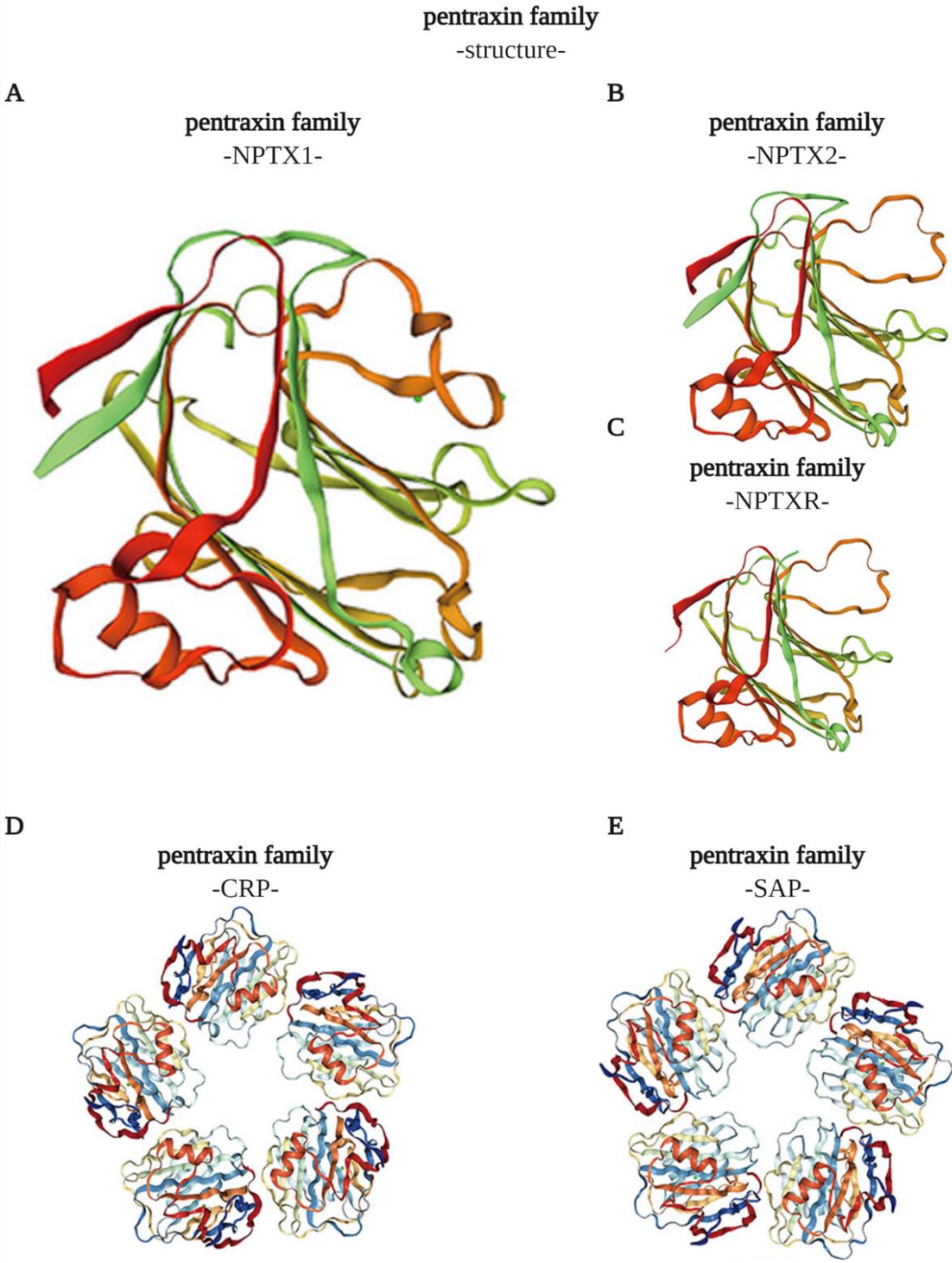


Figure 1. Structure of neuronal pentraxin family members. **A)** Protein structure of CRP. **B)** Protein structure of SAP. **C)** Protein structure of NPTX1. **D)** Protein structure of NPTX2. **E)** Protein structure of NPTXR. Adapted from (Wang et al., 2020).

1. Introduction

1.3.1 Short pentraxins

The first pentraxin to be described was CRP, a protein belonging to the branch of short pentraxins. It was detected in 1930 in human serum and proposed as an acute phase protein product of inflammatory or infectious conditions (Tillet and Francis, 1930). The second pentraxin identified after CRP was SAP, another short pentraxin described as a relative of CRP based on its sequence homology (51%) as well as the similarity in appearance, with a disc-like structure and pentameric symmetry (Noland et al., 1994; Szalai et al., 1999; Pepys and Hirschfield, 2003). Both short pentraxins have similar physiological functions involved in clearance of damaged cells, with CRP targeting nuclear antigens released from damaged cells, primarily binding to small nuclear ribonucleoproteins (snRNPs) (Du Clos, 1989) and SAP binding to chromatin and native DNA (Du Clos, 1996; Pepys and Butler, 1987).

Furthermore, it was shown, that pentraxins present characteristic calcium dependent ligand binding, with CRP and SAP having various pathogens as ligands (Hind et al., 1985; Noursadeghi, et al., 2000; Szalai, 2000). Furthermore, CRP was shown to bind chromatin, glycans and phospholipids (Pepys and Hirschfield, 2003), while SAP was found to bind matrix components, proteoglycans and amyloid fibrils (Loveless et al., 1992; Pepys and Butler, 1987).

The affinity of SAP for binding amyloid fibrils was further found to be involved in amyloidosis, a rare disorder caused by extracellular deposits of insoluble amyloid fibrils in the viscera, connective tissue, and blood vessels. It was proposed that SAP contributes to amyloidogenesis by stabilizing the amyloid fibrils as well as hindering their disposal (Pepys, 2006).

1.3.2 Long pentraxins

Another branch of the pentraxin family are the long pentraxins, which are predominantly expressed in neuronal tissue and include soluble secreted pentraxins: neuronal pentraxin 1 (NPTX1), neuronal pentraxin 2 (NPTX2) and neuronal pentraxin receptor (NPTXR). They possess the same C-terminal pentraxin domain with the pentraxin motif as the short pentraxins, while additionally containing a longer N-terminal domain. The NPTXs share a 20 - 30% similarity to SAP and CRP in terms of their C-terminal amino acid sequence, where the pentraxin motif is located, while sharing

between each other a 50% overlap in amino acid sequence (Downtown and McGrew, 1990; Rassouli et al., 1992; Tsui et al, 1996).

The N-terminal of both NPTX1 and NPTX2 forms coiled copies, while the C-terminal encodes the pentraxin domain, with the NPTXR receptor in turn presenting an amino-terminal transmembrane domain. In terms of structural complexes, the members of the NPTX family form heteromeric complexes which are stabilized by disulphide bonds and are found predominantly at excitatory synapses. Here, they interact via their C-terminal domains with AMPARs N-terminal extracellular domains (Dodds et al., 1997; Kirkpatrick et al., 2000).

Neuronal pentraxins have been described in relation to both synapse formation and synapse remodelling, as well as synaptic plasticity and clearance of synaptic debris. In artificial synapses established in cocultures of neurons and non-neuronal cells, the trans-synaptic localization of AMPAR subunits GluR2 and GluR4 was found to require binding to presynaptically derived NPTXs (Sia et al., 2007). Furthermore, it was shown that the presynaptic complex of NPTXs can be cleaved by TACE, followed by a relocation to the postsynaptic terminal together with their associated AMPARs and entering endosomes, thus increasing the efficacy of AMPAR endocytosis (Cho et al., 2008). The role of NPTXs in functional synaptic transmission was further confirmed by their role in the development of the visual system, where a knockout of NPTX1 and NPTX2 in mice led to disrupted AMPAR recruitment, a step critical for synapse formation (Koch and Ullian, 2010).

Furthermore, NPTX1 was observed in the intrinsic program underlying synaptic scaling in face of activity suppression. Homeostatic scaling in response to activity levels showed amongst others a significant upregulation of NPTX1. Molecularly, the induction of NPTX1 was determined to be mediated by transcription factors SRF and ELK1, as well as calcium influx through T-type voltage-gated calcium channels (Schaukowitch et al., 2017). In line with the involvement of NPTX1 in response to activity changes in the neuron, a possible impact on synapse density was addressed. It was found that NPTX1 negatively regulates excitatory synapse numbers by modulating neuronal excitability. Knockdowns of NPTX1 were shown to increase the number of excitatory synapses as well as increasing neuronal excitability in cortical neurons. In this regard, NPTX1 was found to regulate the surface expression of Kv7.2 a subunit of the Kv7 family of potassium channels, thus modulating neuronal excitability. Finally, NPTX1 knockdown was further shown to enhance excitatory drive and long-term potentiation in the hippocampus of mice (Figueiro-Silva et al., 2015).

Additionally, the individual knockdown of NPTX1 has shown the ability to reduce cell death caused by non-depolarizing culture conditions, suggesting a role in modulation of apoptotic cell death

1. Introduction

(de Gregorio-Rocasolano, et al., 2001). The role of NPTX1 in activity-dependent cell death modulation was further addressed in cultured cerebellar granule neurons (CGN). Low activity was shown to trigger the intrinsic program of apoptosis, which requires the translocation of BAX to the mitochondria. In parallel, the reduction in activity in CGN increased NPTX1 levels. Activity-induced increases in NPTX1 levels were in turn linked to mitochondrial fragmentation in a Bax-dependent manner, whereas the knockdown of NPTX1 showed a clear blockage of mitochondrial fragmentation induced by low activity (Clayton et al., 2012). Furthermore, in hippocampal cultured neurons, mitochondrial motility was shown to be modulated by NPTX1, with NPTX1 knockdown cultures showing a significant increase in mitochondrial transport. Specifically, an increase in anterograde moving mitochondria was detected, with no effect on retrograde transport, nor affecting the transport velocity in either direction (Clayton et al., 2012).

Moreover, a connection between NPTX1 and C1q mediated synaptic pruning by microglial phagocytosis was proposed. Expression levels of proteins related to apoptotic processes such as ubiquitin carboxyl-terminal hydrolase isozyme L1 (UCHL1) and calcineurin subunit B type 1 (PPP3R1), as well as NPTX1, were found to be altered in C1q-tagged synapses analysed in synaptosomal fractions retrieved from mouse cortex. It was in turn proposed, that C1q tagging plays a role in recognition of synapses where local apoptotic-like processes have been initiated, as evidenced by the dysregulation of apoptosis-related proteins, as well as abundant co-localization of the tagged synapses with cleaved caspase-3 (Györfy et al., 2018).

In addition, the role of NPTX1 in cell death modulation has been further addressed in several studies focused on ischemic neuronal death. Elevated NPTX1 levels were found in hippocampal regions CA1 and CA3 after hypoxia-ischemia (HI), while antisense oxyribonucleotides against NPTX1 mRNA (NPTX1AS) significantly inhibited HI-induced increases in NPTX1 and also inhibited neuronal death. Furthermore, NPTX1AS also protected cells against AMPA-induced neuronal death, hinting towards a role of NPTX1 in the excitotoxic cascade (Hossain et al., 2004). The specific role of NPTX1 in modulation of cell death following HI was further addressed in mouse hippocampal cultures of NPTX1 knockout mice and wild-type (WT) littermates. Cell cultures were subjected to oxygen glucose deprivation (OGD). The WT neurons showed an increased interaction of NPTX1 with Bad and Bax, facilitating their mitochondrial translocation, which in turn increased the activation of caspase-3, by inducing an increased release of Cyt C from the mitochondria. The NPTX1 knockouts in contrast showed no translocation of Bad and Bax, with no increase in caspase-3 activity, resulting in significantly less neuronal death (Rahim et al., 2012).

Finally, also extracellularly secreted NPTX1 was proposed to be involved in ischemic neuronal death. Cell culture supernatants from WT cortical cultures exposed to OGD were shown to cause neurotoxicity when added to control WT cultures, suggesting a role for extracellular NPTX1 in neuronal death (Thatipamula et al., 2014).

1.3.3 Involvement of pentraxins in neurodegenerative diseases

In line with its role in amyloidosis, SAP was found to bind to glycosaminoglycans and protein ligands on amyloid fibrils. Amyloid fibrils bound to SAP showed a high resistance to protease digestion, stabilizing and protecting them against degradation by proteases and phagocytic cells (Tennet et al., 1995). From these findings, the involvement of SAP in other amyloid pathologies was questioned, with special interest in brain pathologies, being immunohistologically associated with pathologies of several neurodegenerative diseases, such as Creutzfeldt-Jakob, Alzheimer's disease (AD), and Lewy body disorders (LBD), as well as Parkinson's disease (Akiyama et al., 1991; Kalaria et al., 1991). SAP has been found on amyloid plaques in AD. In regard to its presence in the brain, it has been proposed that SAP interacts with NPTX1 and can enter the brain in case of a compromised blood-brain-barrier, causing similar changes as shown for NPTX1, such as decreased glutamate release (Cummings et al., 2017).

In AD, accumulation of amyloid- β ($A\beta$) is thought to be critical in the degeneration of synapses, neurite damage, and cell death. The ability of NPTX1 to modulate neuronal death in mature neurons, based on reduced neuronal activity, was thus also addressed in relation to the neurotoxicity of $A\beta$. Cultured cortical neurons treated with $A\beta$ elicited a strong increase in NPTX1 protein levels, while the silencing of NPTX1 expression via RNA interference prevented synapse loss and halted apoptosis evoked by $A\beta$. Furthermore, NPTX1 was found increased in dystrophic neurites of brains from sporadic late-onset AD patients, co-localizing with tau deposits as well as synaptosomal-associated protein, 25kDa (SNAP25) (Abad et al., 2006). Finally, NPTX1 was also found to be a potential biomarker for AD, where cerebrospinal fluid retrieved from a group of 40 MCI patients, 40 AD patients and 40 controls showed a significant increase in NPTX1 levels in MCI, with especially high levels of NPTX1 in MCI progressing to AD dementia (Duits et al., 2018).

In sporadic PD, NPTX2 was found to be highly upregulated, with increased NPTX2 mRNA in cortical neurons and glia in the substantia nigra. Furthermore, it was found in close proximity to

1. Introduction

aSyn aggregates in both the substantia nigra and the cerebral cortex of human sporadic PD brains, with approximately one third of LB co-expressing NPTX2 (Moran et al., 2008). NPTX2 has been proposed to potentially contribute to the cell death in the substantia nigra through AMPA receptor-mediated mechanisms, as well as the formation of LB (Moran et al., 2008). Furthermore, an overexpression of NPTX2 was found in the striatum after L-DOPA treatment (Charbonnier-Baupel et al., 2015). L-DOPA-induced dyskinesia (LID) was in turn proposed to be modulated by the expression of NPTX2, with NPTX2 knockout mice showing less severe LID, suggesting a role in the ERK pathway (Charbonnier-Baupel et al., 2015).

Finally, changes in NPTX2 levels in cerebrospinal fluid (CSF) were further correlated with aSyn levels in dementia with Lewy bodies (DLB). Samples from 27 healthy subjects, 48 DLB patients, and 20 AD patients were analysed in terms of aSyn, VGF, and NPTX2 expression levels. Significantly decreased NPTX2 was observed in DLB and AD, with a clinical relation between NPTX2 and global cognitive function, as well as cognitive decline in the visual spatial domain (Boiten et al., 2021).

1.4 Aims of the present study

The technological and scientific development over the last decades has significantly improved the life quality and expectancy for the population worldwide. However, this has also given rise to new challenges in a population reaching ever increasing ages. Amongst these challenges, neurodegeneration significantly worsens the life quality of the aging society. The technological advances have however also provided improved strategies to address the mechanisms accompanying the highly prevalent neurodegenerative diseases. For instance, large scale high-throughput proteomic approaches have enabled addressing with high efficiency a wide range of molecular mechanisms and pathways involved in complex systemic disorders such as Parkinson's disease.

While insight has been gained on the proteomic changes taking place in PD, the focus has been often placed on the widely studied midbrain. However, considering the systemic nature of PD, with a known impact on multiple other brain areas, the availability of such powerful biotechnological tools can be taken advantage of to address the impact of PD in additional regions of the central nervous system.

As such, the main goal of this study was to analyze the hippocampus of PD patients, searching for possible changes in the protein expression levels of synapto-axonal proteins in samples obtained from a cohort of human PD patients and controls, addressing both the global dysregulation of proteins as well as the synaptosome-specific proteome. To this end the following strategies were employed:

- **Mass spectrometry** to identify and quantify hippocampal proteins in total tissue and synaptosomal fractions
- **Differential expression** analysis to establish quantifiable changes in the abundance of proteins in the PD hippocampus
- **Analysis of protein-protein interaction networks and functional annotation**, to characterize the proteomic data sets and address the biological relevance of the differentially abundant proteins, as well as defining a target of interest possibly involved in synaptic dysfunction
- **Modulation of a protein of interest in primary cell cultures** to understand the changes elicited by the differential abundance of this protein on synaptic morphology

Chapter 2: Materials and Methods

2.1 Materials

2.1.1 Human samples

ID	age	sex	duration [y]	PMI [h]	diagnosis
PD					
PD074	85	M	9	17	LBDBS
PD334	87	M	9	21	LBDN
PD458	73	M	19	10	LBDBS
PD666	93	F	15	24	LBDBS
PD039	82	F	15	12	LBDBS
PD125	74	M	25	20	LBDN
PD134	74	M	10	21	LBDBS
PD180	85	F	15	15	LBDN
PD182	75	M	10	3	LBDN
PD184	71	M	7	24	LBDE
PD187	72	M	8	11	LBDN
PD201	87	M	11	19	LBDN
PD203	84	F	18	19	LBDN
PD207	81	M	10	11	LBDN
PD229	85	F	18	7	LBDN
PD102	81	M	25	16	LBDBS
CTR					
PDC035	89	F		13	Diffuse hypoxic damage
PDC023	78	F		23	n.a.
PDC034	90	M		12	n.a.
PDC040	61	F		15	n.a.
PDC087	92	F		24	n.a.
PDC088	96	F		24	n.a.
C054	66	M		16	n.a.
C064	63	F		21	n.a.
C074	84	F		22	n.a.
PD529	70	F		18	n.a.
PD549	76	M		25	Age associated changes
C030	75	M		17	n.a.
C075	88	M		8	n.a.
PDC078	91	M		18	n.a.

Table 1. Human sample clinical and demographic information. PMI: post-mortem intervals; LBD-BS: Lewy body disease -brain stem predominant-; LBDN: Lewy body disease -neocortical- ; LBDE Lewy body disease -early-neocortical- (Alafuzoff et al., 2009; Lachén-Montes et al., 2018), n.a: not available.

2. Materials and Methods

2.1.2 Reagents

Reagent	Supplier
2-Propanol	AppliChem (Germany)
APS	Sigma Aldrich (Germany)
Acrylamide	Applichem (Germany)
B-27 Supplement	Gibco (Germany)
Bromophenol blue	Sigma Aldrich (Germany)
Bovine serum albumin (BSA)	Applichem (Germany)
DAPI	Sigma Aldrich (Germany)
Ethanol absolute	AppliChem (Germany)
Fetal calf serum (FCS)	Biochrom (Germany)
Glucose	Merck (Germany)
Glutamax	Lonza (Germany)
Glycerol	Roth (Germany)
Glycine	Applichem (Germany)
GlycoBlue Coprecipitant	ThermoFisher Scientific (USA)
Hanks balanced salt solution (HBSS)	Gibco (Germany)
Ketamine	Medistar (Germany)
Laminin	Sigma Aldrich (Germany)
Methanol	Applichem (Germany)
Mowiol 488	Sigma Aldrich (Germany)
Neurobasal medium	Gibco (Germany)
Non-fat dried milk	Applichem (Germany)
Paraformaldehyde (PFA)	Applichem (Germany)
Phosphate buffered saline (PBS)	AppliChem (Germany)
Precision Plus Dual Colour Standard	BIO-RAD (Germany)
Sodium dodecyl sulphate polyacrylamide gel electrophoresis (SDS)	Applichem (Germany)
Sucrose	Applichem (Germany)

TEMED	Roth (Germany)
Tris base	Applichem (Germany)
Tris HCl	Applichem (Germany)
TritonX 100	Applichem (Germany)
Trypsin	Biochrom (Germany)
Tween20	Applichem (Germany)

2.1.3 Buffers and solutions

Antibody solution for immunohistochemistry (IHC): 1% NGS; 0.1% TritonX 100 in PBS

Basic reverse-phase buffer A: 10 mM NH₄OH in water, pH ~10; buffer

Basic reverse-phase buffer B: 10 mM NH₄OH and 80% (v/v) ACN in water, pH ~10

Blocking solution for IHC: 10% NGS; 0.1% TritonX 100 in PBS

Blocking solution for Western Blots (WB): 5% non-fat milk in TBS-T

Culture medium: 2% B27 supplement; 1% Glutamax; 1% Pen/Strep; 1% 45% Glucose; 95% Neurobasal

DAPI solution: 1 µg/ml DAPI in PBS

Electrophoresis buffer [pH 8.3]: 192mM Glycine; 0.1% SDS; 25mM Tris HCl

Homogenization buffer: 320 mM sucrose, 5 mM HEPES in water

Laemmli buffer [pH 6.8]: 312.5mM Tris; 10% SDS; 50% Glycerin; 0.005% Bromophenolblue; 100mM DTT

Mowiol [pH 7.2]: 6g Glycerol; 2.4g Mowiol; 6ml H₂O; 12ml Tris

PBS: 9.5mg/ml PBS; distilled water

PBS-T: 0.1% TritonX 100 in PBS

PFA (4x) solution: 40mg/ml PFA; 9.5mg/ml PBS

Primary antibody solution for WB: 5% non-fat milk in TBS-T

RIPA buffer: 10mM HEPES; 142nM KCl; 5nM MgCl₂; 2.1mM EGTA and IGEPAL; Complete proteasome inhibitor 1:25; Phosphatase inhibitor 1:20

2. Materials and Methods

Secondary antibody solution: 5% non-fat dried milk; TBS-T

Synaptosomal fractions lysis buffer: 4% SDS, 100 mM HEPES, 1 mM EDTA, 1 × Halt Protease and phosphatase inhibitor cocktail in water

TBS: 10mM Tris HCl; 150mM NaCl in distilled water

TBS-T [pH 7.6]: 0.1% Tween20; TBS

Transfer buffer [pH 8.3]: 192mM Glycine; 20% Methanol; 25mM Tris HCl

Tris [pH 8.0]: 10mM Tris-buffered saline

Urea lysis buffer: [added 20% weight/vol]: 7M Urea; 2M Thiourea; 4% Chaps; ASB14 2%; 4% Complete, Mini, EDTA-free Protease inhibitor; 5% Phos Stop Phosphatase inhibitor

2.1.4 Equipment

Equipment	Producer
6-and 24-well cell culture plates	Sarsted (Germany)
Agilent 1100 HPLC system	Agilent (USA)
Bioruptor ultrasonic device	Diagenode (Belgium)
Chrommatography Pre-column (0.18 mm ID x 20 mm; symmetry C18, 5 µm)	Waters (USA)
Chrommatography RP-C18 column	Waters (USA)
Cover slide Ø 18mm	Menzel (Germany)
Cover slips 24 x 60mm	Menzel (Germany)
Cover slide Ø 12mm	Menzel (Germany)
Cover slips 24 x 55mm	Menzel (Germany)
Cryostat CM 3050S	Leica Microsystems (Germany)
C18 PepMap100-trapping column (0.3 x 5 mm, 5 µm)	Thermo Fisher Scientific (USA)
C18-X-Bridge column (3.5 µm particles, 1.0 mm inner diameter, 150 mm length)	Waters (USA)
Eksigent nanoLC425 nanoflow chromatography system	AB Sciex (USA)
Hybrid triple quadrupole-TOF mass spectrometer (TripleTOF 5600+)	AB Sciex (USA)
Micro-centrifuge 5415R	Eppendorf (Germany)
Orbitrap Fusion Lumos Tribrid mass spectrometer	Thermo Fisher Scientific (USA)
Parafilm sealing film	Starlab Int. GmbH (Germany)
Pre-packed 18 spin columns	Harvard Apparatus (USA)
Savant SpeedVac	Thermo Fisher Scientific (USA)
Spark 10M multimode microplate reader	Tecan (Switzerland)
SS-34 fixed angle rotor centrifuge	Thermo Fisher Scientific (USA)

SW-41 swinging bucket rotor ultra-centrifuge	Beckman Coulter (Germany)
UltiMate 3000 RSLC nanosystem	Thermo Fisher Scientific (USA)

Table 2. List of used equipment.

2.1.5 Software

Software	Producer
AxioVision SE64 Rel. 4.9	Carl Zeiss
limma	(Smyth, 2005; Ritchie et al., 2015)
Matlab v.R2020b	MathWorks
MaxQuant v.1.6.10.2	(Cox, et al., 2011; Tyanova, et al., 2016)
OriginPro v.8.5.0 SR1	OriginLab
PeakView Software version 2.1	AB Sciex (USA)
Perseus 1.5.6.0	Institute, Martinsried Germany (Tyanova et al., 2016)
ProteinPilot Software version 5.0	AB Sciex (USA)
Python v.3.8.11	Python Software Foundation
R software	R Core Team, 2017
SWATH quantification microApp version 2.0	AB Sciex (USA)
WGCNA package	Langfelder

Table 3. List of used software.

2.2 Methods

2.2.1 Human brain samples

2.2.1.1 Source and ethics

Human hippocampal samples were provided by the Parkinson's UK Brain Bank (Imperial College London, London, England) and conceded to the Lingor Lab (Department of Neurology of the University Medical Center Göttingen, Göttingen, Germany), with the ethical approval of the Multicenter Research Ethics Committee (07/MRE09/72) as well as the Ethics Committee of the University Medical Center Göttingen (18/3/17).

2.2.1.2 Hippocampus sampling

Snap frozen hippocampal post-mortem human blocks were handled at -20°C in a cryostat chamber for brief periods of time, preventing damage by thawing. Samples were acquired from the tissue blocks (n = 16 PD and n = 14 CTR) via needle biopsies with a 20G Quinke spinal needle (Beckton Dickson, Madrid, Spain), collecting ~13mg of tissue per block. Samples were kept overnight at -80°C and lysed the next day for the proteomic approach via mass spectrometry.

A second collection on a sub-cohort of samples, from brain-blocks with enough material (n = 6 PD and n = 4 CTR), was done by fractioning off a block of tissue, aiming for ~600mg. The fractioned blocks were processed on the same day for synaptosomal fraction isolation and subsequent proteomics via mass spectrometry.

2.2.2 Proteomics

2.2.2.1 Whole tissue lysate preparation

To obtain proteomic data from the whole tissue lysates, samples were lysed in Urea/Thiourea/Chaps lysis buffer (detailed composition in **Error! Reference source not found.**). Samples were homogenized with a bead homogenizer, followed by a brief centrifugation to reduce the formation of bubbles. Further, sonication was performed on ice, with two 15s intervals, followed by a second brief centrifugation to remove bubbles.

2.2.2.2 Whole tissue sample protein quantification

Protein content quantification of the whole tissue lysates was performed using a modified-Bradford Roti-Nanoquant protein quantification kit as per manufacturer's instructions, with colorimetric reactions being read in the TECAN Spark 10M Plate reader. For the subsequent mass spectrometry 50µg of protein were aliquoted and the remaining lysate was stored at -80°C for subsequent validations.

2.2.2.3 Whole tissue sample mass spectrometry

The previously prepared whole tissue lysate samples with 50µg of total protein were loaded onto a 4-12% NuPAGE Novex Bis-Tris Minigel (Invitrogen, USA) and run for 1.5cm by electrophoresis, followed by Coomassie Brilliant Blue staining to identify protein bands. The bands were removed and diced, followed by a reduction with dithiothreitol and alkylation with iodoacetamide with a final trypsin digestion over night.

The extracted peptides were dried in a SpeedVac (Atanassov and Urlaub 2013). Aliquots (80µg per sample) were pooled and separated into eight fractions via a reverse spin column (Pierce High pH Reversed-Phase Peptide Fractionation Kit, Thermo Fisher Scientific), to generate a peptide library. A Synthetic peptide standard was spiked into all samples for retention time alignment (iRT Standard, Schlieren, Switzerland).

Peptides from the protein digests were dissolved in a loading buffer (2% acetonitrile, 0.1% formic acid in water), with 1.5µg of digested protein being enriched on a precolumn (0.18 mm ID x 20 mm, Symmetry C18, 5 µm, Waters, Milford/MA, U.S.A), followed by a separation on an analytical RP-C18 column (0.075 mm ID x 250 mm, HSS T3, 1.8 µm, Waters) with linear gradient of 5-35 % acetonitrile/0.1% formic acid (v:v) at 300nl min⁻¹ for 90 minutes.

2.2.2.4 Whole tissue sample mass spectrometry analysis

The analysis of LC/MS/MS data was done via a data dependent Top25 acquisition method, with a m/z 350-1250 survey scan, accumulated for 350s with a resolution of 30 000 full width and at half maximum (FWHM). The accumulation of m/z scans 180-1600 was in turn 100ms at 17 500 FWHM, with a precursor isolation width of 0.7 FWHM, totalling a cycle time of 2.9s. A threshold was set for precursors at 125cps with charge states 2+, 3+ and 4+, with precursors above the threshold being selected for MS/MS. CID with nitrogen as collision gas and rolling collision energy settings at

2. Materials and Methods

the manufacturer's default were used for MS/MS activation, while analysing triplicates per reversed phase fraction as technical replicates in the spectral library construction.

2.2.2.5 Synaptosomal fraction homogenate preparation and fractions isolation

After sampling of ~600mg of tissue from frozen post-mortem human hippocampal samples, the collected samples were homogenized in cold homogenization buffer with nine strokes of a Teflon/glass homogenizer. The homogenized solution was centrifuged for two minutes at 2988xg in a SS 34 fixed angle rotor centrifuge, collecting the supernatant and centrifuging again for 12 minutes at 14462xg, obtaining crude synaptosomes. For the final fractioning of the sample, the pellet of crude synaptosomes was gently resuspended in homogenization buffer, layered on a discontinuous Ficoll gradient with 6%, 9% and 13% wt/v Ficoll in homogenization buffer and centrifuged for 35 minutes at 86575xg in an SW 41 swinging bucket rotor ultracentrifuge. From the resulting layers, the interfaces between 6% and 9% as well as between 9% and 13% were carefully collected and pooled, obtaining enriched synaptosomal fractions.

2.3.2.6 Synaptosomal fraction protein sample preparation for mass spectrometry

The obtained synaptosomal fraction was pelleted, lysed and sonicated for 10 minutes at maximum output on a Bioruptor ultrasonication device with 30s on and off cycles. Protein concentrations were assessed with a BCA protein assay kit and 200µg of protein were used for further processing. Samples were reduced and alkylated, followed by an incubation in 10mM TCEP and 40mM CAA for 30 minutes at 37°C and protein purification following the protocol by Hughes et al. 2019. An overnight digestion with trypsin was followed by the labelling of 10 individual samples (n=6 PD and n=4 CTR) as well as a technical replicate using TM11 labelling reagents following the manufacturer's instructions. Further, pooled samples were cleaned in pre-packed C18 spin columns and concentrated in a Savant SpeedVac vacuum concentrator.

2.3.2.7 Basic reversed-phase (bRP) chromatography of synaptosomal fraction

The labelled peptides were injected into a C18-X-Bridge column in a Agilent 1100 series HPLC system and separated at a 60µl/min flow rate under basic pH, with the columns being equilibrated with 95% buffer A and 5% buffer B and a linear gradient for 74 minutes ranging from 5% to 50% buffer B. A washing step was conducted at 90% buffer B for 5 minutes and following the suggestions by Wang et al. 2011 one-minute fractions were retrieved and concatenated into 24 final fractions, snap frozen in liquid nitrogen and dried in the SpeedVac.

2.3.3.8 Synaptosomal fraction mass spectrometry analysis

Technical duplicates, obtained from re-dissolving the dried peptides, were injected onto a C18 PepMap100-trapping column connected to an in-house packed C18 analytical column, with column pre-equilibration conducted with a mixture of 98% buffer A. Liquid chromatography was controlled by Ultimate 3000 RSLC nanosystem, with an elution using a linear gradient from 2% to 7% buffer B over 1 minute followed by a 7% to 45% buffer B gradient for 105 minutes, finished off by a 5 minute 90% buffer B washing step. The eluted peptides were sprayed into an Orbitrap Fusion Lumos Tribid mass spectrometer, acquiring MS1 scans in a positive ion mode with a resolution of 120 000 at 200 m/z, 5e5 automatic gain control (AGC) target and 50ms maximum injection time. With a 1.6 m/z isolation window, precursor ions with charges 2-7 were isolated and fragmented at 38% normalized collision energy (NCE). A resolution of 15 000, 2.5e5 AGC target and 40ms maximum injection time were used for MS2 fragment spectra. Finally, using an isolation window of 2 m/z and NCE of 45%, ten most intense fragments were selected for SPS-MS3, acquiring the spectra at a resolution of 60 000 and maximum injection time of 118ms.

2.2.4 Bioinformatic analysis

The differential expression analyses were done in collaboration with the lab of Prof. Stefan Bonn by Hannes Wartmann (UKE, Hamburg) and the lab of Prof. Henning Urlaub by Dr. Christof Lenz and Ivan Silbern (UMG Göttingen).

2.2.4.1 Mass spectrometry whole tissue lysate data processing and mapping

Following the qualitative analysis, proteins were identified with the ProteinPilot Software v.5 build 4769 on thorough settings, searching the MS/MS spectra against the human reference proteome revision 04-2018 from UniProtKB with the addition of a set of 52 known common laboratory contaminants. Proteins were identified with a false discovery rate of 1%, with a spectral library generation and SWATH peak extraction being conducted in PeakView software v.2.1 build 11041, using the SWATH quantitation microApp v.2.0 build 2003. Peak areas were assessed after retention time correction via iRT standard, with peak areas being summed to peptides, obtaining final protein area values for further statistical analysis.

2.2.4.2 Differential expression analysis of whole tissue lysates

The obtained final protein values were normalized, and log transformed for the analysis, using the limma R package for the differential expression analysis. A $Y \sim \text{control} + \text{PD}$ model was fitted via

2. Materials and Methods

lmFit, with the differential expression being established using limma's eBayes function, followed by a Benjamini-Hochberg (BH) correction for multiple testing. Statistical significance was considered for proteins with an adjusted p-value < 0.05 .

2.2.4.3 Mass spectrometry processing of synaptosomal fraction data and differential expression analysis

For the processing of the raw files MacQuant v.1.6.10.2 was used with default settings, using cysteine carbamidomethylation as fixed modification and methionine oxidation and acetylation of protein-N-termini being kept as variable modifications. The quantification was conducted using reporter ions in MS2, with MS1 and MS2 tolerances kept at 4.5ppm and 20ppm respectively. Protein contaminants and matches to reverse sequences were filtered out, as well as excluding protein groups with less than two razor or unique peptides and protein groups with four or more missing quantitative values. Remaining missing values were imputed for the individual TMT-channels by random sampling from a Gauss distribution with a mean at the 10% percentile and a half standard deviation of the log-transformed intensities. Finally, log2-transformed reporter ion intensities were normalized via Tukey median polishing and an eBayes function was used to establish the differential expression, followed by a BH correction. Samples were further considered as differentially expressed based on the mod p value prior to BH correction, with $p_{mod} < 0.05$.

2.2.4.4 Functional annotation

To characterize the biological relevance of the obtained proteomic data sets, functional annotation analyses as well as protein-protein interaction networks were created using STRING Platform v.11.0b (Szklarczyk et al., 2019), with statistical significance considered for $FDR < 0.05$. Additionally, a second functional annotation was performed as conducted for the re-scaled data set after module formation by WGCNA, utilizing the WEB-based Gene SeT AnaLysis Toolkit (WebGestalt, Liao et al., 2019), using the redundancy reducing affinity propagation method for post-processing.

2.2.4.5 Weighted correlation network analysis of whole tissue lysates and synaptosomal fractions

To reduce the complexity of the obtained proteomic data set of both whole tissue lysates and synaptosomal fractions, the data sets were re-scaled into sub-sets of proteins assigned to individual modules based on the correlation of their expression patterns, grouping together proteins with highly similar expression patterns. The reduction was conducted using the WGCNA R package, following

the available tutorial (Langfelder and Horvath, 2008), using an automatic network construction with default settings, a thresholding power of 4 and minModuleSize of 25 for the whole tissue lysate data set and a thresholding power of 10 with an adjusted minModuleSize of 80 to generate 10 modules for the synaptosomal fraction data set.

2.2.4.6 Synaptic morphology analysis of cultured treated hippocampal neurons

From the imaged cell cultures rectangular areas of a constant size were manually selected using custom written Matlab scripts, with regions of interest containing signal being determined by a threshold setting. Signal strength above background was set to the mean plus standard deviation of the signal within the selected rectangular area. Signal strengths above the threshold within the delimited area were considered as synapses and variables of a fitted ellipse were measured using the regionprops function of Matlab [R2020b], including mean intensity, major and minor axis and area.

2.2.5 Cell culture

Primary cell cultures of hippocampal mouse neurons were used to address the protein of interest NPTX1 *in vivo*, both to characterize endogenous expression and to describe morphological changes to the synapse elicited by an artificial increase in NPTX1 mimicking the increases measured in the hippocampus of PD. The cultured cells were treated chronically for seven days prior to fixation and analysis.

2.2.5.1 Culture plates

For the culture of hippocampal mouse neurons, 6-and 24-well plates were coated with PLL and stored at 37°C in the incubator over night, a day prior to the seeding of cells. On the day of seeding, the PLL was removed, and plates were washed two times with PBS, filled with Neurobasal and stored at 37°C in the incubator until usage.

2.2.5.2 Primary hippocampal neuron cultures

C57BJ/6J newborn pups (P0) were used for primary hippocampal neuron cultures. The extracted brains were held in ice-cold CMF and dissected under aseptic conditions on an ice-battery to ensure low temperatures. Meninges were removed from the brains and hippocampi were isolated and gathered in ice-cold CMF. After dissection, the collected hippocampi were centrifuged at 1rcf for 2 minutes at room temperature (RT). CMF was removed and the pellet was incubated in 1ml trypsin at 37°C for 12 minutes with occasional shaking. DNase (150µl) was added and incubated for additional 2 minutes at 37°C, followed by a minute of centrifugation at 1rcf, removing the supernatant

2. Materials and Methods

liquid and adding 1ml of FCS to stop the reacting trypsin. Tissue was homogenized using a fire polished Pasteur pipette, followed by 4 minutes of centrifugation at 1rcf, discarding the supernatant and resuspending the pellet in cell culture medium. The suspended cells were counted in a Neubauer counting chamber and 200,000 cells/well were plated on PLL-covered coverslips in 24-well plates with a total volume of 500 μ l per well. For 6-well PLL-coated plates, 1,000,000 cells/well were seeded, with a final volume of 3ml. Half of the culture medium was exchanged for new medium one day after seeding, with the addition of AraC (2 μ M per well) to decrease the amount of glia contamination.

2.2.5.3 Recombinant NPTX1 treatment

After seeding, the first exchange of medium was accompanied by the first of seven treatments of recombinant NPTX1. 0.2 μ g/ μ l of recombinant NPTX1 were solubilized in culture medium, aliquoted and kept at -20°C until use. Daily treatment was applied by removing ~100 μ l per well individually, adding and mixing in 0.23 μ g of recombinant NPTX1 to each 100 μ l removed and returning the treated culture medium to the respecting wells with the seeded cells. Control cells underwent the same procedure of removal of culture medium, substituting the recombinant NPTX1 with cell culture medium.

2.2.5.4 Fixation of cells

After 7 days of treatment, medium was collected from the cells in the 24-well plates, 5% ice cold glucose was added and rinsed and 4% PFA was applied for 10 minutes at RT for fixation. After the fixation, wells were washed 3 times with PBS and plates were stored at 4°C until further usage.

2.2.5 Molecular biology and biochemical techniques

2.2.5.1 Immunocytochemistry

Cells in 24-well plates previously fixated and washed with PBS were incubated with 25mM glycine in PBS for 20 minutes and washed subsequently two times for 5 minutes each with PBS. An incubation for 1.5h with blocking solution at RT was followed by the incubation of primary antibodies solutions at 1:50 for NPTX1(mouse, Becton Dickinson) and 1:500 for SYN1 (rabbit, Synaptic Systems) at 4°C overnight. On the second day, cells were washed thrice for 5 minutes each with PBS, followed by the incubation of the secondary antibody at a dilution of 1:250 for both Cy3 AffiniPure fluorescent dye (1:250, anti-mouse, Biozol) and AlexaFluor AffiniPure fluorescent dye (1:250, anti-rabbit, Biozol) conjugated secondary antibodies, incubating for 1.5h at RT. After the secondary

antibody incubation cells were washed thrice with PBS for 5 minutes each, followed by the addition of DAPI for 2 minutes for nuclei staining, finished by three washing steps with PBS for 5 minutes each. Finally, cells were mounted with Mowiol and stored at 4°C until use.

2.2.6 Microscopy *in vivo*

2.2.6.1 Image processing

To characterize the NPTX1 expression both in endogenous conditions as well as in treated cultures with increased NPTX1 abundance, cells were immunostained and imaged with a Zeiss Axioplan microscope (Zeiss, Göttingen, Germany). The AxioVision SE64 Rel. 4.9 software was used to generate images of the cells with a magnification of 63x using an immersion objective. The same exposure was used for all images across the same experiment, with same intensities used for each channel imaged. NPTX1 signal was used to analyze endogenous expression levels and expression patterns over time from DIV01-DIV11. SYN1 signal was used to characterize morphological changes to the synapse by fitting of ellipses to individual SYN1 signals and quantifying defined variables.

2.2.7 Validation of NPTX1 via Western Blots

The differential expression of NPTX1 abundance in PD was established by measuring NPTX1 expression ratios to house keeping protein GAPDH in both PD and CTR samples. All 16 PD and 14 CTR samples were lysed in RIPA cell lysis buffer (Pierce) and protein concentrations were assessed with a BCA protein assay kit (Pierce). Equal amounts of protein were loaded onto a 12% Mini-PROTEAN TGX gels (BioRad), adding a pooled sample from all samples to each of the three membranes loaded and run at 80V until the 10kDa marker band of the ladder reached the bottom of the gel. Gels were transferred to a PVDF membrane (GE Healthcare) over night at 4°C with 15V. On the second day, membranes were blocked for 1h with 5% dry milk in TBST and washed thrice for 15 minutes each with TBS. Incubation of primary antibody solution in TBST-milk of NPTX1 (1:100; mouse; Becton Dickinson) or SYN1 (1:1,000; rabbit; Synaptic Systems) or GAPDH (1:1,000; mouse; HyTest) was done overnight at 4°C, followed on the third day with 3 washing steps of 15 minutes each with TBS. Secondary antibodies, goat-anti-rabbit-HRP or horse-anti-mouse-HRP (Cell Signalling) at a dilution of 1:10,000 in TBST-milk were incubated for 1.5h at RT, followed by three washing steps of 15 minutes each with TBS. Finally, membranes were developed using ECL Primer Western Blotting Detection Reagent (TH Geyer) and visualised with FusionPulse (Vilber). Signals were quantified with EvolutionCapt (Vilber), normalized to housekeeping GAPDH to correct for

2. Materials and Methods

possible differences in loading as well as normalized to signal of the pooled sample applied to all three membranes measured to enable multiple membrane comparison.

2.2.8 Statistical analysis

In addition to the previously mentioned analyses, statistical analysis for the validation of NPTX1 via Western Blots were conducted using OriginPro 8.5.0 SR1. Signal intensities of NPTX1 were normalized to GAPDH intensities and intensity ratios were in turn normalized to the GAPDH intensity of the pooled sample. A PD sample and a CTR sample were removed due to presenting outlier values in GAPDH signal. Data were tested for normality with Shapiro-Wilk and Kolmogorov-Smirnov normality tests and a two sample t test for significance.

Development of endogenous NPTX1 expression over time was assessed by normalizing NPTX1 signal to GAPDH housekeeping signal. Data were tested for normality with Shapiro-Wilk and Kolmogorov-Smirnov normality tests and a one way ANOVA with a Tukey Test for evaluation.

Finally, morphological changes in the synapse were assessed by comparing the total measurements of all identified synapses for the different variables (area, mean intensity, major axis and minor axis) by means of two sample t tests .

For all previously mentioned analyses data were considered significant if $p < 0.05$ and indicated with $p < 0.05$ (*), $p < 0.01$ (**), and $p < 0.001$ (***) .

2.2.9 Figures

All schemes presented in this thesis were created or formatted in BioRender.

Chapter 3: Results

3.1 Differential abundance of proteins in whole tissue lysate samples retrieved from human hippocampal PD samples.

3.1.1 Aims

The aim of the experiments described in this chapter, was to identify, quantify and characterize differences in the hippocampus of PD patients, by addressing quantifiable expression levels of proteins and comparing them to CTR samples. Firstly, label free mass spectrometry enabled the identification and quantification of a wide range of proteins. Secondly, a differential expression analysis enabled to calculate significant changes in the abundance of proteins in PD compared to CTR. Thirdly, two methods to analyze the data set were employed to address the biological relevance and to identify possible areas of interest in terms of mechanistic effects: protein-protein-interaction networks and network reduction via co-expression analysis of expression patterns. In a fourth step, a validation of results was conducted using a mass spectrometry-independent approach for identification and quantification of the target protein expression levels via western blots. Finally, the results were compared to a transgenic mouse model of PD, addressing similarities in protein expression changes.

3.1.2 Results

3.1.2.1 Protein quantification and differential expression analysis of whole tissue lysate samples

In order to analyse changes in the PD hippocampus, protein expression levels of human hippocampal tissue samples were quantified and compared to control samples. Tissue was collected from human fresh frozen hippocampal samples via needle biopsies, retrieving ~13mg of tissue, which was lysed with a Urea/Thiourea/Chaps lysis buffer (**Figure 2**).

3. Results

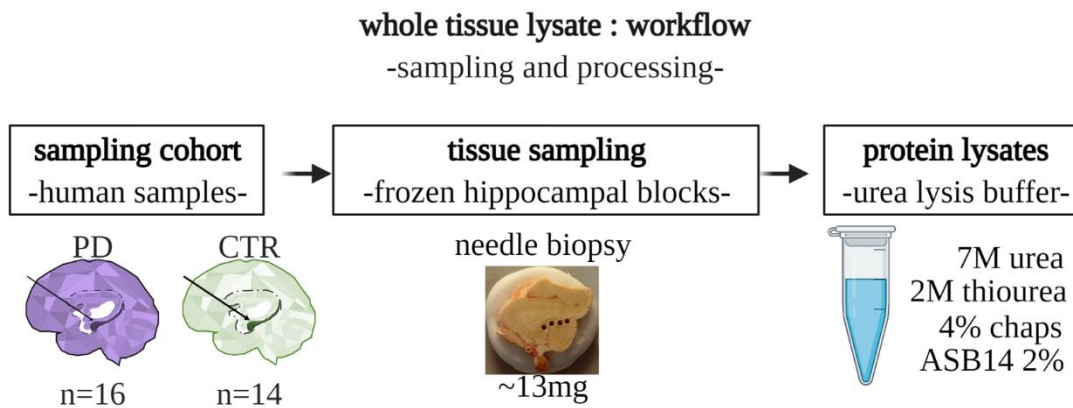


Figure 2. Workflow for sample collection of whole tissue lysate samples. Workflow for tissue sampling from human fresh frozen hippocampal samples for whole tissue proteome cohort. Needle biopsies were performed with a 20-G spinal needle. Protein lysates were prepared using a urea lysis buffer.

The protein composition of the whole tissue lysates was assessed by the group of Dr. C. Lenz¹, using the Sequential Window Acquisition of all Theoretical Mass Spectra (SWATH-MS). To establish peptide libraries, equal amounts of proteins were run in electrophoresis gels and digested with trypsin. Peptides were identified by means of a spectral library and peak areas were obtained for mass quantification. A data set of protein expression levels of a total of 2089 unique proteins was obtained after peptide mapping and normalization of protein content, adhering to a 1% false discovery rate (FDR).

Due to unknown spatial folding of the sampled frozen brain blocks, the precise histological composition of the needle biopsies was not determinable. Thus, to verify for an unbiased tissue sampling, the identified protein data set was compared to a reference set of marker proteins for individual cell types. To this end, we established a set of cell type specific proteins based on the proteomic data set presented in Sharma et al. 2015. The study of Sharma and colleagues presented a proteome analysis based on high-resolution mass spectrometry, with an identification of 12,934 proteins. The study covered astrocytes, microglia, oligodendrocytes and neurons. We focused on cell type specific proteins with a reported significant increase in abundance compared to the other cell types, considering only proteins with a reported fold change (FC) > 2. From the obtained list of proteins we constructed four unique lists of cell type markers by removing proteins present in more than one cell type category. Finally we compared the individual lists to the proteomic data set from the whole tissue lysates, to assess the representation of cell type specific proteins in the quantified

¹ Proteomic services, Universitätsmedizin Göttingen (UMG), Göttingen.

proteome. We found that 1565 proteins were not cell-type specific. From the remaining 524 proteins, 318 proteins were neuron markers, 104 were astrocyte markers, 61 were microglia markers, and 41 were oligodendrocyte markers (**Figure 3**).

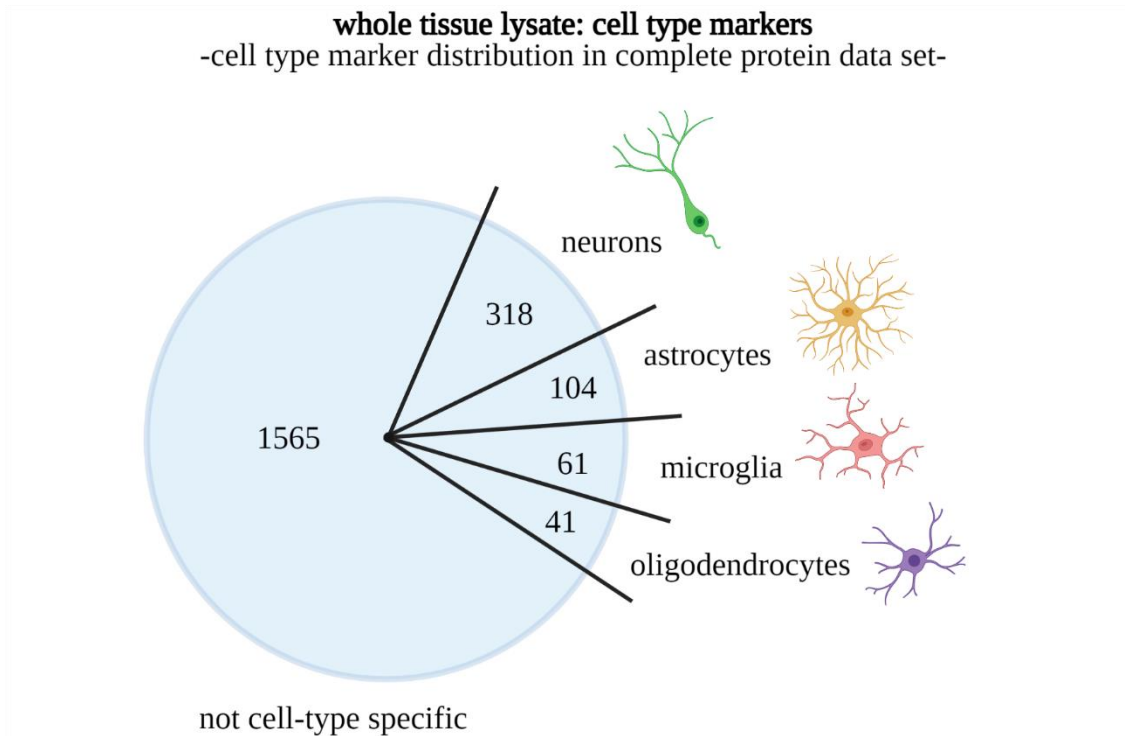


Figure 3. Cell type specific markers mapped onto proteins from whole tissue samples. Total cell type markers mapped onto 2089 unique whole lysate proteins with distribution of DE proteins.

The proteomic data set was then analysed by Hannes Wartmann², to establish differential expression (DE) in PD samples compared to CTR samples, using the limma R package, applying the eBayes function for differential expression and a Benjamini-Hochberg (BH) correction for multiple testing. The differential analysis, considering BH adjusted p-values <0.05, yielded a total of 55 proteins that were identified as significantly differentially expressed in the hippocampal samples of the PD patients (**Figure 4A; Table 4**). From the 55 DE proteins, 37 were more abundant in PD compared to CTRs, while 18 had significantly lower abundance in PD compared to CTRs (**Figure 4B**).

² Research group of Prof. S. Bonn, Universitätsklinikum Hamburg-Eppendorf (UKE), Hamburg.

3. Results

A

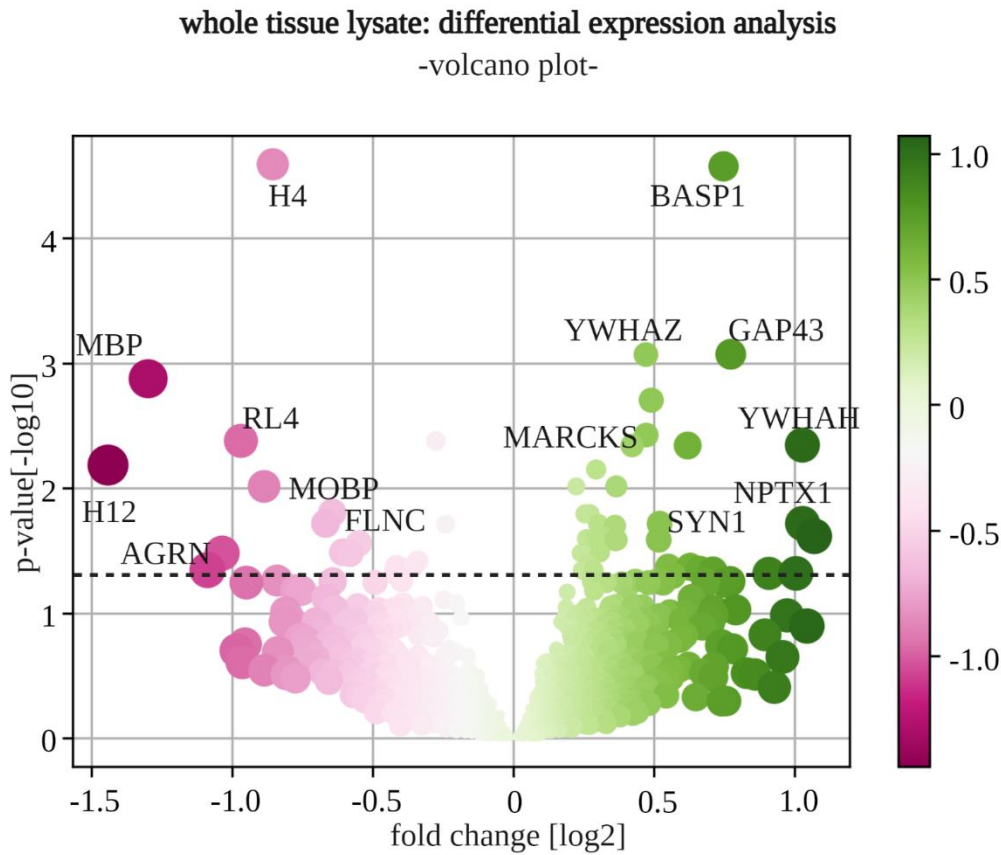


Figure 4. Differential expression analysis of proteins from whole tissue lysate samples. **A)** Volcano plot showing all identified proteins. P-values $[-\log_{10}]$ are shown in the y-axis, fold change values $[\log_2]$ are shown in the x-axis. Colour code shows protein abundance in PD compared to CTR, with lower abundance in PD in magenta tones and higher abundance in PD in green tones. Circumference of protein dots correlates to fold change. Dotted line at p-value 0.05. Proteins above dotted line are considered significantly differentially abundant in PD vs. CTR. **B)** Overview scheme of all identified proteins from whole tissue lysate samples as well as differential expression analysis. Green arrows show increased abundance in PD, magenta arrows show decreased abundance in PD.

3.1 DE of hippocampal lysate samples

#	gene	uniProt accession	fold change [log]	adjusted p-Value
1	H4C1	P62805	-0.8542	2.56E-05
2	BASP1	P80723	0.7486	2.66E-05
3	GAP43	P17677	0.7742	8.49E-04
4	YWHAZ	P63104	0.4727	8.53E-04
5	MBP	P02686	-1.2974	1.33E-03
6	YWHAH	Q04917	0.4913	1.98E-03
7	MARCKS	P29966	0.4737	3.76E-03
8	RPL4	P36578	-0.9675	4.18E-03
9	ST13P4	Q8IZP2	-0.2741	4.18E-03
10	LY6H	O94772	1.0289	4.52E-03
11	NPTX1	Q15818	0.6210	4.56E-03
12	PEA15	Q15121	0.4234	4.56E-03
13	H1-2	P16403	-1.4402	6.54E-03
14	CCT2	P78371	0.2954	7.10E-03
15	MDH2	P40926	0.3672	9.70E-03
16	MOBP	Q13875	-0.8852	9.70E-03
17	PPP2R1A	P30153	0.2250	9.70E-03
18	FLNC	Q14315	-0.6429	1.57E-02
19	YWHAQ	P27348	0.2729	1.61E-02
20	RAN	J3KQE5	0.2554	1.61E-02
21	GLIPR2	Q9H4G4	-0.6668	1.92E-02
22	ACYPI	G3V2U7	1.0296	1.92E-02
23	SYN1	P17600	0.5211	1.92E-02
24	CORO1A	P31146	0.3033	1.94E-02
25	BSG	P35613	-0.2397	1.94E-02
26	CAPZA2	P47755	0.3628	2.00E-02
27	NUTF2	P61970	1.0710	2.43E-02
28	PEBP1	P30086	0.3205	2.43E-02
29	ALDOA	P04075	0.3089	2.43E-02
30	ATP6V1B2	P21281	0.2609	2.54E-02
31	ATP6V1H	Q9UI12	0.2920	2.60E-02
32	NIPSNAP1	Q9BPW8	0.5180	2.60E-02
33	OXCT1	P55809	0.3681	2.60E-02
34	CEND1	Q8N111	0.3090	2.60E-02
35	PTPRZ1	P23471	0.3637	2.61E-02
36	TST	Q16762	-0.5480	2.76E-02
37	GNAO1	P09471	0.3085	3.26E-02
38	TF	P02787	-0.6053	3.26E-02
39	HSPA8	P11142	0.2416	3.32E-02
40	RPS9	A0A024R4M0	-1.0344	3.32E-02
41	CPVL	H7C0X5	-0.5797	3.34E-02
42	MYADM	Q96S97	-0.3390	3.85E-02
43	BCAN	Q96GW7	0.2680	4.01E-02
44	FLOT2	J3QLD9	0.5522	4.27E-02
45	SLC1A4	P43007	0.6296	4.27E-02

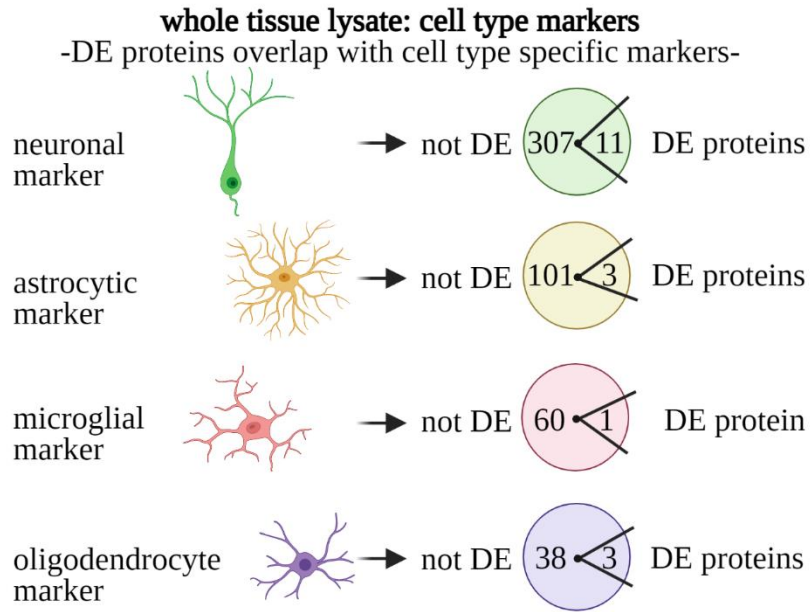
3. Results

46	SLC12A2	P55011	-0.4140	4.27E-02
47	DPYSL5	Q9BPU6	-0.3565	4.28E-02
48	AGRN	O00468	-1.0865	4.54E-02
49	CRIP2	H0YFA4	0.6643	4.54E-02
50	TUBB	P07437	0.2456	4.56E-02
51	TUBB3	Q13509	0.2869	4.56E-02
52	CDH13	P55290	0.7105	4.63E-02
53	RPS16	M0R210	-0.4194	4.80E-02
54	NECAB2	Q7Z6G3	0.9099	4.82E-02
55	IGHA1	A0A286YEY1	1.0063	4.82E-02

Table 4. List of all proteins with differential abundance in PD vs. CTR sorted by pValue .

The proteins found to be differently abundant in PD were further compared to the previously described list of cell-type specific marker proteins. From the 55 DE proteins, 11 were neuron markers, 3 were astrocytic markers, 1 was a microglia marker and 3 were oligodendrocyte markers (**Figure 5**).

A



B

whole tissue lysate: cell type markers
 -DE proteins overlap with cell type specific markers-

neurons	astrocytes	microglia	oligodend.	not-cell type specific		
GAP43	BSG	CORO1A	MBP	H4C1	ATP6V1B2	FLNC
LY6H	TST		BCAN	BASP1	ATP6V1H	YWHAQ
SYN1	GLIPR2		SLC12A2	YWHAZ	OXCT1	RAN
NIPSNAP1				YWHAH	PTPRZ1	ACYP1
CEND1				MARCKS	TF	CAPZA2
GNAO1				RPL4	HSPA8	IGHA1
SLC1A4				ST13P4	RPS9	NUTF2
DPYSL5				NPTX1	CPVL	PEBP1
TUBB3				PEA15	MYADM	ALDOA
CDH13				H1-2	FLOT2	NIPSNAP1
NECAB2				CCT2	AGRN	PPP2R1A
				MDH2	CRIP2	RPS16
				MOBP	TUBB	

Figure 5. Cell type specific markers mapped onto DE proteins from whole tissue samples. A) DE proteins overlapping with cell-type specific marker proteins. Colour coded green for astrocytes, yellow for microglia, red for oligodendrocytes and purple for neurons. **B)** List of overlapping DE proteins and the respective cell-type specific category.

3.1.2.2 Functional annotation analysis of DE proteins from the whole tissue lysate samples

As a first characterization step of the identified whole tissue lysate DE proteins, a protein-protein interaction (PPI) network was created using the STRING platform v.11.0b (D. Szklarczyk et al., 2019). The PPI network visualized the interactions between the different DE proteins, based on current literature findings, enabling thus the detection of potentially interesting clusters of highly interactive DE proteins. Considering at first the PPI network of all 55 identified DE proteins, two prominent clusters of high protein interaction were discernible. The first cluster featured amongst others, proteins known to be important for axonal growth cones, such as brain acid soluble protein 1 (BASP1), growth associated protein 43 (GAP43) and myristoylated alanine-rich C-kinase substrate (MARCKS). In addition, the same cluster included synaptic proteins like synapsin 1 (SYN1) and agrin (AGRN).

The second prominent cluster was composed of several isoforms of the signal transduction mediating 14-3-3 protein family, such as 14-3-3 protein eta (YWHAH), 14-3-3 protein theta (YWHAQ) and 14-3-3 protein epsilon (YWHAE). Further, the second cluster of the PPI network included several ribosomal proteins such as the 40S ribosomal protein S16 (RPS16), the 60S ribosomal protein L4 (RPL4) and the 40S ribosomal protein S9 (RPS9) (**Figure 6A**).

A second approach was used for the PPI network construction, by separating the DE proteins based on the found abundance in PD, creating two separate PPI networks of more abundant proteins and less abundant proteins respectively. With an overall higher number of proteins found to be more abundant in PD (37) compared to lower abundance (18), the PPI of higher abundant proteins showed a high interacting network of proteins with high similarity to the overall PPI network. The network shows a very similar distribution with two main clusters, one containing amongst others aforementioned proteins such as 14-3-3 isoforms eta, theta and epsilon and the other encompassing proteins such as BASP1, GAP43 and SYN1. In contrast, PPI networks of proteins found to be lower abundant in PD show less clustering, with mostly ribosomal proteins as well as myelin-related proteins such as myelin basic protein (MBP) and myelin-associated oligodendrocyte basic protein (MOBP) representing interaction clusters in the PPI network (**Figure 6B-C**).

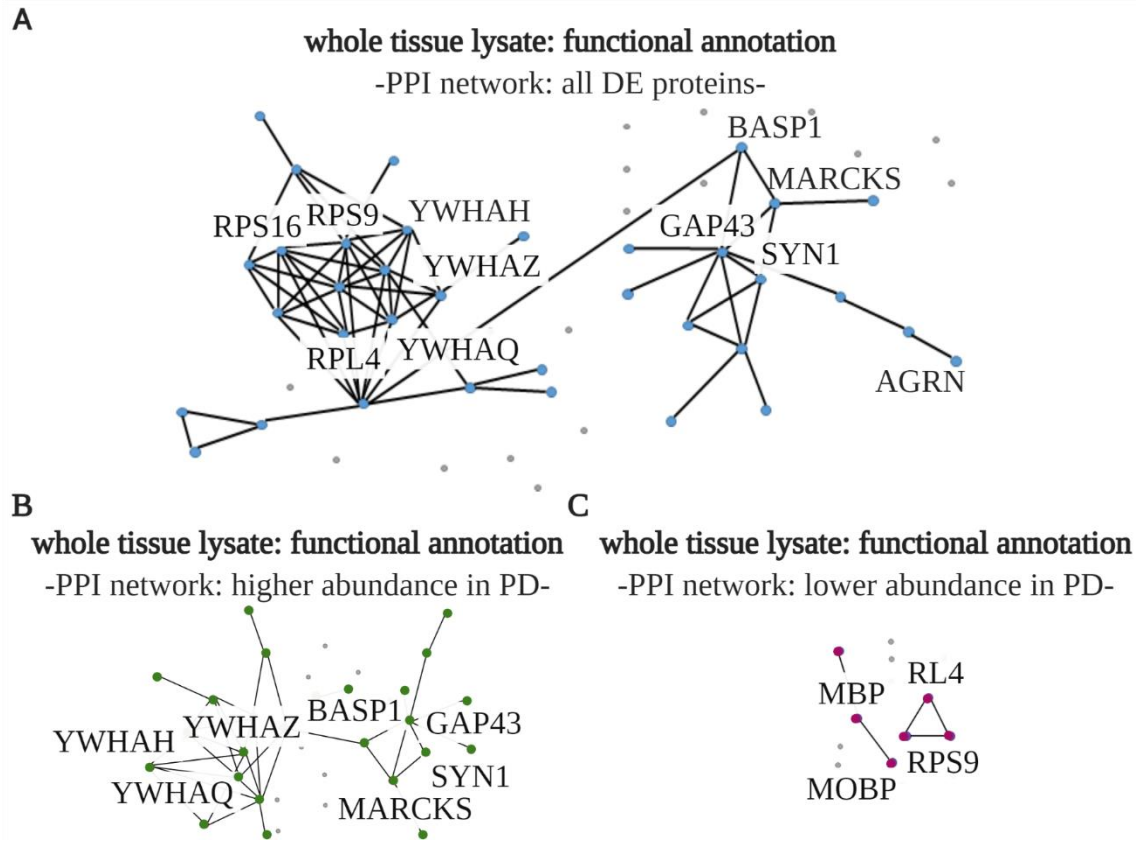


Figure 6. Protein-protein interaction (PPI) networks of differentially expressed proteins. **A)** PPI network of all 55 differentially expressed proteins of the whole tissue lysate samples. **B)** PPI of all 37 proteins found to be more abundant in PD. **C)** PPI of all 18 proteins found to be less abundant in PD. For all panels known interactions are shown with connecting lines. Proteins with at least one interaction are shown in blue for the overall PPI network and in green/magenta in higher or lower abundance PPI networks, respectively. Proteins without known interactions are shown in grey.

In addition to addressing the known interactions between the proteins that show significant alteration in expression levels in PD, the biological relevance of the established DE proteins was assessed via functional annotation analyses using the STRING platform v.11.0b (D. Szklarczyk et al., 2019). Starting with the functional annotation of the overall set of 55 DE proteins, the top 10 gene ontology (GO) terms found to be significantly enriched for *biological processes* included terms related to *localization* and *transport*. In turn, the top 6 terms enriched for *molecular function* range from *binding*, such as *actin binding* and *cytoskeletal protein binding* to *structural constituent of myelin sheath*. Finally, the top 10 GO-terms enriched for *cellular compartment* display terms like *myelin sheath*, *cytoskeleton*, and *neuron projection*, as well as *cell periphery* and *cytoplasm*. (**Figure 7**).

3. Results

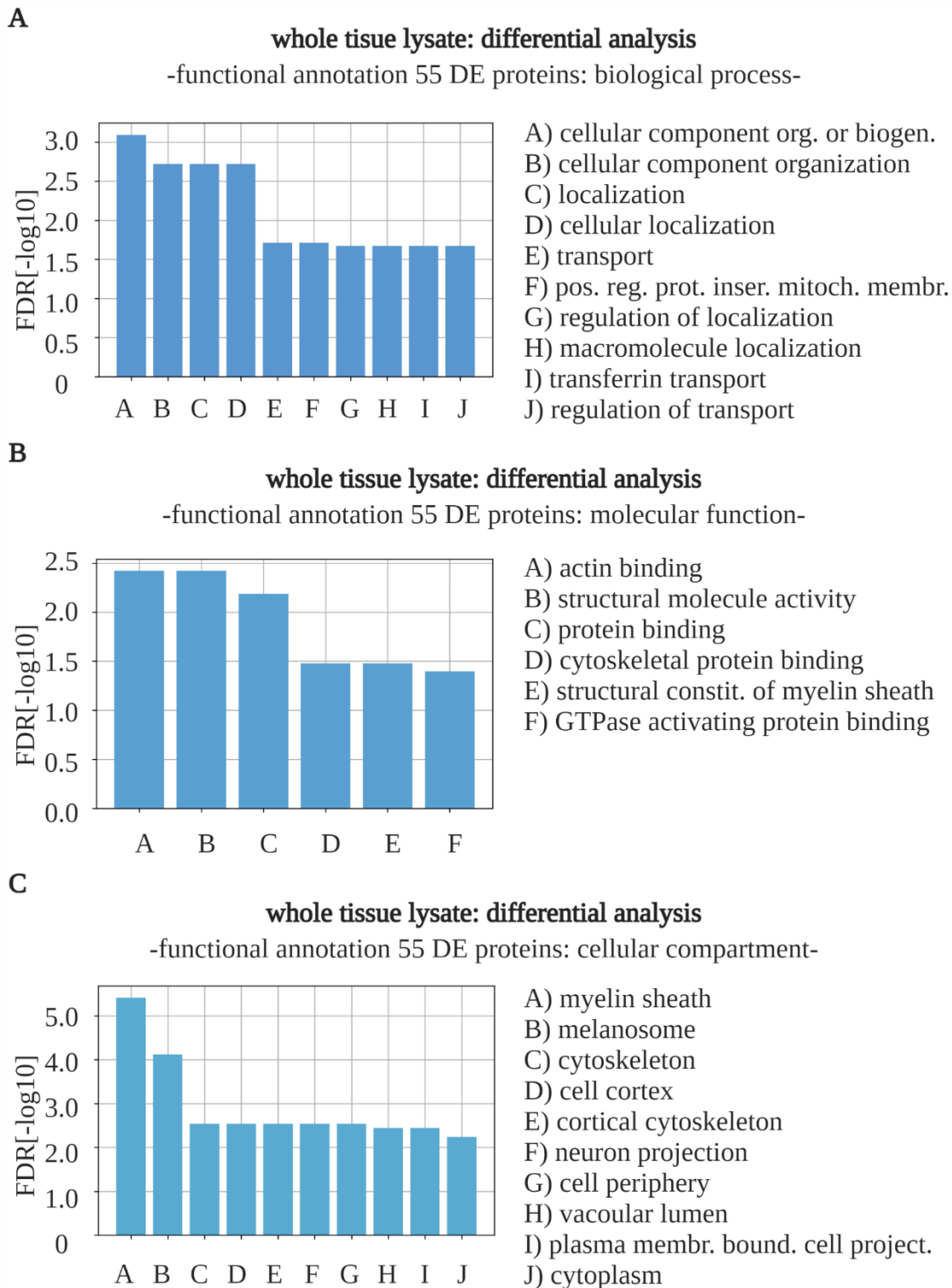


Figure 7. Functional annotation of 55 DE proteins. **A)** Enrichment ratio plot of top 10 gene ontology (GO) terms significantly enriched for *biological process*. **B)** Enrichment ratio plot of top 6 GO terms significantly enriched for *molecular function*. **C)** Enrichment ratio plot of top 10 GO terms significantly enriched for *cellular compartment*. Significance with FDR < 0.05. In all plots FDR [-log10] is shown in y-axis, while individual GO terms are displayed in the x-axis.

A second functional annotation analysis was done, separating the data sets into proteins found more abundantly in PD and proteins found less abundantly in PD. Significantly enriched GO-terms for *biological process* showed mostly an overlap with the functional annotation analysis of the non-divided proteins in terms regarding *transport* and *localization*. Similar to the PPI networks, the functional analysis of the proteins more abundant in PD showed higher similarity to the undivided analysis. In turn, *biological processes* significantly enriched in the functional annotation analysis of proteins less abundant in PD showed additional terms related to *translation* (**Table 5**).

abundance in PD	GO term	FDR [-log10]
higher	regulation of transport	1,9355
higher	regulation of cellular localization	1,9355
higher	pos. reg. of protein insertion into mitochondrial membrane	1,9355
higher	pos. reg. of cellular protein localization	1,9355
higher	pos. reg. of protein localization to membrane	1,9355
higher	pos. reg. of apoptotic signalling pathway	1,9355
higher	plasma membrane bounded cell projection organization	1,9318
higher	positive regulation establishment protein localization	1,9318
higher	cellular component organization	1,7545
higher	regulation of protein localization	1,7545
lower	protein localization to membrane	3,2218
lower	nuclear-transcribed mRNA catabolic process	1,8601
lower	SRP-dependent co-translational protein targeting to membrane	1,8601
lower	negative regulation heterotypic cell-cell adhesion	1,8601
lower	translational initiation	1,8268
lower	cellular component organization or biogenesis	1,8268
lower	macromolecule localization	1,8125
lower	cellular nitrogen compound catabolic process	1,6289
lower	protein localization	1,5331
lower	macromolecule catabolic process	1,4724

Table 5. Functional annotation of the top 10 *biological process* of DE proteins from whole tissue lysate samples, divided into data sets of higher and lower abundance in PD.

Similarly, there was an overlap in enriched terms for *molecular functions*, with the higher abundance protein displaying several terms related to *binding* and lower abundance proteins including *structural* terms. Additionally, the functional annotation of higher abundance proteins added *ATPase* and *GTPase activity* to the significantly enriched *molecular functions* (**Table 6**).

3. Results

abundance in PD	GO Term	FDR [-log10]
higher	actin binding	1,6162
higher	protein binding	1,6162
higher	hydrolase activity	1,6162
higher	nucleoside-triphosphatase activity	1,6162
higher	GTPase activating protein binding	1,6162
higher	proton-transporting ATPase activity	1,6162
higher	proton-exporting ATPase activity	1,6073
higher	identical protein binding	1,6073
higher	carbohydrate derivative binding	1,5591
higher	GTPase activity	1,5114
lower	structural molecule activity	2,7212
lower	structural constituent of myelin sheath	2,5528
lower	structural constituent of ribosome	1,9666
lower	rRNA binding	1,4123

Table 6. Functional annotation of top 10 molecular functions of DE proteins from whole tissue lysate samples, divided into data sets of higher and lower abundance in PD.

Finally, the functional annotation for *cellular compartments* of the divided DE protein data sets yielded significantly enriched terms only for the proteins found in higher quantities in PD, showing a high overlap of terms with the *cellular compartments* found for the overall proteins (Table 7).

abundance in PD	GO Term	FDR [-log10]
higher	myelin sheath	3,9208
higher	melanosome	3,6778
higher	neuron projection	2,7447
higher	cytoskeleton	2,6383
higher	plasma membrane bounded cell projection	2,3979
higher	proton-transporting V-type ATPase	2,2596
higher	cytoplasm	2,2441
higher	anchored component of membrane	2,2441
higher	cell periphery	2,2366
higher	vacuolar lumen	2,2147

Table 7. Functional annotation of top 10 cellular compartments of DE proteins from whole tissue lysate samples, divided into data sets of higher abundance in PD.

3.1.2.3 WGCNA network construction and functional annotation analysis of protein modules in the whole tissue lysate samples

A second approach towards the characterization of the proteomic data set of the whole tissue lysates was a network analysis approach. In contrast to reducing the amount of data by only considering proteins found to be significantly differentially expressed in PD, the second approach utilized the entire data set of identified and quantified proteins in the whole tissue lysate samples.

The goal of this approach was to downscale the entire proteomic data set into several smaller sub-groups of proteins. The assignment of proteins into these sub-groups or modules, was done by constructing a co-expression network, correlating the expression patterns of all 2089 proteins. In terms of analysed data, for each protein the expression pattern represents all protein expression levels measured across the entire sample cohort (both PD and CTRs), thus having 30 individual values of protein abundance for each of the 2089 proteins identified. This set of values per protein was in turn correlated in a pairwise fashion to each of the remaining 2088 proteins, creating a co-expression network. In turn, individual modules were identified by combining all proteins sharing highly similar expression patterns.

The construction of the co-expression network, as well as subsequent rescaling of the data set into modules of proteins with highly correlated expression patterns was conducted via the R package WGCNA, following the corresponding manual and tutorial (Langfelder and Horvath, 2008) (**Figure 8A**). The network rescaling yielded 10 modules of correlated proteins, comprising 70% of the data set, with 1459 out of the 2089 proteins being assignable to a specific module based on their expression patterns. The remaining 30% of proteins showed no significant correlation to any of the established modules. Protein amounts per module averaged 149 proteins, ranging from 361 in module W01 to 30 in module W10 (**Figure 8B**).

3. Results

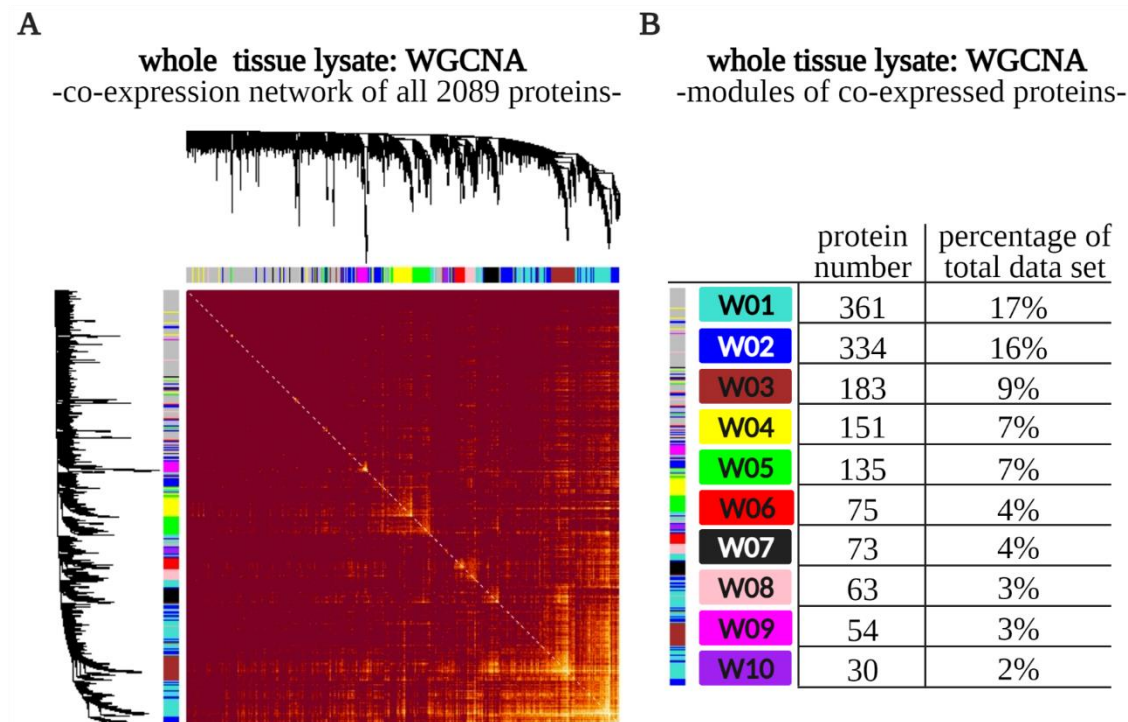


Figure 8. Network analysis based on co-expression of all 2089 identified proteins from the whole tissue lysates. A) Heatmap plot of adjacency. Rows and columns correspond to single proteins, light colours represent low adjacency calculated from pair-wise correlations. Darker colours represent higher adjacency. Protein dendrograms and module assignment shown on top and to the left. **B)** Amount of assigned proteins per module, as well as percentage of the entire 2089 protein data set.

Next, the 55 previously identified differentially abundant proteins were tracked in the 10 modules, with more than 60% being distributed in modules W01 (20 DE proteins) and W03 (14 DE proteins). Further, 11% were assigned to W09, while another 11% were distributed between W02, W05, W07 and W08. The final 16% were proteins that had not been assigned to any particular module, thus having no strong similarities in expression patterns (**Figure 9**).

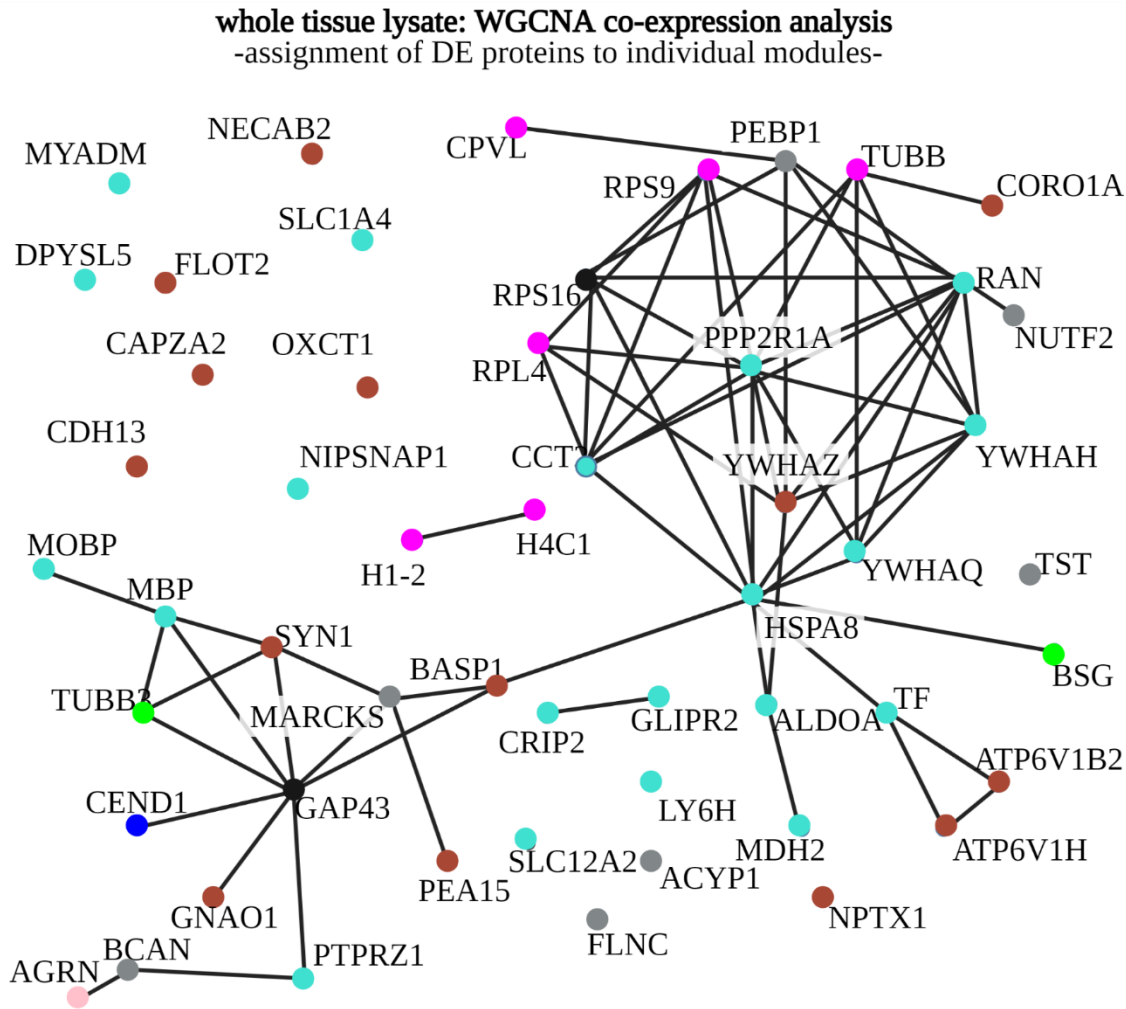


Figure 9. Location of the 55 DE proteins of the whole tissue sample cohort in the individual WGCNA modules. PPI of 55 DE proteins with color-coded designation of the module in which the individual proteins can be found. Turquoise = W01; Blue= W02; Brown= W03; green= W05; black= W07; pink= W08 and magenta= W09. Proteins not assigned to a specific module are shown in grey.

Subsequently, the complete data set of proteins from each module were further analysed for biological relevance by means of functional annotation. The data set of proteins from each module were analysed using the WEB-based Gene SeT AnaLysis Toolkit (WebGestalt, Y. Liao et al., 2019), assessing *biological processes*, *molecular function* and *cellular compartments*. Based on a non redundant analysis of significant enrichment of categories as well as employing the R package *apcluster* available in the online WebGestalt platform, significantly enriched GO-terms were obtained for each module for the aforementioned categories (**Table 8-Table 10**).

3. Results

module	GO term	description <i>biological process</i>	FDR[-log10]
W01	GO:0009141	nucleoside triphosphate metabolic process	7.1703
W01	GO:0072350	tricarboxylic acid metabolic process	6.2204
W01	GO:0046390	ribose phosphate biosynthetic process	6.0033
W02	GO:0072350	tricarboxylic acid metabolic process	7.5735
W02	GO:0006732	coenzyme metabolic process	5.8181
W02	GO:0009141	nucleoside triphosphate metabolic process	4.9763
W03	GO:0099504	synaptic vesicle cycle	> 16
W03	GO:0072512	trivalent inorganic cation transport	7.8849
W04	GO:0006730	one-carbon metabolic process	0.8187
W04	GO:0051648	vesicle localization	0.6615
W04	GO:0002446	neutrophil mediated immunity	0.5248
W04	GO:0097193	intrinsic apoptotic signalling pathway	0.4515
W05	GO:0002446	neutrophil mediated immunity	3.1887
W05	GO:0031532	actin cytoskeleton reorganization	2.7842
W05	GO:0007015	actin filament organization	2.2149
W06	GO:0002446	neutrophil mediated immunity	6.1904
W06	GO:0006081	neutrophil mediated immunity	4.8151
W06	GO:0044282	small molecule catabolic process	3.1626
W06	GO:0072524	pyridine-containing metabolic process	2.1200
W07	GO:0099504	synaptic vesicle cycle	3.9335
W07	GO:0140029	exocytic process	2.2375
W07	GO:0050817	coagulation	2.0592
W07	GO:0072593	reactive oxygen species metabolic process	1.9869
W07	GO:0043270	positive regulation of ion transport	1.3734
W08	GO:0006520	cellular amino acid metabolic process	2.1777
W08	GO:0070972	protein localization to endoplasmic reticulum	1.6435
W09	GO:0009112	nucleobase metabolic process	1.6611
W09	GO:0034113	heterotypic cell-cell adhesion	1.3175
W10	GO:0009141	nucleoside triphosphate metabolic process	0.8972
W10	GO:0048193	golgi vesicle transport	0.7585
W10	GO:0046390	ribose phosphate biosynthetic process	0.6756
W10	GO:0010498	proteasomal protein catabolic process	0.6756
W10	GO:0002446	neutrophil mediated immunity	0.6522
W10	GO:0051602	response to electrical stimulus	0.6294

Table 8. Functional annotation of *biological processes* for each module of co-expressed proteins from the whole tissue lysate sample.

module	GO term	description <i>molecular function</i>	FDR[-log10]
W02	GO:0050839	cell adhesion molecule binding	2.9556
W03	GO:0030276	clathrin binding	7.2906
W04	GO:0001882	nucleoside binding	0.8953
W05	GO:0001882	nucleoside binding	5.3335
W05	GO:0042578	phosphoric ester hydrolase activity	2.3483
W06	GO:0050839	cell adhesion molecule binding	2.8094
W08	GO:0016790	thiolester hydrolase activity	2.4822
W09	GO:0005201	extracellular matrix structural constituent	10.5019

Table 9. Functional annotation of *molecular function* for each module of co-expressed proteins from the whole tissue lysate sample.

module	GO term	description <i>cellular compartment</i>	FDR[-log10]
W01	GO:0043209	myelin sheath	> 16
W02	GO:0044455	mitochondrial membrane part	6.3652
W03	GO:0098978	glutamatergic synapse	> 16
W03	GO:0098984	neuron to neuron synapse	11.5568
W04	GO:0099568	cytoplasmic region	0.4515
W05	GO:0005874	microtubule	3.5631
W08	GO:0005775	vacuolar lumen	1.3488
W08	GO:0005743	mitochondrial inner membrane	1.0331
W09	GO:0005796	golgi lumen	1.6158
W10	GO:0070469	respiratory chain	0.7585

Table 10. Functional annotation of *cellular component* for each module of co-expressed proteins from the whole tissue lysate sample.

From the obtained terms, a summary was constructed manually, considering the most represented terminologies found in the functional annotation analysis. These terms were then combined into single representative terms, which best described the majority of individual enriched GO-terms and their biological relevance (**Figure 10**).

3. Results

whole tissue lysate: WGCNA co-expression analysis -biological relevance of modules-


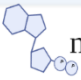








module		description	DE proteins
W01		mitochondria	MPB; YWHAH; LY6H; CCT2; MDH2; MOBP; PPP2R1A; YWHAQ; RAN; GLIPR2; ALDOA; NIPSNAP; PTPRZ1; TF; HSPA8; MYADM; SLC1A4; SLC12A2; DPYSL5; CRIP2
W02		metabolite precursor metabolism	CEND1
W03		synapse	BASP1; YWHAZ; NPTX1; PEA15; SYN1; CORO1A; CAPZA2; ATP6V1B2; ATP6V1H; OXCT1; GANO1; FLOT2; CDH13; NECAB2
W04		intrinsic apoptotic signaling	none
W05		cytoskeleton	BSG; TUBB3
W06		white blood cells	none
W07		synapse	GAP43; RPS16
W08		translation initiation	AGRN
W09		ribosome	H4C1; RPL4; H1; RPS9; CPVL; TUBB
W10		complex I	H4C1; RPL4; H1; RPS9; CPVL; TUBB

Figure 10 Summarized biological relevance of individual modules of the whole tissue lysate reduced data set. Individual manual characterization of biological relevance is annotated per module. DE proteins present in the respective module are listed.

The characterization of the biological relevance of the identified modules was further used to narrow down the available options for the selection of a potential target protein for further studies. The selection relied on a targeted approach based on the focus of the present study: a possible synapto-axonal dysfunction in the PD hippocampus.

In this regard, the functional annotation analysis of proteins in module W03 was particularly interesting. The analysis yielded significant enrichment of synaptic GO terms, presenting *biological processes* such as *synaptic vesicle cycle*, *vesicle-mediated transport in synapse* and *synapse organization* as well as terms from the category of *cellular compartment* such as *presynapse*, *synaptic membrane* and *postsynaptic specialization* (**Figure 11**). Furthermore, amongst the 183 proteins comprising the W03 module, 14 proteins had been quantified with significantly altered abundance in PD, amongst which were proteins such as NPTX1, GAP43, BASP1, SYN1 and PEA15.

Finally, the results gathered from the characterization of the whole tissue lysate samples were combined with the known literature to isolate a single protein of interest for further experiments. As such, in line with the special focus on synaptic dysfunction, the proteins of module W03 that had been determined as being differentially abundant in PD, were taken into consideration as possible target proteins. From these, NPTX1 was profiled as a protein of special interest based on the known links to other neurodegenerative diseases. In the context of AD, NPTX1 had been proposed as early biomarker with an increase of NPTX1 levels being correlated to the progression from MCI to AD dementia (Duits et al., 2018). In addition, NPTX1 had been previously linked to the synaptic compartment, negatively modulating synapse density and synapse numbers as well as negatively affecting the expression levels of synaptic proteins such as PSD95 and synaptophysin (Figueiro-Silva et al., 2015).

3. Results

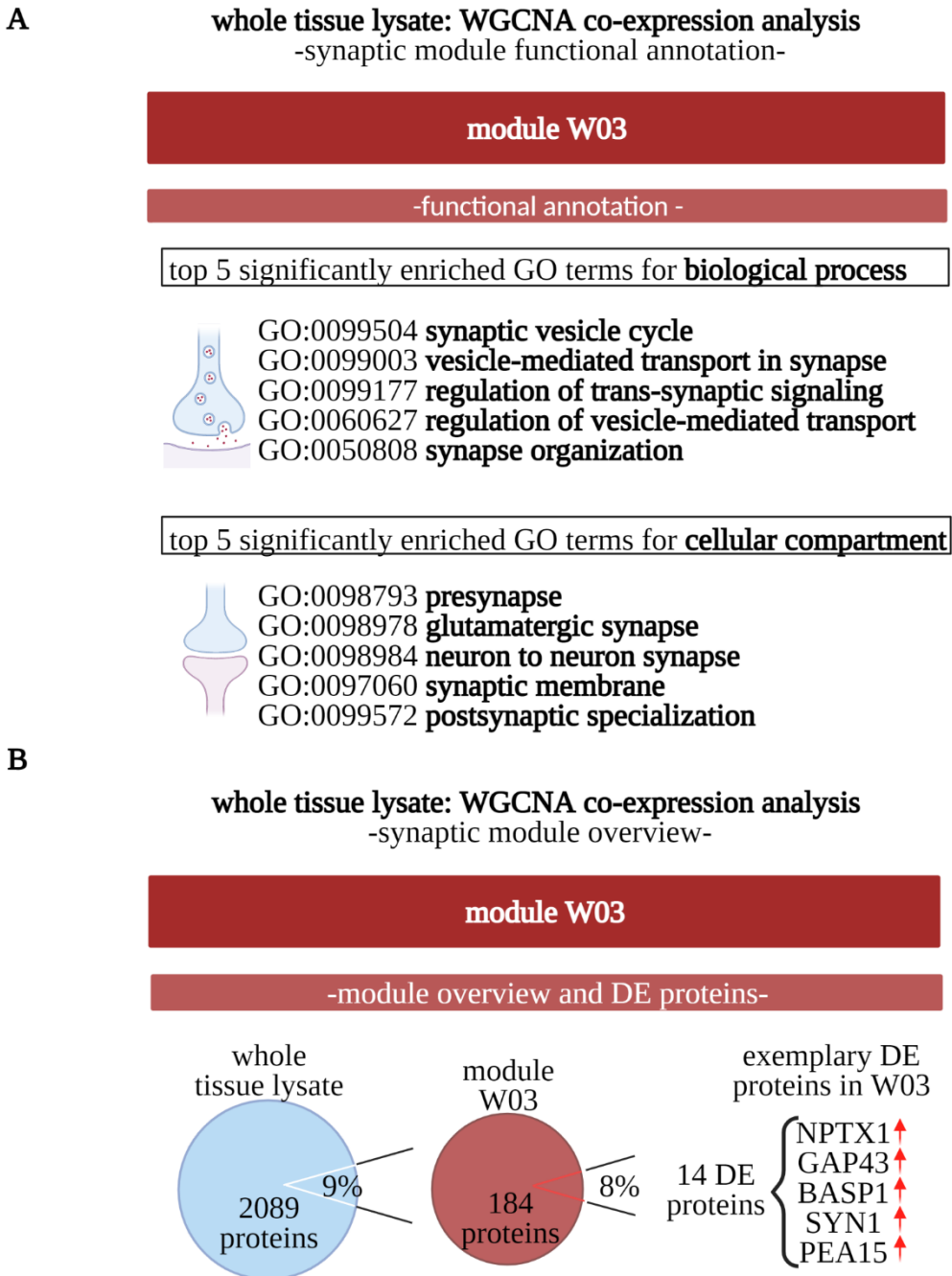


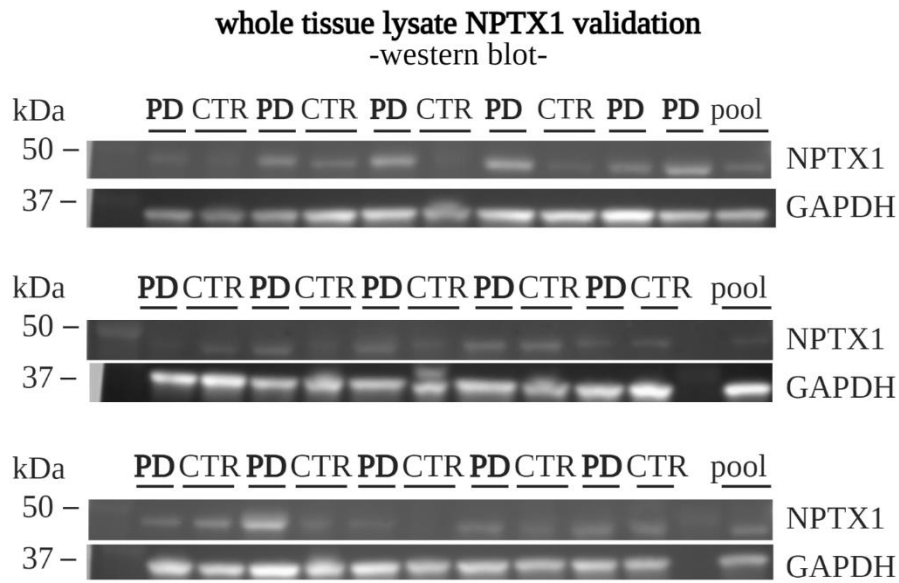
Figure 11. Synaptic module W03 overview. **A)** Overview of top 5 enriched GO terms from functional annotation analysis of categories *biological process* and *cellular compartment*. **B)** Scheme showing number of proteins assigned to module W03 and differentially expressed proteins. Red arrows signify higher abundance in PD.

3.1.2.4 Validation of differentially expressed NPTX1 via western blots

Increased abundance of NPTX1 was validated in a mass spectrometry independent way, via western blots. Lysis samples obtained from the same whole tissue lysates used for the mass spectrometry analysis were used for the validation. The 30 samples were loaded onto 3 gels for electrophoresis, alternating PD and CTRs as well as including a pooled sample containing equal amounts of most samples, PD and CTR alike. The obtained intensities of the NPTX1 antibody were normalized both to the housekeeping protein glyceraldehyde-3-phosphate dehydrogenase (GAPDH) to control for variation in loading amounts and to the pool to account for multiple membranes and minimize individual effects on signal development, enabling a comparison of NPTX1 signal intensity ratios for all membranes. From the 16 PD samples and 14 CTRs, 1 PD and 1 CTR sample displayed abnormally strong NPTX1 expression levels compared to the range from the rest of the cohort, being determined as outliers, and left out of the final quantification. The quantification of the remaining samples (n = 15 PD and n = 13 CTRs), NPTX1 was shown to be significantly more abundant in PD samples, compared to the CTRs (**Figure 12**).

3. Results

A



B

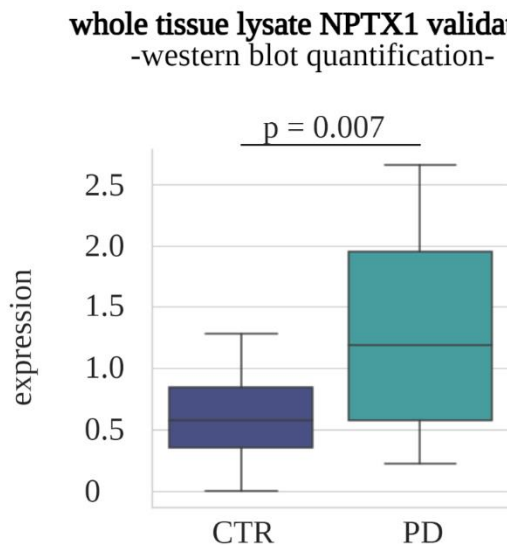


Figure 12. Whole tissue lysate validation of NPTX1 differential expression via western blot. A) NPTX1 and housekeeping gene GAPDH antibody signals of all patients from the whole tissue lysate cohort divided into three membranes. Pooled samples were loaded onto each gel as means of comparison between membranes. **B)** Normalized NPTX1 signal of PD and CTR.

3.1.2.5 Differential protein expression over time in the hippocampus and cerebellum of a transgenic mouse model of PD

Finally, a transgenic PD mouse model (B6;C3-Tg(Prnp-SNCA*A53T)83Vle/J, short A53T model) was chosen to compare alterations in protein expression that are elicited in mice by expression of mutated alpha-synuclein[A53T] mimicking PD. In the A53T mouse model, animals express the mutated human aSyn protein, with an A53T point mutation. Transgenic mice exhibit PD similar symptoms, such as progressive motor symptoms as well as cognitive dysfunction (Giasson et al., 2002; Paumier et al., 2013).

We assessed the proteomic changes of the hippocampus and the cerebellum in A53T animals, quantifying protein expression levels at two different ages. Samples were gathered from a cohort of 10 homozygous young animals (n= 5 transgenic and n= 5 wild type), which were sacrificed and analysed at 250 days of age. Similarly, samples were obtained from 10 homozygous old animals (n= 5 transgenic and n= 5 wild type) which were sacrificed and analysed at 400 days of age. The tissue used for the proteomic analysis was previously dissected, snap frozen and stored by Lucas Caldi Gomes³ (Caldi Gomes, 2019). Only left hippocampi and left cerebella of each animal were used for the analysis. Samples were handled, lysed, and processed in the same fashion as previously described for the human whole tissue lysate samples, obtaining proteomic data for the differential expression analysis.

A total of 1734 proteins were detected in all samples, with all transgenic animals both 250 days old and 400 days old showing a strong increase of aSyn in the hippocampus and in the cerebellum. In addition to the increase of aSyn in the hippocampus, 13 proteins were found differentially abundant for 250 days old animals. Similarly, 13 proteins were found differentially expressed in the hippocampus of 400 days old animals (**Figure 13**). For the cerebellar tissue, 9 proteins were found differentially abundant in 250 days old animals, and 9 proteins were found to be significantly altered in 400 days old animals (**Figure 14**).

³ Research group of Prof. P. Lingor, Department of Neurology, Klinikum rechts der Isar, Technical University of Munich, München

3. Results

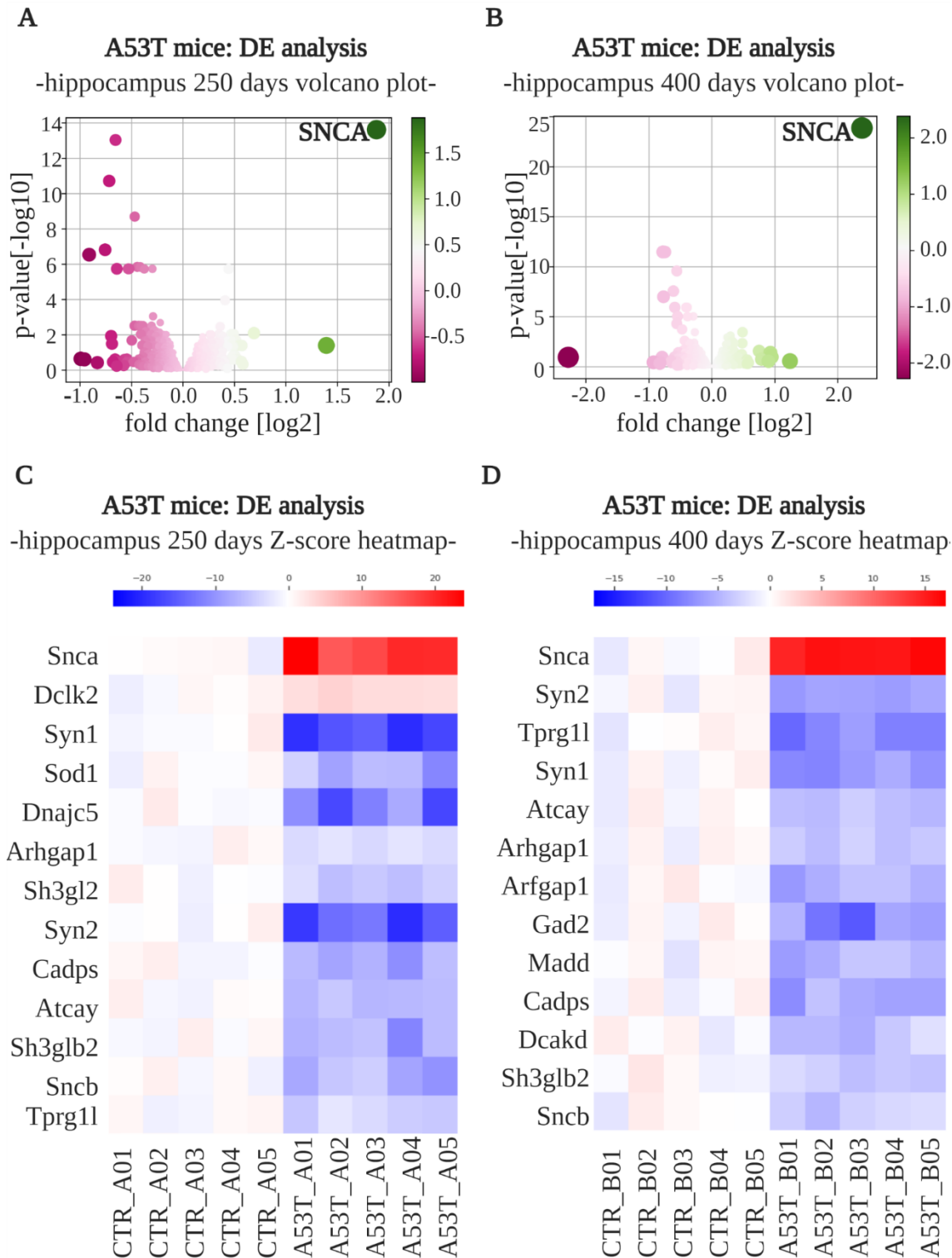


Figure 13. Differential expression analysis of proteins from hippocampus of A53T mice. A-B) Volcano plot showing all identified proteins of animals aged 250 days and 400 days, respectively. P-values $[-\log_{10}]$ are shown on the y-axis, fold change values $[\log_2]$ are shown on the x-axis. Colour code shows protein abundance in PD compared to controls, with lower abundance in transgenic animals in magenta tones and higher abundance in transgenic animals in green tones. Circumference of protein dots correlates to fold change. C-D) Heat map of Z-scores of all DE proteins in the 250 days old hippocampus and 400 days old hippocampus respectively. Z-scores are color-coded with blue colours showing proteins less abundant in transgenic mice and red colours showing higher abundance.

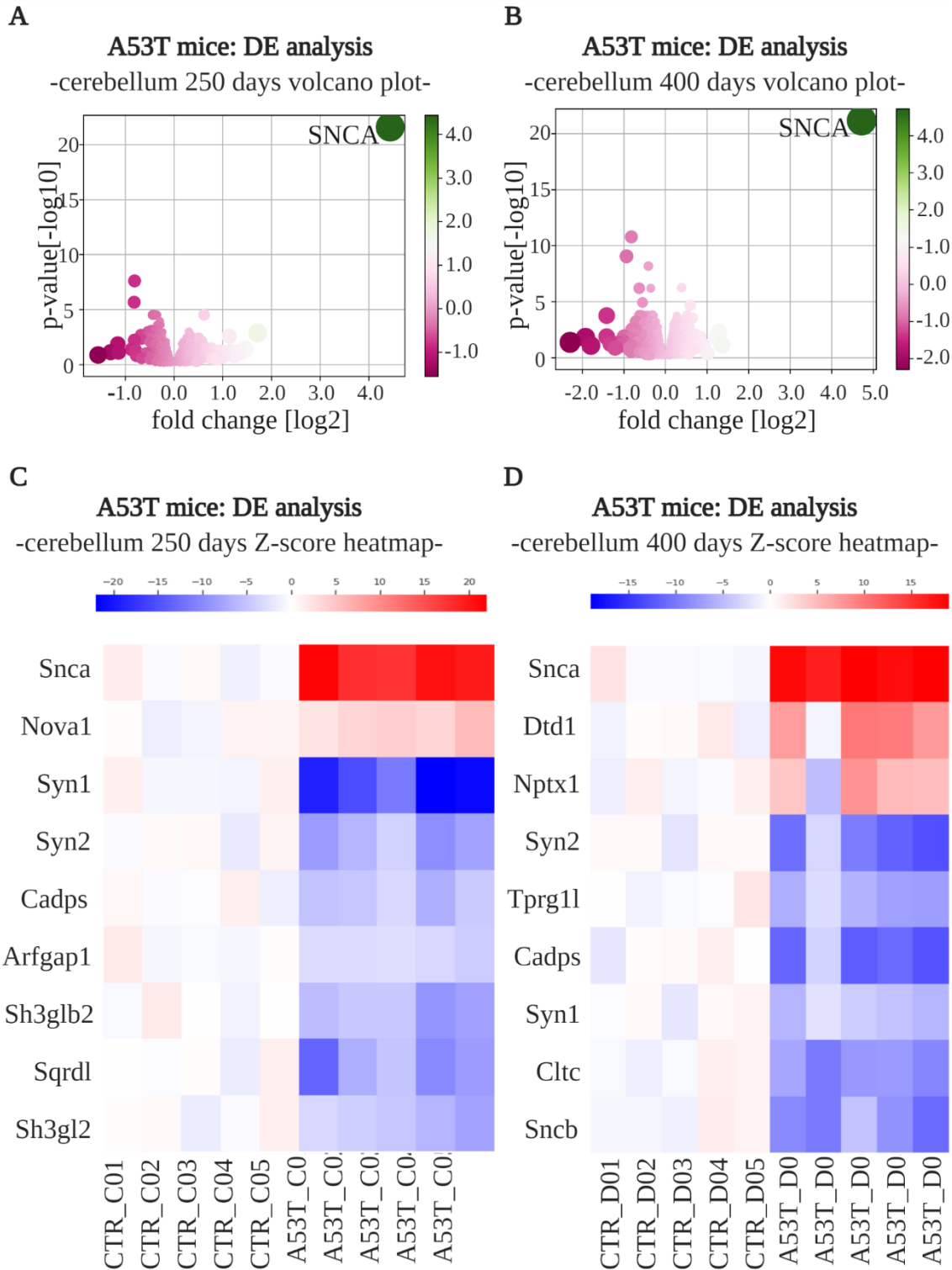


Figure 14. Differential expression analysis of proteins from cerebellum of A53T mice. **A-B)** Volcano plot showing all identified proteins of animals aged 250 days and 400 days, respectively. P-values $[-\log_{10}]$ are shown on the y-axis, fold change values $[\log_2]$ are shown on the x-axis. Colour code shows protein abundance in PD compared to controls, with lower abundance in transgenic animals in magenta tones and higher abundance in transgenic animals in green tones. Circumference of protein dots correlates to fold change. **C-D)** Heat map of Z-scores of all DE proteins in the 250 days old cerebellum and 400 days old cerebellum respectively. Z-scores are color-coded with blue colours showing proteins less abundant in transgenic mice and red colours showing higher abundance.

3. Results

The proteomic data obtained from the A53T mice had an overlap of 1300 proteins with the proteins identified in the human whole tissue lysate samples. In the remaining set of 789 proteins found only in the whole tissue lysates and not in the corresponding homologous mouse proteome in the A53T mice, 15 proteins had been previously determined as DE in PD. From the remaining 40 proteins found differentially expressed in the human hippocampal samples, only Syn1 and NPTX1 were found to be also significantly altered in abundance in the mice proteomic data set.

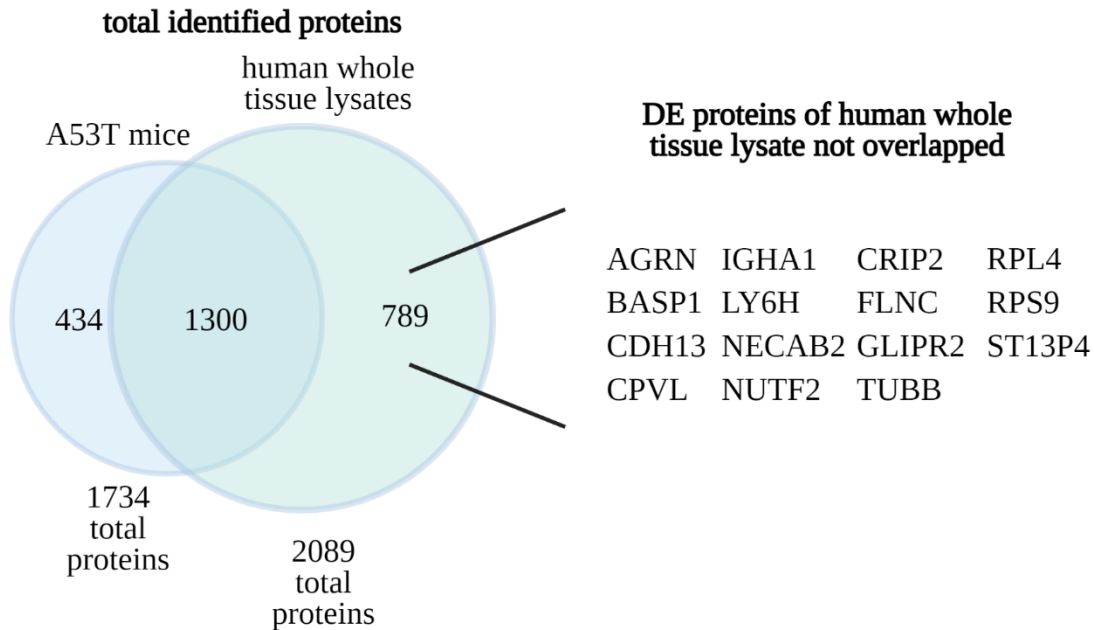
Syn1 was found to be DE at both ages, at 250 and 400 days, showing altered abundance in both the hippocampus and the cerebellum. NPTX1 abundance was found to be significantly altered in 400 day old animals, with a detectable difference measured in the cerebellum of the transgenic animals (**Figure 15**).

Furthermore, the longitudinal development of protein expression levels was tracked for the obtained proteomic data set of the A53T mice. In the hippocampus, young animals (250 days old) showed a total of 13 proteins with significantly altered abundance in the transgenic animals compared to wild type littermates. In the older animals (400 days old), from the initial 13 proteins 9 were still identified, with the remaining 4 being substituted by 4 new proteins. In the cerebellum, young animals presented 9 proteins with significant dysregulation. From these, 4 were identified as significantly dysregulated in the cerebellum of old (400 days old) animals, with the remaining 5 being replaced by 5 new proteins. Overall, alpha-synuclein (SNCA), synapsin 1 (SYN1), synapsin 2 (SYN2) and calcium-dependent secretion activator (CADPS) were found to be DE in both brain regions in 250 days old and 400 days old animals (**Figure 16**).

A

A53T mice: protein quantification

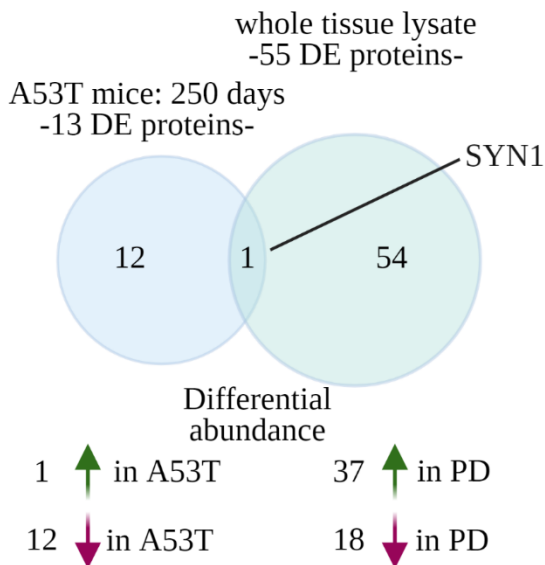
-overview -



B

250 days A53T hippocampus

-overview DE proteins-



C

400 days A53T hippocampus

-overview DE proteins-

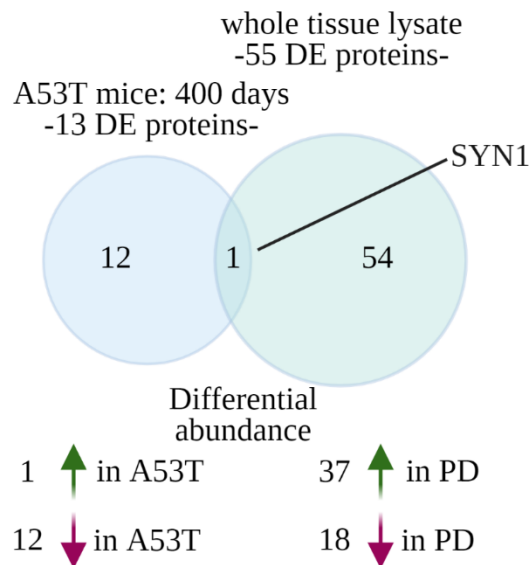


Figure 15. Overview of overlaps of proteomic data sets of A53T mice and whole tissue lysate samples. A) Overlap between all identified proteins from A53T mice in blue and human whole tissue lysate samples in green. B-C) Overlap of DE proteins from hippocampi of 250 days old A53T mice and 400 days old mice in blue and human whole tissue lysates in green. Green arrows show increased abundance in PD/ A53T mice , red arrows symbolise decreased abundance in PD/A53T.

3. Results

A53T mice: DE analysis
-longitudinal changes accross brain regions-

	hippocampus 250d	hippocampus 400d	cerebellum 250d	cerebellum 400d
SNCA	Green	Green	Green	Green
NOVA1			Green	
SYN1	Magenta	Magenta	Magenta	Magenta
SYN2	Magenta	Magenta	Magenta	Magenta
CADPS	Magenta	Magenta	Magenta	Magenta
ARFGAP1			Magenta	
SH3GLB2	Magenta	Magenta	Magenta	
SQRDL			Magenta	
SH3GL2	Magenta		Magenta	
DTD1				Magenta
NPTX1				Green
TPRG1L	Magenta	Magenta		Magenta
CLTC				Magenta
SNCB	Magenta	Magenta		Magenta
DCLK2	Magenta			
SOD1	Magenta			
DNAJC5	Magenta			
ARHGAP1	Magenta	Magenta		
ATCAY	Magenta	Magenta		
GAD2		Magenta		
MADD		Magenta		
DCAKD		Magenta		

Figure 16. Longitudinal progression of DE in hippocampal and cerebellar proteins in A53T mice. Magenta rectangles represent proteins less abundant in transgenic mice, green rectangles represent proteins more abundant in transgenic mice compared to wild-type litter mates.

3.2 Differential abundance of proteins in synaptosomal fractions retrieved from human hippocampal PD samples

3.2.1 Aims

To characterize in more depth the protein changes in the synaptic compartment that already became apparent in the analysis of the whole tissue lysate samples, we additionally enriched synaptic proteins in isolated synaptosomal fractions.

In this chapter, the experiments described, aimed to gain synaptosomal fractions, to identify, quantify and characterize differences in the abundance of enriched synaptic proteins in PD compared to CTR samples. In a first step, synaptosomal fractions of a suitable sub-set of the initial cohort of hippocampal samples were isolated by following a series of centrifugation steps, combined with the fractionation of the samples using a discontinuous Ficoll gradient. In a second step, the isolated synaptosomal fraction was assessed by identifying and quantifying protein expression levels via mass spectrometry. In a third step, a differential expression analysis quantified differential abundance of proteins in the synaptosomal fractions obtained from the PD hippocampus. Finally, a characterization of the biological relevance of the obtained data set provided additional insight, complementing the previous results obtained from the whole tissue lysates.

3.2.2 Results

3.2.2.1 Protein quantification and differential expression analysis of synaptosomal fraction samples

From the initial cohort of hippocampal samples ($n = 16$ PD and $n = 14$ CTRs), only a subset of samples provided adequate amounts of tissue for a successful isolation of the synaptosomal fraction ($n = 6$ PD and $n = 4$ CTRs). The synaptosomal isolation was conducted in collaboration with Ivan Silbern⁴. To this end ~600mg of tissue were fractioned off the fresh frozen hippocampal sample blocks from a third of the initial cohort, both from PD and CTR samples (**Figure 17A**). The fractionated tissue was in turn processed to obtain enriched synaptosomal fractions. In brief, the collected tissue was homogenised in a sucrose buffer and subjected to a series of centrifugal steps to

⁴ Research group of Prof. H. Urlaub, Max Planck Institute for Biophysical Chemistry, Göttingen

3. Results

obtain crude synaptosomes (**Figure 17B**). The crude synaptosomes were in turn loaded on a discontinuous Ficoll gradient and ultracentrifuged, obtaining enriched synaptosomal fraction bands, which were retrieved and further analysed (**Figure 17C**).

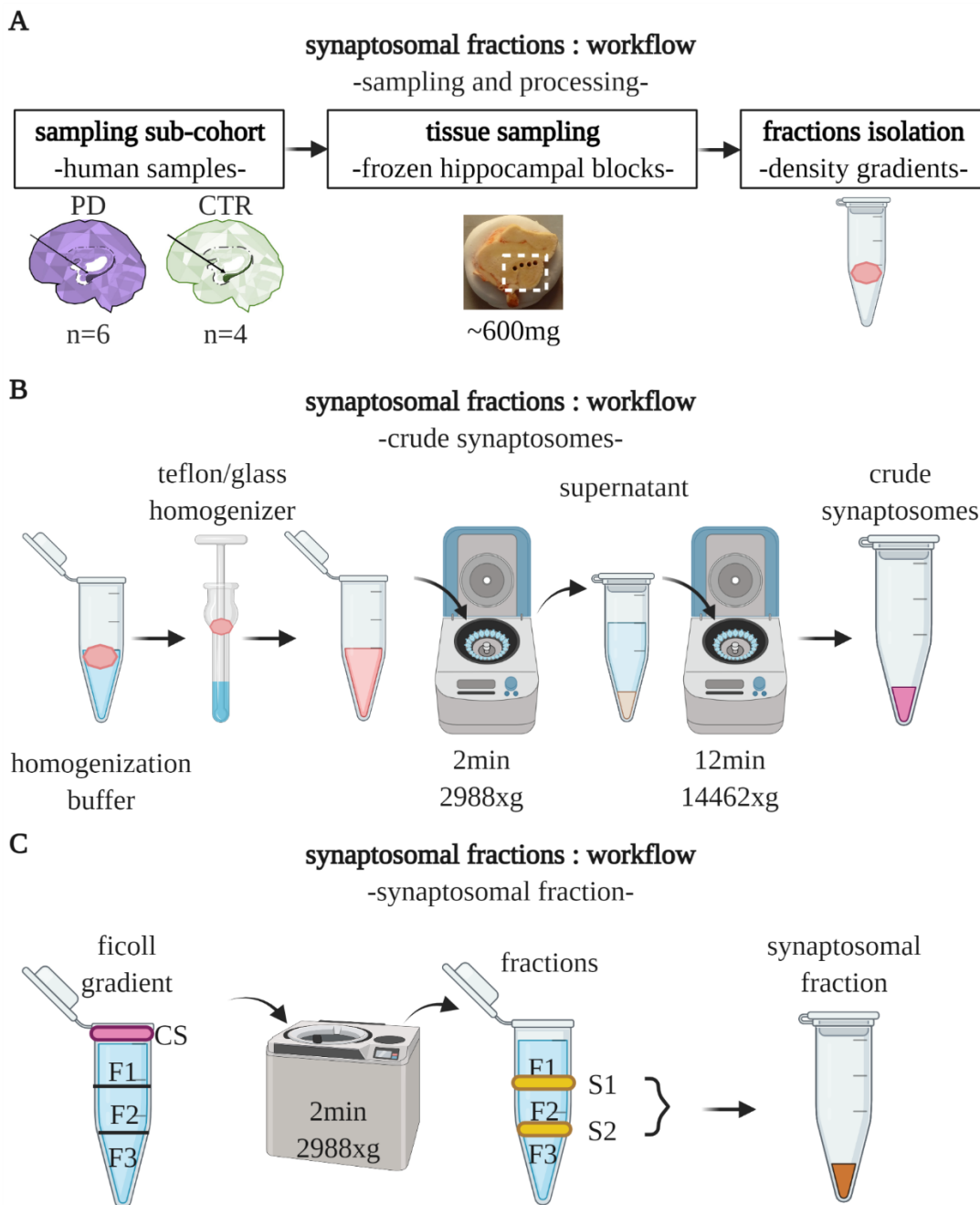


Figure 17. Workflow for sample collection and enrichment of synaptosomal fractions. **A)** Tissue sampling from a suitable sub-cohort of the human fresh frozen hippocampal samples for synaptosomal fraction enrichment. **B)** Crude synaptosome enrichment via centrifugation steps after homogenization. **C)** Synaptosomal fraction enrichment from crude synaptosomes. A Ficoll discontinuous gradient (F1=6%; F2= 9% and F3=13% wt/v Ficoll) was used for density gradient fractioning. Synaptosomal bands between F1-F2 and F2-3 were gathered and pooled for further analyses.

A quality control check for the protocol of synaptosomal fraction enrichment was conducted by quantifying synapsin 1 (SYN1) enrichment in a test run of ~700mg tissue retrieved from two human hippocampal samples not used in the main cohort, with fractionation conducted under the same experimental workflow as done for the main cohort. The enrichment was assessed comparing the levels of SYN1 detected in the initial homogenate of the tissue, the crude synaptosomes and the pooled synaptosomal fractions.

Samples from the preparation steps as well as the individual fractionations on the Ficoll gradient were gathered and run on a electrophoresis gel. SYN1 signals from the crude synaptosomes (CS), each of the synaptosome bands (S1 and S2) as well as the fractions above and below the synaptosome bands (F1 and F3) and the remaining pellet (PE) were compared to the SYN1 signal in the starting homogenate (H0) to address synaptosomal enrichment.

The synaptosomal fractions isolated showed a combined increase of SYN1 signal of ~7,500% in sample 1 compared to H0 (1,319% in S1 and 6,277% in S2). Sample 2 had a combined increase of ~3,850% of SYN1 signal in the synaptosomal fraction (926% in S1 and 3,031% in S2). A strong increase in SYN1 signal was also detected in the F3 fraction and the PE of both samples, with an increase of 9,823% in F3 and 6,088% in the PE for sample 1 and 3,516% in F3 and 3,947% in the PE for sample 2. This increase hinted towards a loss of synaptic proteins in the fractions below S2, however, the yield of protein content in the pooled S1 and S2 fractions, proved to be sufficient for a subsequent proteomic approach (**Figure 18**).

3. Results

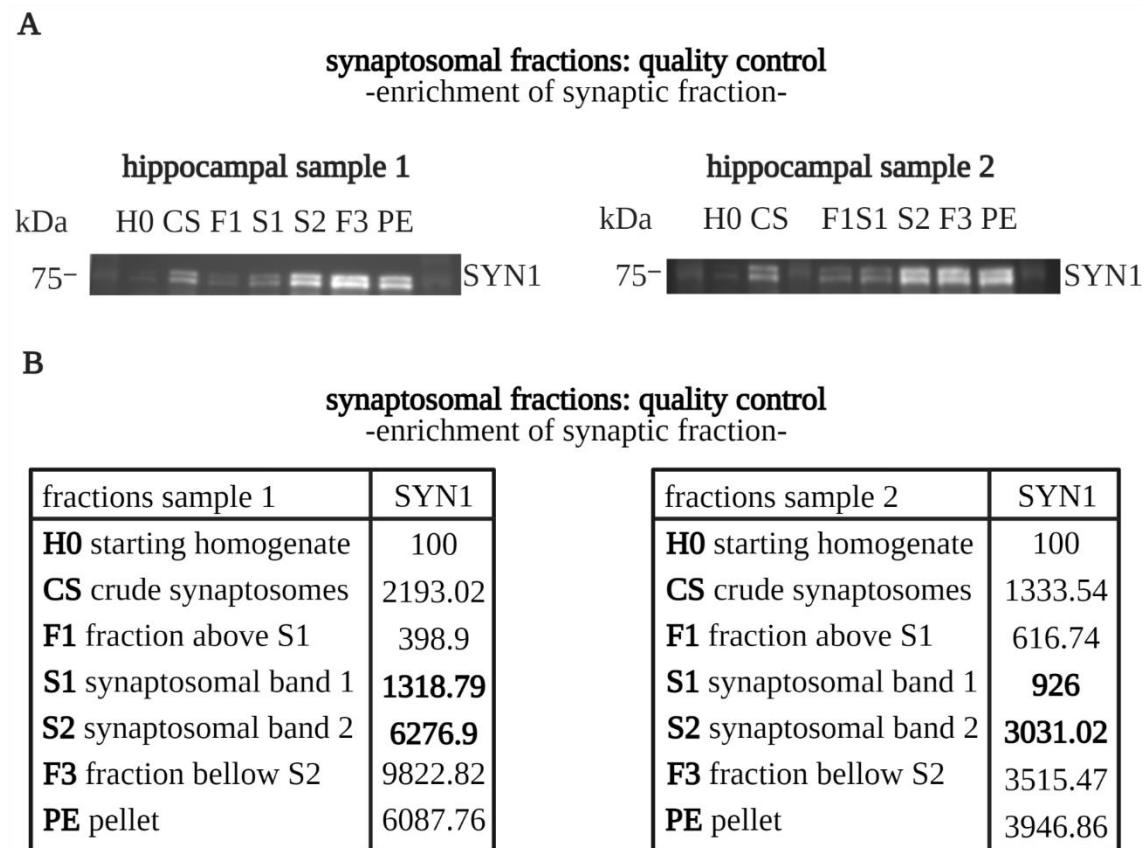


Figure 18. Synaptosomal fraction quality control. **A)** Quality control runs of fractionation of ~700mg of frozen hippocampal tissue not used in the experimental cohort. Samples compared are starting homogenate (H0), crude synaptosomes (CS) and density gradient fractions (F1-3, S1-2) for hippocampal samples 1 and 2. Synaptosomal fraction bands are located at S1 and S2. **B)** Quantification of enrichment normalized to SYN1 content measured in starting homogenates. Equal amounts of total protein from all fractions were loaded into gels.

Further processing of the obtained synaptosomal fractions as well as the quantification of protein expression levels via mass spectrometry and the assessment of differential expression were conducted by Ivan Silbern⁵. In total, 2413 unique proteins were identified and quantified from the synaptosomal fractions.

In comparison to the protein data set of the whole tissue lysate samples, there was an overlap of 2009 proteins, with 80 proteins being unique to the whole tissue lysate samples and 404 proteins uniquely identified in the synaptosomal fraction. In comparison to the DE proteins quantified in the whole tissue lysate samples, only 3 proteins are found in both data sets, (YWHAH, CORO1A and ATP6V1H) (**Figure 19**).

⁵ Research group of Prof. H. Urlaub, Max Planck Institute for Biophysical Chemistry, Göttingen

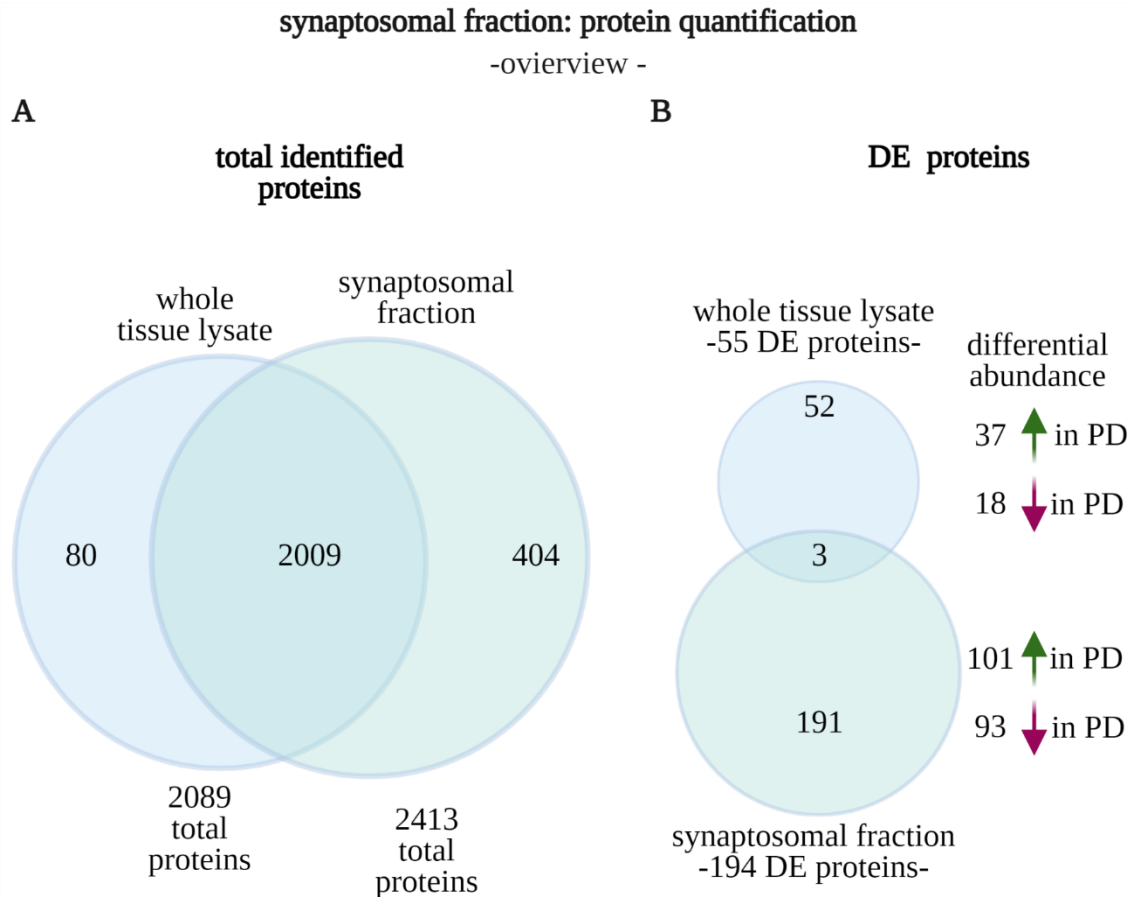


Figure 19. Overview of overlaps in proteomic data sets of human synaptosomal fractions and human whole tissue lysate samples. A) Overlap between all identified proteins from whole tissue lysate samples in blue and synaptosomal fractions in green. B) Overlap of DE proteins from whole tissue lysates in blue and synaptosomal fractions in green. Green arrows show increased abundance in PD, red arrows symbolise decreased abundance in PD.

In terms of differential expression, no significantly altered protein levels were found in the synaptosomal fractions after correcting for multiple testing via BH . The lack of significance may be explained by a smaller number of samples coupled with an inherent inter-patient variability. Heterogeneity is particularly present among the CTRs, likely due to the clinical heterogeneity of control patients and the presence of comorbidities in the age range which is required as control for the PD cohort. In comparison, a higher homogeneity can be seen in the PD samples, which share the same neurodegenerative diagnosis (**Figure 20**).

3. Results

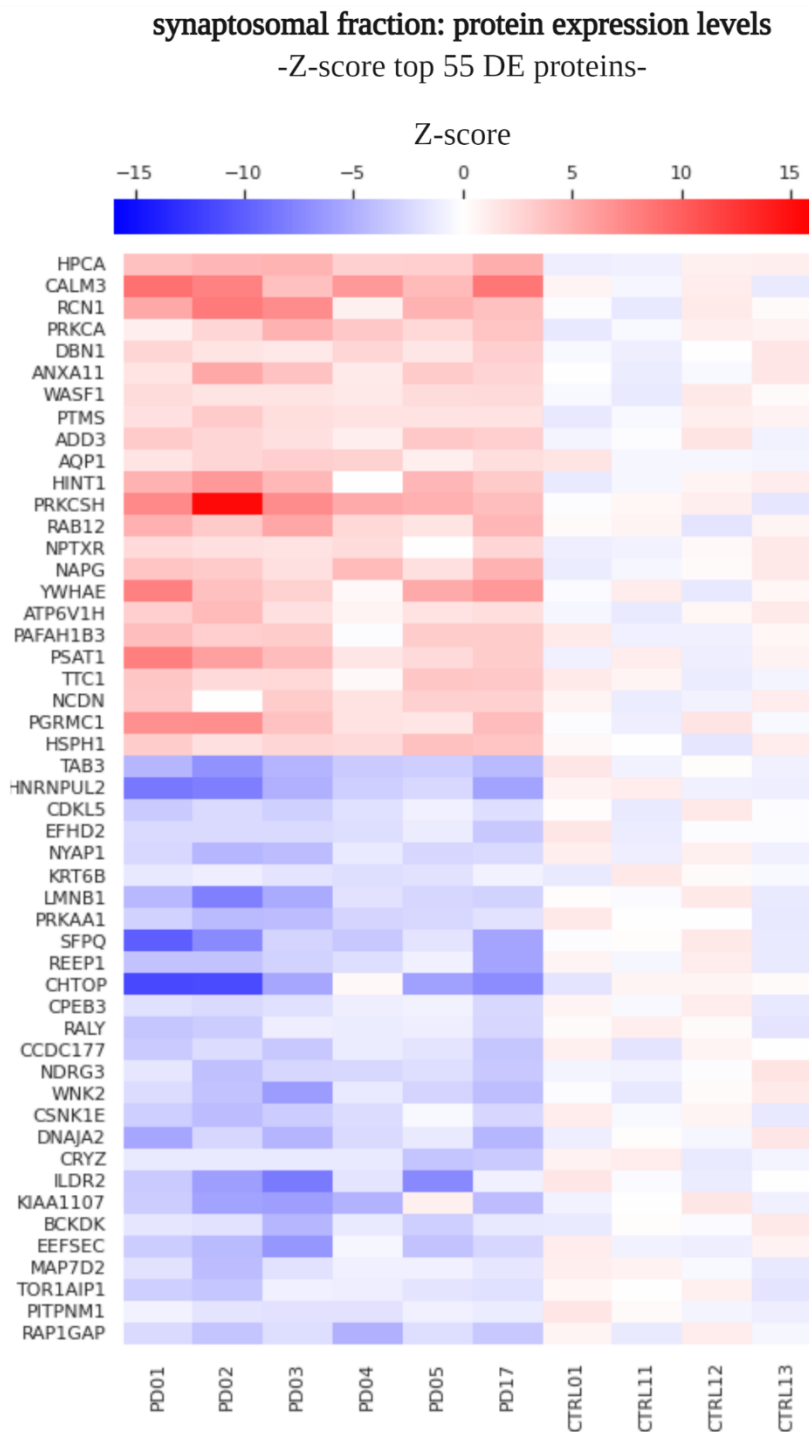
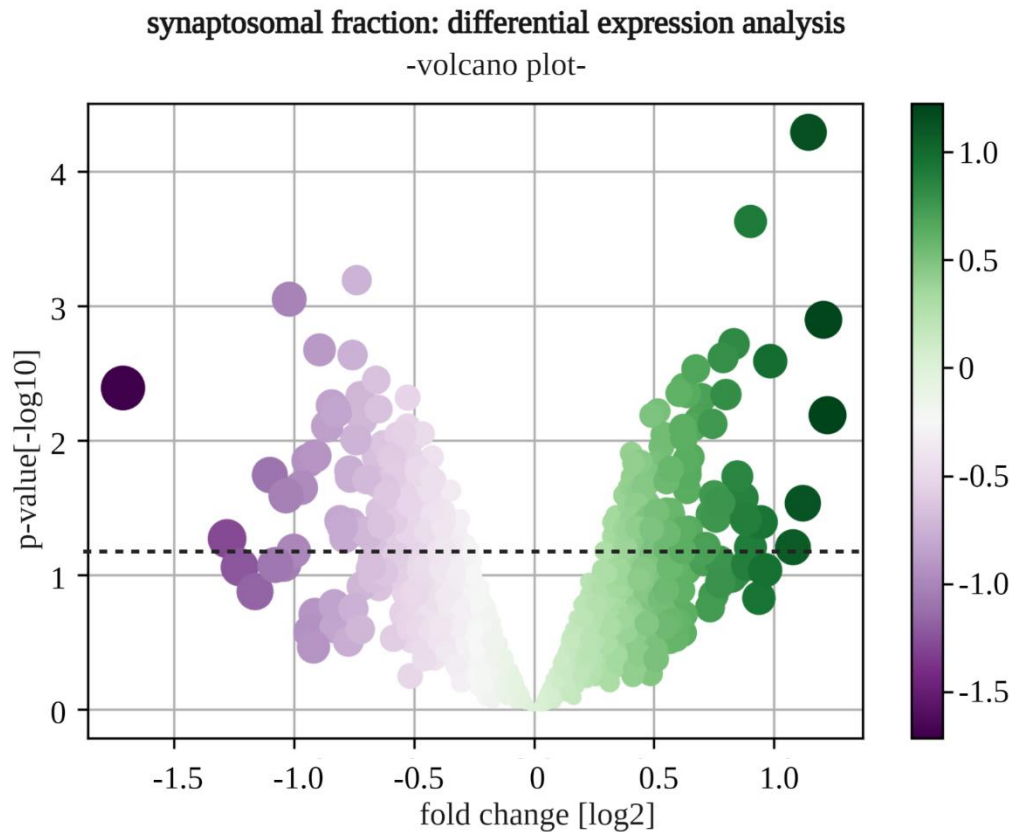


Figure 20. Heat map of Z-scores of top 55 DE proteins of the synaptosomal fraction. Z-scores are color-coded with blue colours showing proteins in less abundance in PD and red colours showing higher abundance.

For further analyses, we therefore used a less stringent cut-off and considered proteins with p-values <0.05 prior to BH correction as significantly differentially expressed in PD, yielding 194 proteins with altered abundance in PD (**Figure 21**).

A



B

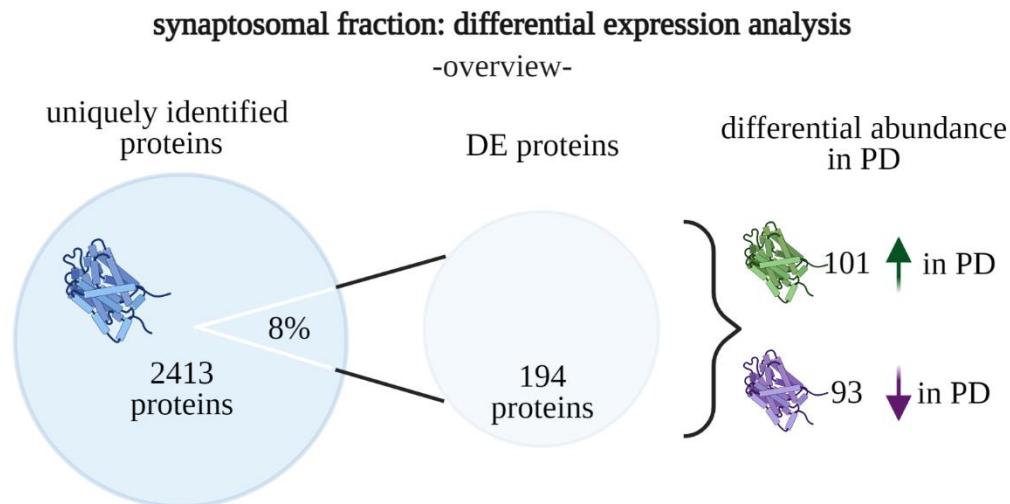


Figure 21 Differential expression analysis of proteins from synaptosomal fractions. **A)** Volcano plot showing all identified proteins. P-values $[-\log_{10}]$ are shown on the y-axis, fold change values $[\log_2]$ are shown on the x-axis. Colour code shows protein abundance in PD compared to controls, with lower abundance in PD in purple tones and higher abundance in PD in dark green tones. Circumference of protein dots correlates to fold change. Dotted line at moderated p-value 0.05. Proteins above dotted line are considered significantly differentially abundant in PD. **B)** Overview scheme of all identified proteins from whole tissue lysate samples as well as differential expression analysis. Dark green arrows show increased abundance in PD, purple arrows show decreased abundance in PD.

3. Results

3.2.2.2 Functional annotation analysis of DE proteins from the whole tissue lysate samples

Similarly to the experimental workflow conducted on the whole tissue lysates, the data set of DE proteins obtained from the synaptosomal fraction was firstly characterised establishing a PPI network of known interactions using the STRING platform v.11.0b (D. Szklarczyk et al., 2019).

The larger data set of 194 proteins yielded a more complex PPI network, with a central cluster of protein interactions encompassing the vast majority of the DE proteins of the synaptosomal fraction. Within the main central cluster, a set of densely interacting sub-clusters of proteins was visible (**Figure 22**).

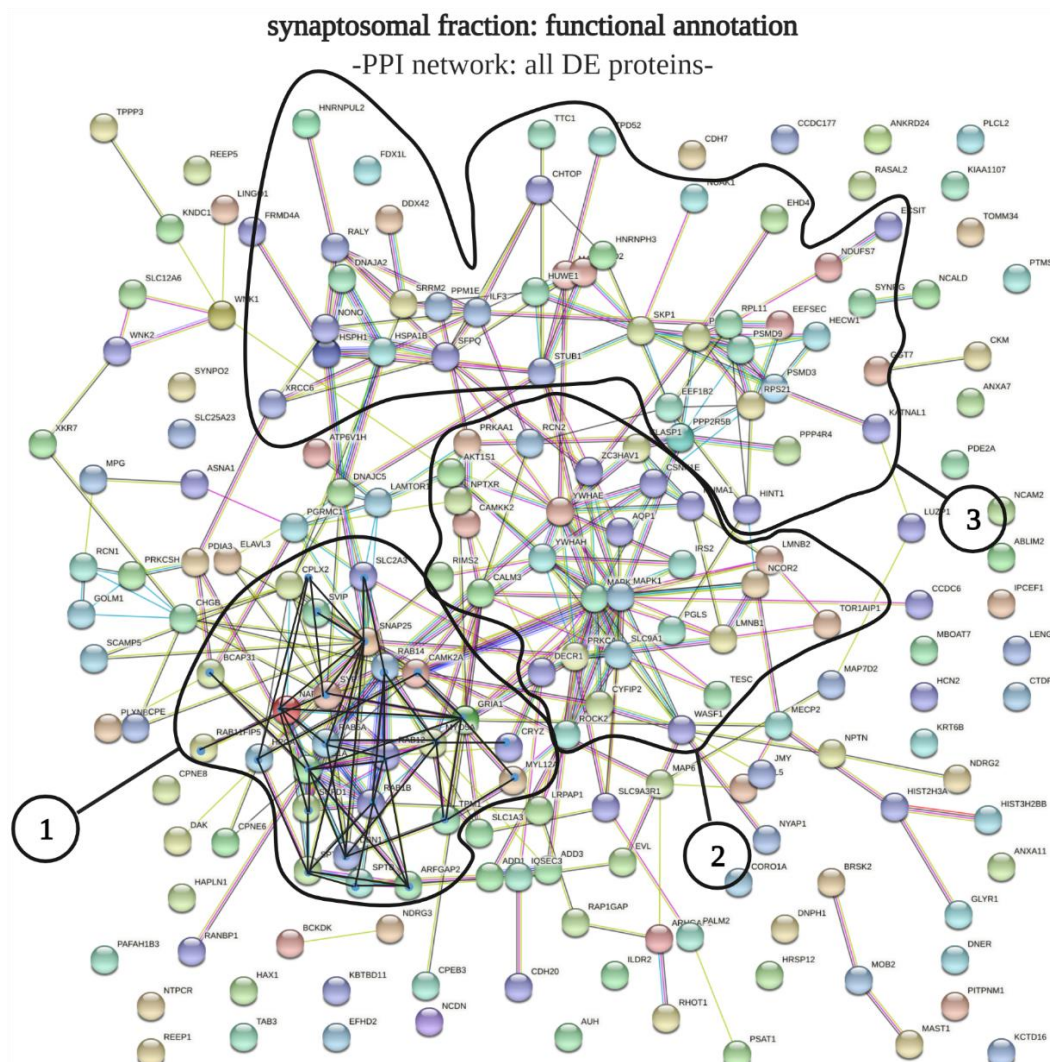


Figure 22. Protein-protein interaction network of DE proteins from synaptosomal fractions. Three sub-clusters of strongly interacting proteins are identified (1-3).

The first sub-cluster (1) displayed several key regulators of intracellular membrane trafficking, with Ras-related proteins such as Ras-related protein Rab-1B (RAB1B) and Ras-related

protein Rab-6A (RAB6A) amongst others, as well as synaptic proteins like synaptophysin (SYP) and synaptosomal-associated protein, 25 kDa (SNAP25) (**Figure 23A**).

The second sub-cluster (2) contained essential components of the MAP kinase signal transduction pathway such as mitogen-activated protein kinase 1 (MAPK1), mitogen-activated protein kinase 3 (MAPK3) and rho-associated protein kinase 2 (ROCK2), as well as isoforms of the 14-3-3 protein family with 14-3-3 protein epsilon and 14-3-3 protein eta (YWHAH), the later being one of the three shared DE proteins between whole tissue lysates and synaptosomal fractions (**Figure 23B**).

The final sub-cluster (3) displayed chaperone heat shock 70kDa protein 1B (HSPA1B) pivotal in protein quality control system and protein folding handling, as well as it's nucleotide-exchange factor heat shock protein 105kDa (HSPH1), as well as incorporating ribosomal proteins like ribosomal protein S21 (RPS21) and 60S ribosomal protein L11 (RPL11) (**Figure 23C**).

3. Results

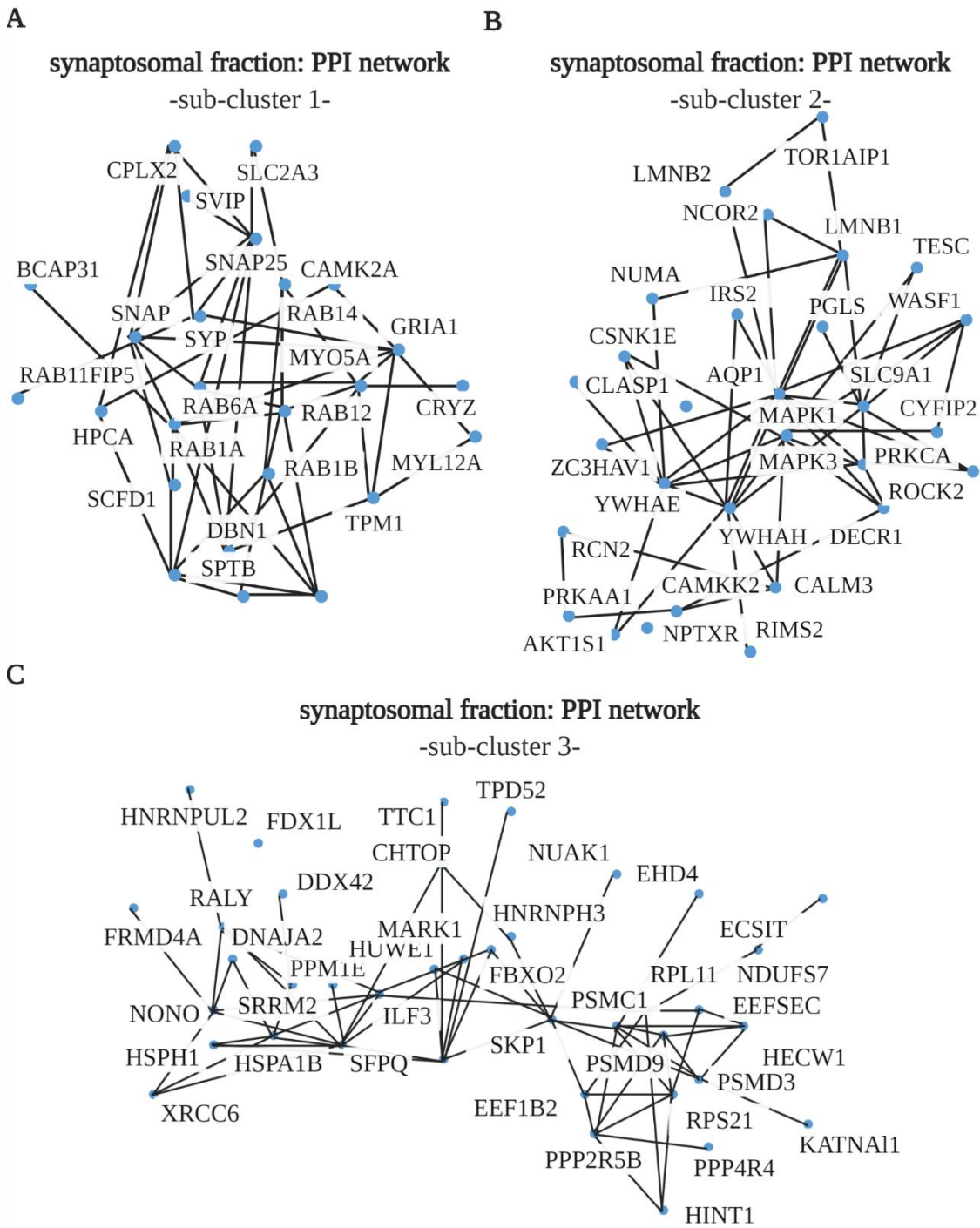


Figure 23. Protein-protein interaction network sub-clusters of DE proteins from synaptosomal fractions. A-C) Sub-clusters 1 to 3 of the PPI of the DE proteins from the synaptosomal fraction.

The functional annotation of the DE proteins from the synaptosomal fractions showed among the top 10 highest ranking terms enriched for *biological processes* terms overlapping with the functional annotation of the whole tissue lysates, with several terms involved in *localization* and *transport* (**Table 11**).

# term ID	term description	FDR [-log10]
GO:0051128	regulation of cellular component organization	7.2668
GO:0016192	vesicle-mediated transport	7.2418
GO:0051234	establishment of localization	5.1785
GO:0016043	cellular component organization	5.1349
GO:0051179	localization	5.1349
GO:0065008	regulation of biological quality	5.1349
GO:0006810	transport	5.0246
GO:0007399	nervous system development	5.0246
GO:0048699	generation of neurons	5.0246
GO:0051493	regulation of cytoskeleton organization	5.0246

Table 11. Functional annotation of top 10 *biological processes* of DE proteins from synaptosomal fraction samples.

The functional annotation of the *molecular functions* yielded several GO-terms related to *binding*, including *protein binding*, *cytoskeletal protein binding* and *actin binding*, a molecular function also previously seen in the top-ranking enriched terms of the functional annotation analysis of whole tissue lysates (**Table 12**).

# term ID	term description	FDR [-log10]
GO:0005515	protein binding	6.5834
GO:0005488	binding	5.5157
GO:0008092	cytoskeletal protein binding	5.3363
GO:0036094	small molecule binding	4.0477
GO:0000166	nucleotide binding	3.7447
GO:0043168	anion binding	3.7447
GO:0005509	calcium ion binding	3.6778
GO:0003779	actin binding	3.4089
GO:0004674	protein serine/threonine kinase activity	3.0809
GO:0032555	purine ribonucleotide binding	3.0655

Table 12. Functional annotation of top 10 *molecular functions* of DE proteins from synaptosomal fraction samples.

3. Results

Finally, the category *cellular compartment* yielded enriched terms such as *neuron projection* and *cytoskeleton*, also significantly enriched in the functional annotation analysis of the whole tissue lysates (**Table 13**).

# term ID	term description	FDR [-log10]
GO:0005829	cytosol	8.1599
GO:0005737	cytoplasm	7.9872
GO:0043005	neuron projection	5.6655
GO:0005622	intracellular	5.3990
GO:0005856	cytoskeleton	4.8097
GO:0036477	somatodendritic compartment	4.4498
GO:0005623	cell	4.2899
GO:0042995	cell projection	4.2899
GO:0120025	plasma membrane bounded cell projection	4.2899
GO:0098805	whole membrane	4.0227

Table 13. Functional annotation of top 10 cellular components of DE proteins from synaptosomal fraction samples.

3.2.2.3 WGCNA network construction and functional annotation of synaptosomal fraction

The data set of identified proteins from the synaptosomal fractions was further characterized, by downscaling the entire set into modules of co-expressed proteins as was done with the data set of the whole tissue lysates, using the R package WGCNA as previously described in chapter 3.1.2.3 (**Figure 24A**).

The network rescaling was aimed at the construction of 10 modules of corelated proteins in order to facilitate comparisons to the results gathered from the modules of whole tissue lysates. From the 2413 proteins in the data set, 2358 were assigned to a specific module, with only 2% of proteins not showing significant correlation to any given set of proteins in the identified modules. The resulting 10 modules contain an average of 236 proteins per module, ranging from 495 in module S01 to 100 proteins in module S10. (**Figure 24B**).

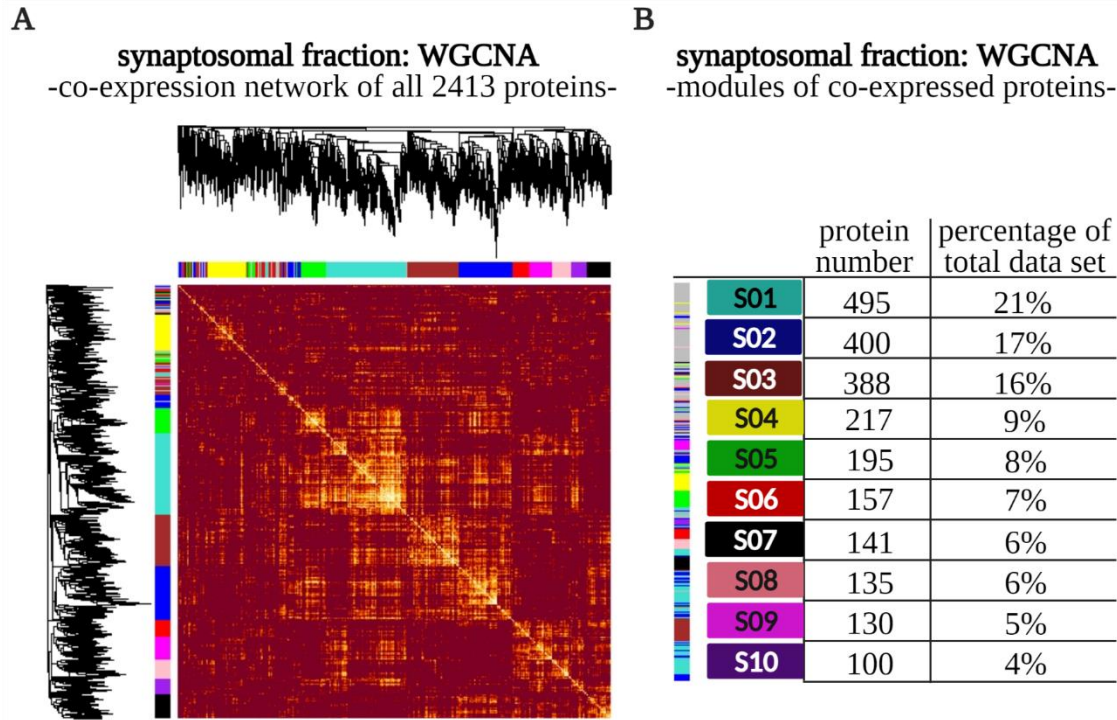


Figure 24. Network analysis based on co-expression of all 2413 identified proteins from the synaptosomal fraction. A) Heatmap plot of adjacency. Rows and columns correspond to single proteins, light colours represent low adjacency calculated from pair-wise correlations. Darker colours represent higher adjacency. Protein dendrograms and module assignment shown on top and to the left. B) Amount of assigned proteins per module, as well as percentage from the entire 2413 protein data set.

The biological relevance of the obtained modules were in turn assessed via functional annotation as described in 3.1.2.3 (Table 14-Table 16).

module	GO term	description <i>biological process</i>	FDR [-log10]
S01	GO:0099504	synaptic vesicle cycle	7.1645
S01	GO:0010975	regulation of neuron projection development	4.9403
S02	GO:0060491	regulation of cell projection assembly	3.5858
S02	GO:0099003	vesicle-mediated transport in synapse	3.4640
S03	GO:0009141	nucleoside triphosphate metabolic process	11.1169
S03	GO:0010257	NADH dehydrogenase complex assembly	7.5233
S04	GO:0010257	NADH dehydrogenase complex assembly	5.2917
S04	GO:0009123	nucleoside monophosphate metabolic process	5.0488
S04	GO:0002181	cytoplasmic translation	4.3931
S05	GO:0099504	synaptic vesicle cycle	9.7298
S05	GO:0010975	regulation of neuron projection development	6.3407
S05	GO:0051668	localization within membrane	5.1942
S05	GO:0035418	protein localization to synapse	4.6275
S06	GO:1902903	regulation of supramolecular fiber organization	4.7344
S06	GO:0010975	regulation of neuron projection development	3.9867

3. Results

S06	GO:0009896	positive regulation of catabolic process	3.8079
S07	GO:0019932	second-messenger-mediated signaling	2.2856
S07	GO:0002446	neutrophil mediated immunity	1.3038
S08	GO:0008380	RNA splicing	6.9114
S08	GO:0006403	RNA localization	2.6040
S09	GO:0051258	protein polymerization	2.5095
S09	GO:0031109	microtubule polymerization or depolymerization	1.6343
S09	GO:0006898	receptor-mediated endocytosis	1.5044
S10	GO:0034976	response to endoplasmic reticulum stress	2.9754
S10	GO:0070671	response to interleukin-12	1.6523
S10	GO:0051656	establishment of organelle localization	1.2409

Table 14. Functional annotation of *biological processes* for each module of co-expressed proteins from the synaptosomal fractions.

module	GO term	description <i>molecular function</i>	FDR [-log10]
S01	GO:0099572	postsynaptic specialization	11.5383
S02	GO:0099572	postsynaptic specialization	7.1509
S02	GO:0033267	axon part	5.6982
S02	GO:0005911	cell-cell junction	3.4208
S03	GO:0005759	mitochondrial matrix	>16
S04	GO:0098798	mitochondrial protein complex	5.2917
S04	GO:0043209	myelin sheath	3.8990
S04	GO:0005874	microtubule	3.8309
S05	GO:0098984	neuron to neuron synapse	>16
S05	GO:0015629	actin cytoskeleton	7.6468
S06	GO:0101031	chaperone complex	3.8428
S07	GO:0005905	clathrin-coated pit	2.0779
S09	GO:0098793	presynapse	2.5095
S09	GO:0008180	COP9 signalosome	1.7258
S10	GO:0097060	synaptic membrane	2.9754
S10	GO:0019898	extrinsic component of membrane	2.5818
S10	GO:0033267	axon part	1.9161
S10	GO:0098589	membrane region	1.7851
S10	GO:0099572	postsynaptic specialization	1.6448

Table 15. Functional annotation of *molecular function* for each module of co-expressed proteins from the whole tissue lysate sample.

module	GO term	description <i>cellular compartment</i>	FDR [-log10]
S01	GO:0005200	structural constituent of cytoskeleton	9.1226
S04	GO:0050839	cell adhesion molecule binding	5.3724
S06	GO:0050321	tau-protein kinase activity	4.5989
S06	GO:0060589	nucleoside-triphosphatase regulator activity	3.9418
S07	GO:0003924	GTPase activity	3.0509
S08	GO:0036002	pre-mRNA binding	2.9322

Table 16. Functional annotation of *cellular compartments* for each module of co-expressed proteins from the whole tissue lysate sample.

A series of umbrella terms were manually established to summarize similar GO-terms from the functional annotation of *biological processes*, in order to facilitate comparisons between the biological relevance of modules from the whole tissue lysates and synaptosomal fractions. A total of 12 umbrella terms were determined (**Table 17**).

module	umbrella term	description of <i>biological process</i>
W01	metabolic process	nucleoside triphosphate metabo. process
W01	metabolic process	tricarboxylic acid metabolic process
W01	metabolic process	ribose phosphate biosynthetic process
W02	metabolic process	tricarboxylic acid metabolic process
W02	metabolic process	coenzyme metabolic process
W02	metabolic process	nucleoside triphosphate metabolic process
W03	cellular localization	synaptic vesicle cycle
W03	transport	trivalent inorganic cation transport
W04	metabolic process	one-carbon metabolic process
W04	cellular localization	vesicle localization
W04	immune system process	neutrophil mediated immunity
W04	response to stimulus	intrinsic apoptotic signaling pathway
W05	immune system process	neutrophil mediated immunity
W05	cytoskeletal organization	actin cytoskeleton reorganization
W05	cytoskeletal organization	actin filament organization
W06	immune system process	neutrophil mediated immunity
W06	immune system process	neutrophil mediated immunity
W06	metabolic process	small molecule catabolic process
W06	metabolic process	pyridine-containing comp. metabo. process
W07	cellular localization	synaptic vesicle cycle
W07	transport	exocytic process
W07	not considered	coagulation
W07	metabolic process	reactive oxygen species metabolic process
W07	transport	positive regulation of ion transport
W08	metabolic process	cellular amino acid metabolic process

3. Results

W08	cellular localization	protein localization to ER
W09	metabolic process	nucleobase metabolic process
W09	cell adhesion	heterotypic cell-cell adhesion
W10	metabolic process	nucleoside triphosphate metabolic process
W10	transport	golgi vesicle transport
W10	metabolic process	ribose phosphate biosynthetic process
W10	metabolic process	proteasomal protein catabolic process
W10	immune system process	neutrophil mediated immunity
W10	response to stimulus	response to electrical stimulus
S01	cellular localization	synaptic vesicle cycle
S01	nervous system development	reg. of neuron projection development
S02	regulation of cellular process	reg. of cell projection assembly
S02	transport	vesicle-mediated transport in synapse
S03	metabolic process	nucleoside triphosphate metabo. process
S03	cellular component organization	NADH dehydrogenase complex assembly
S04	cellular component organization	NADH dehydrogenase complex assembly
S04	metabolic process	nucleo. monophosphate metabo. process
S04	metabolic process	cytoplasmic translation
S05	cellular localization	synaptic vesicle cycle
S05	nervous system development	reg. of neuron projection development
S05	cellular localization	localization within membrane
S05	cellular localization	protein localization to synapse
S06	biological regulation	reg. of supramolecular fiber org.
S06	nervous system development	reg. of neuron project. development
S06	metabolic process	positive regulation of catabolic process
S07	signaling	second-messenger-mediated signaling
S07	immune system response	neutrophil mediated immunity
S08	metabolic process	RNA splicing
S08	metabolic process	RNA localization
S09	cellular component organization	protein polymerization
S09	cytoskeletal organization	microtub. Polymeriz. or depolymeriz.
S09	transport	receptor-mediated endocytosis
S10	response to stimulus	response to ER stress
S10	response to stimulus	response to interleukin-12
S10	cellular localization	establishment of organelle localization

Table 17. Break down of biological processes assigned to the different umbrella terms created for comparison of functional annotation of both whole tissue lysates and synaptosomal fractions.

Umbrella terms such as *metabolic process*, *cellular localization* and *transport*, encompassed GO-terms significantly enriched for several of the ten modules as well as being present in both whole tissue lysates modules and synaptosomal fractions modules. Several other umbrella terms such as

signalling, nervous system development and cell component organization contained respectively GO-terms significantly enriched only for modules created from the data set of synaptosomal fractions (Figure 25).

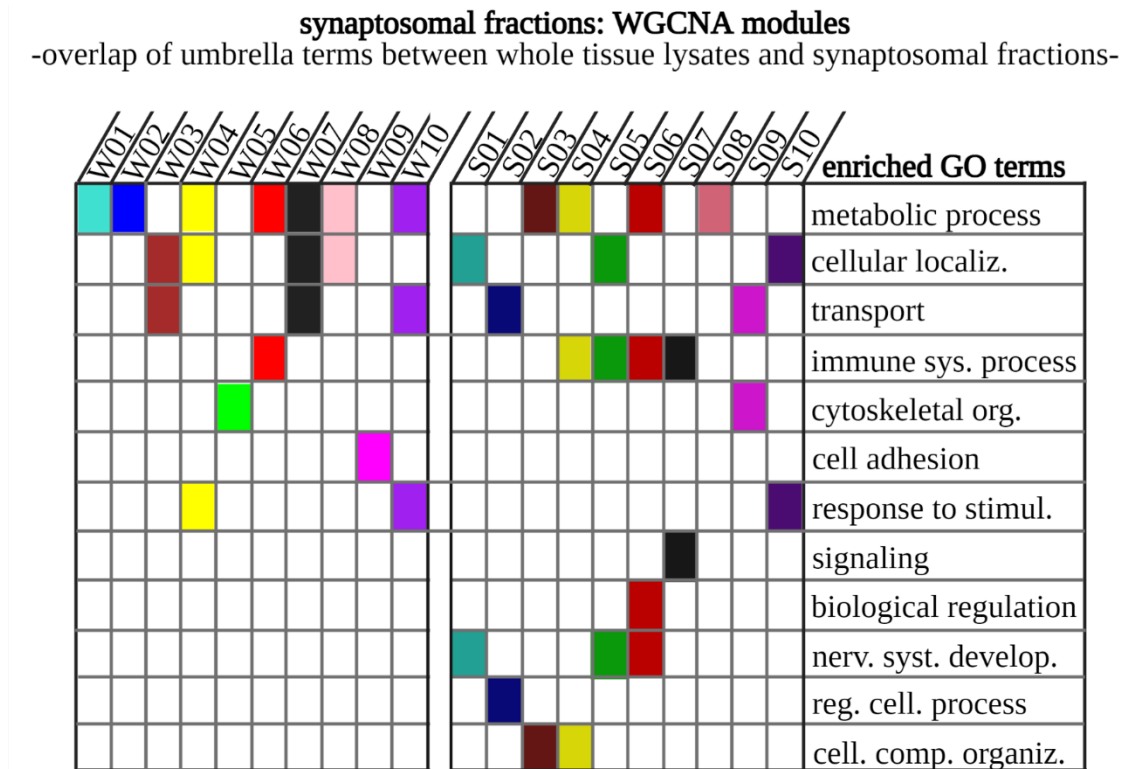


Figure 25. Summary of modules from both whole tissue lysates and synaptosomal fractions assigned to one of twelve umbrella terms. Coloured rectangles at each module W01-W10 and S01-S10 symbolize at least one GO-term enriched for that module that belongs to the umbrella term on the right.

Finally, from the 10 modules of the synaptosomal fractions, module S01, the module containing the largest number of proteins, showed several enriched terms from both *biological processes* and *cellular compartments* related to the synaptic compartment.

This module showed high similarity to the previously established synaptic module, W03, from the whole tissue samples. Modules W03 from the whole tissue lysates and S01 from the synaptosomal fractions had an almost perfect overlap between the top 5 terms enriched for both *biological processes* and *cellular compartments*, varying slightly in the ranking of the terms (Figure 26A).

Furthermore, the synaptic module of the synaptosomal fractions contained 23 DE proteins, amongst which were complexin-2 (CPLX2), a protein negatively regulating synaptic vesicle formation at the active zone, calcium/calmodulin-dependent protein kinase type II subunit alpha (CAMK2A), a kinase involved in synaptic plasticity and neurotransmitter release and long-term potentiation and neuronal pentraxin receptor (NPTXR), a protein mediating the synaptic clustering

3. Results

of AMPA glutamate receptors and receptor to NPTX1, a DE protein found in the synaptic module W03 from the whole tissue lysates (**Figure 26B**).

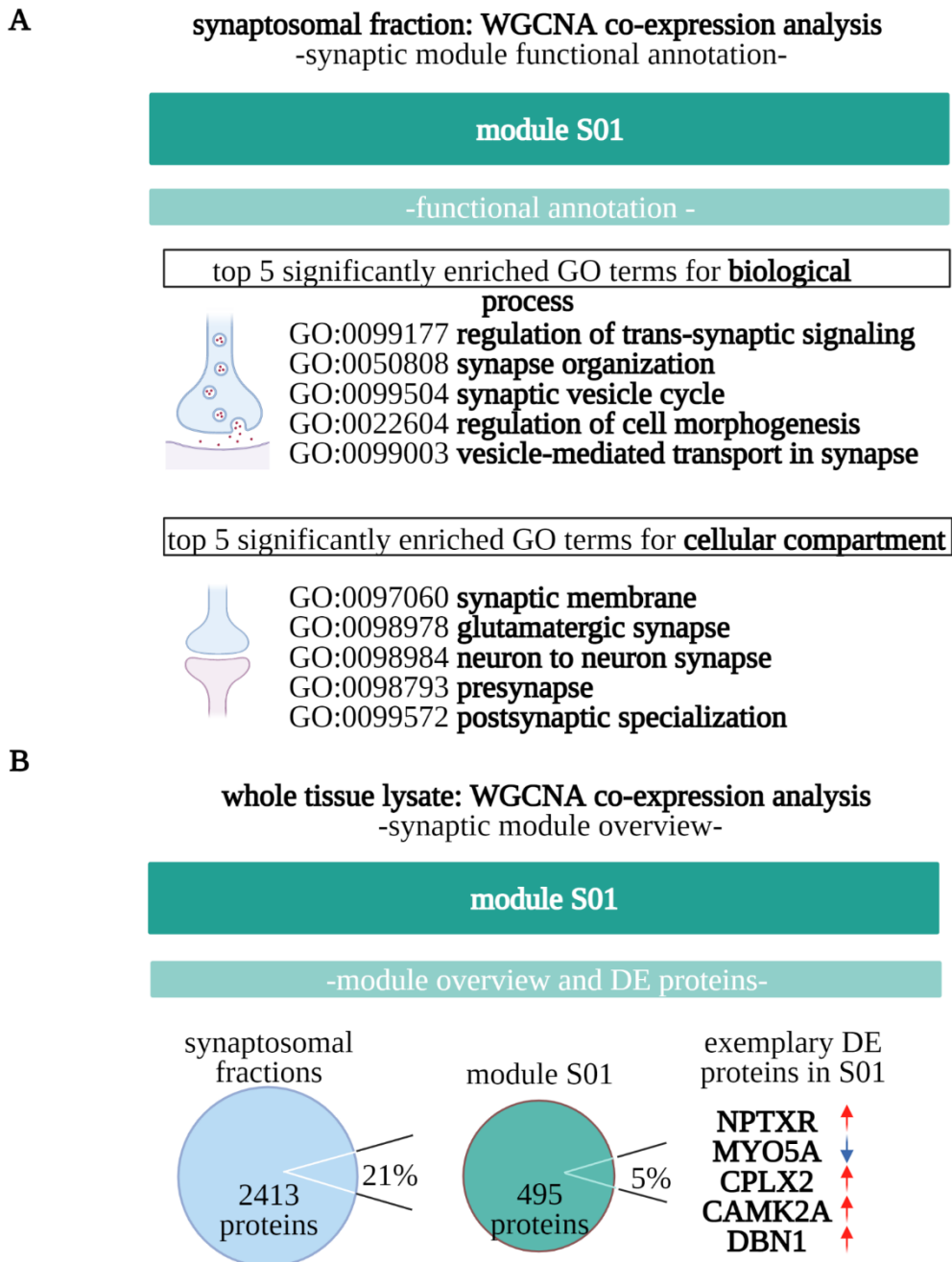


Figure 26. Synaptic module S01 overview. **A)** Overview of top 5 enriched GO terms from functional annotation analysis of categories *biological process* and *cellular compartment*. **B)** Scheme showing the number of proteins assigned to module W03 and exemplary differentially expressed proteins. Red arrows signify higher abundance in PD, blue arrow signifies lower abundance in PD.

protein	fold change [log]
NPTXR	1.2230
CHGB	1.1202
MBOAT7	0.8835
DBN1	0.7879
CPLX2	0.7505
CAMK2A	0.5569
PDE2A	0.5099
NAPG	0.4908
GOLM1	0.4575
SLC25A23	0.4521
TPM1	0.4445
RAB1A	0.3366
KATNAL1	-0.3203
MYO5A	-0.4314
FBXO2	-0.4529
SPTB	-0.4921
HSPA1B	-0.5010
HECW1	-0.5759
LUZP1	-0.7931
NUMA1	-0.8086
RALY	-0.8620
HCN2	-1.0336
HIST2H3A	-1.1006

Table 18. All DE proteins contained in the synaptic module S01 from synaptosomal fractions.

3.3 Changes in synaptic morphology induced by dysregulation of NPTX1 in primary cell cultures

3.3.1 Aims

From the focussed target selection enabled by the characterization of the proteomic data sets, combined with a special interest on a potential synaptic dysfunction, we identified NPTX1 as a candidate for further characterization.

As such, the work presented in this chapter aimed to characterize NPTX1 and the potential consequences of an increased abundance on a neuronal network. In order to address this, we employed primary cell cultures obtained from hippocampal mouse neurons.

The first aim was to characterize the endogenous expression of NPTX1 in cultured cells by quantifying expression changes over time. The second aim was to characterize changes elicited by the increase in abundance of NPTX1. In order to mimic the observed increase in abundance of NPTX1 in the human hippocampus, the cultured mouse hippocampal cells were exposed to a chronic 7-day treatment with recombinant NPTX1. Treatment effects were measured by characterizing synapse morphology and comparing the treated cells to control cultures.

3.3.2 Results

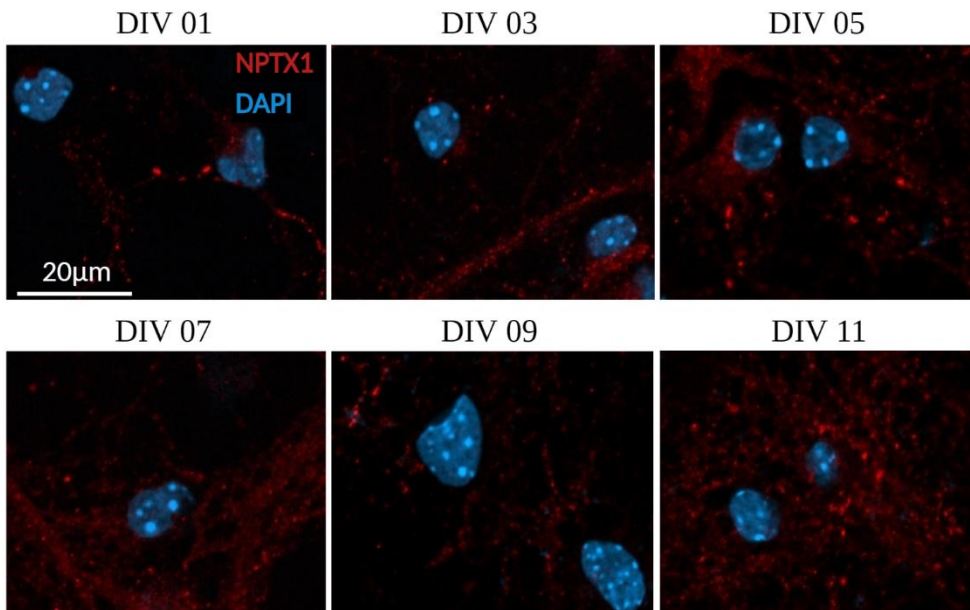
3.3.2.1 Endogenous expression of NPTX1 in primary mouse hippocampal cell cultures

First, the endogenous expression of NPTX1 was characterized in the maturing hippocampal neuron culture. Secondly, NPTX1 levels were increased by adding recombinant NPTX1 to the culture.

The characterization of endogenous NPTX1 expression showed an increase of expression over time, with a distinct punctate expression pattern emerging around day in vitro (DIV) 07, which started to diffuse into the cytoplasm at DIV11 (**Figure 27**).

A

endogenous NPTX1 expression in mouse primary hippocampal neurons
-expression over time-



B

endogenous NPTX1 expression in mouse primary hippocampal neurons
-expression development quantification-

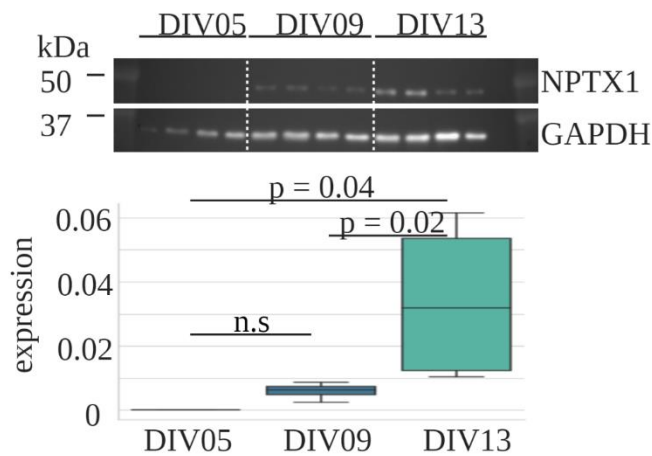


Figure 27. Endogenous NPTX1 expression in mouse hippocampal primary cell cultures. A) Exemplary immunostainings of P0 mouse hippocampal primary cell cultures at different developmental stages. NPTX1 signal in red. Scale bar 20 μm. B) Quantification of NPTX1 protein levels at different developmental stages. Signals normalized to housekeeping GAPDH.

3. Results

3.3.2.2 Morphological changes in the synapse induced by increase of NPTX1 protein levels in primary hippocampal cell cultures

To mimic the increase of NPTX1 in PD samples quantified in the whole tissue lysates, recombinant NPTX1 protein (0.23 μ g) was added daily to primary hippocampal neurons from DIV01 to DIV07 with a starting concentration of 10nM at DIV01 and an end concentration of 70nM at DIV07, fixating cells on DIV08 for the characterization of effects on synapse morphology (**Figure 28**).

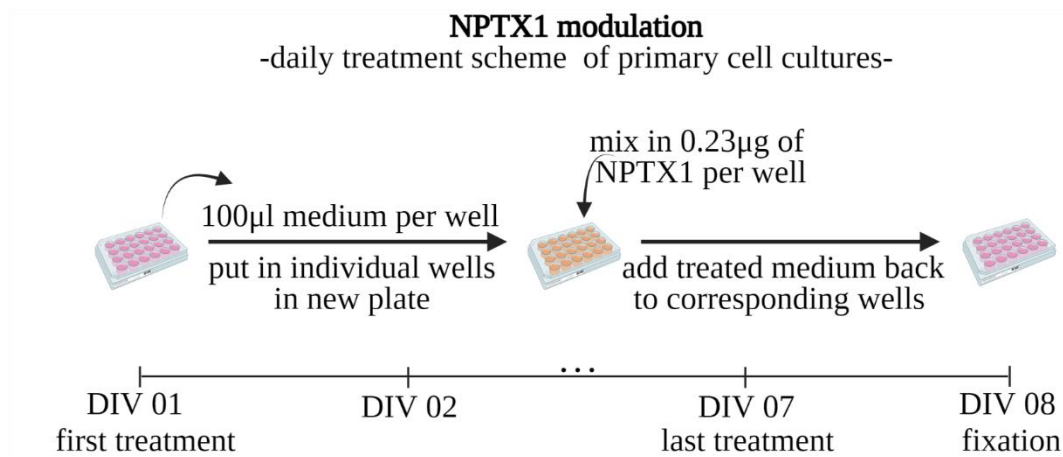


Figure 28. Treatment scheme for daily NPTX1 dosages on primary hippocampal cell cultures. Medium from cell cultures was gathered individually from each well, 0.23 μ g of recombinant NPTX1 was mixed thoroughly within each well of medium and the treated medium was added back unto the corresponding wells with cells.

To quantify changes in synapse morphology elicited by the increase in NPTX1 protein levels of cells receiving a chronic treatment with recombinant NPTX1, fixated cultures were co-immunostained for NPTX1 and SYN1. Signals from SYN1 were used to fit ellipses to ~10,300 individual synapses of treated cells and control cells respectively (**Figure 29A**).

Ellipse characteristics such as area, major and minor axis and mean intensity were quantified for each fitted ellipse using a semi-automatic algorithm, assessing the morphology of individual synapses, (**Figure 29B**).

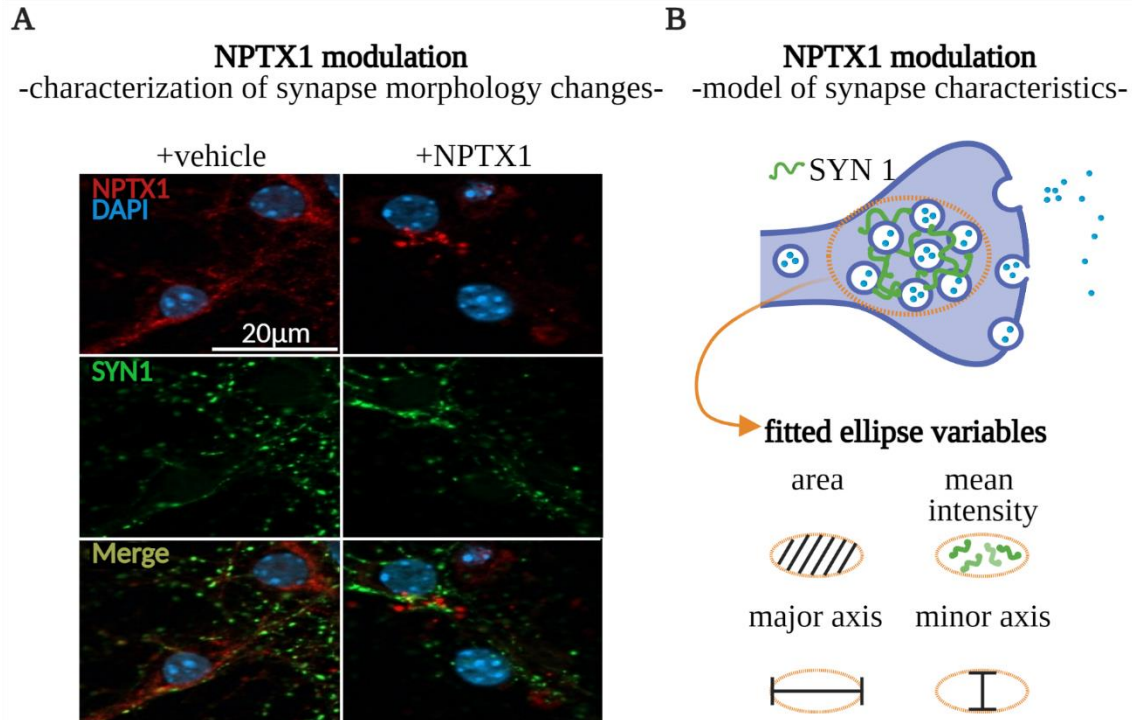


Figure 29. Characterization of morphological changes of the neuronal synapse treated with NPTX1. A) Cell cultures treated with NPTX1 were co-immunostained for NPTX1 in red and SYN1 in green. SYN1 signal was used for synapse morphology characterization. Scale bar 20µm. B) Model for semi-automatic synapse morphology characterization. Ellipses were fitted to SYN1 signal. Synapse morphology was assessed based on ellipse characteristics: area, mean intensity, major axis and minor axis.

The quantification of the individual variables of each fitted ellipse, showed a significant change in the area of synapses (p -value = 0.01) with treated cells having smaller areas (37.7 a.u.) compared to the vehicle-treated cultures (39.7 a.u.). The synaptic shape was also significantly altered in treated cultures, with the major axis of the fitted ellipses showing no significant alteration, while the minor axis had a highly significant increase in the treated cells (5.3 a.u. vs. 5.3 a.u., p -value = $2.52 \cdot 10^{-5}$), hinting thus towards a more stubby shape of synapses in cultures treated with NPTX1. Finally, also the mean intensity of the fitted ellipses was significantly higher for treated cells (16.2 a.u. vs. 15.2 a.u., p -value < $2.2 \cdot 10^{-16}$) (**Figure 30**).

NPTX1 modulation
-morphological changes of treated synapses-

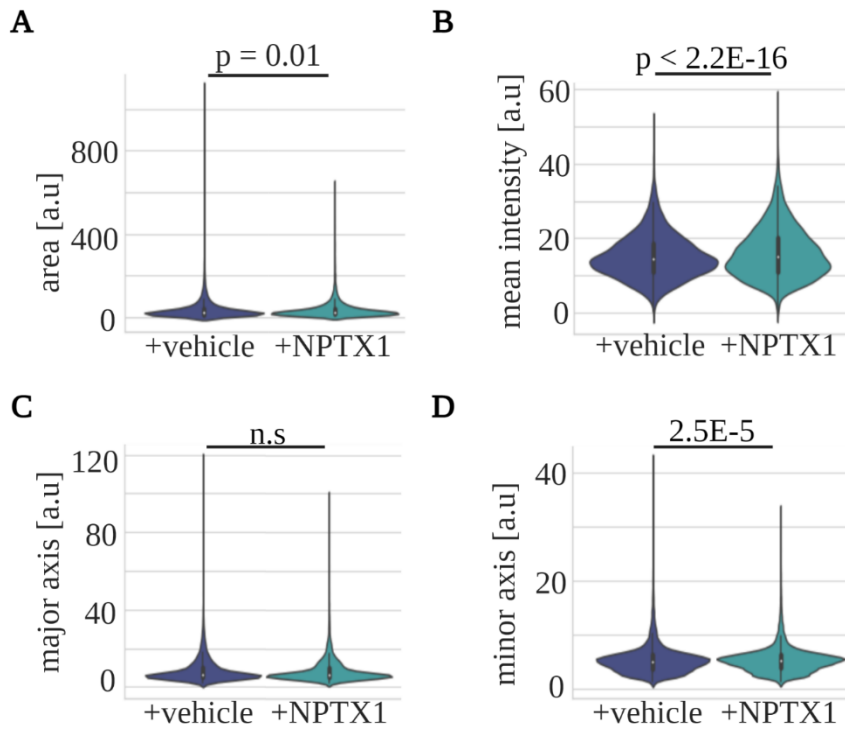


Figure 30. Quantification of morphological changes of synapses from neurons treated with NPTX1. Ellipses were fitted to ~10,300 individual synapses for both treated cultures and controls respectively. **A)** Areas of treated synapses show a significant decrease (37.7 a.u. vs. 39.7 a.u.). **B)** Mean intensity of treated synapses show significant increase in signal (16.2 a.u. vs. 15.2 a.u.). **C)** Major axis of the synapse have no significant change. **D)** Minor axis significantly increased in treated cells (5.3 a.u. vs. 5.3 a.u.), representing an overall stubbier synapse.

3.4 Summary of Results

In summary, we identified and characterized changes in the human hippocampus elicited by PD by quantifying protein abundances compared to controls via mass spectrometry. As such, we showed that the PD hippocampus shows altered abundance of 55 proteins, with 37 being more abundant in PD and 18 being less abundant in PD compared to CTRs (**Figure 4**). Furthermore, we addressed the biological relevance of these altered proteins by means of a PPI network and functional annotation analysis. We found two main clusters of proteins with known interactions. The first cluster comprised amongst others GAP43, BASP1, MARCKS, AGRN and SYN1, all of which were found to be upregulated in PD. These proteins were represented in the annotation of significantly enriched GO terms in the functional annotation analysis of the *molecular functions* of the data set, with prominent enriched GO terms like *cytoskeleton* and *actin binding* (**Figure 6A and Figure 7B**).

The second cluster of known interacting proteins included several isoforms of the 14-3-3 protein family, such as YWHAZ, YWHAH and YWHAQ, all in higher abundance in PD. These were represented in the functional annotation analysis by enriched *biological processes* such as *transport*, *localization* and *organization*. In addition, this second cluster showed ribosomal proteins such as RPS9, RPS16 and RPL4, all less abundant in PD. These were annotated in the enriched *biological processes* such as *rRNA binding* and *structural constituent of ribosome* (**Figure 6A and Figure 7B**).

As an additional step of characterization of the obtained proteomic data set, we re-sized the entire data set of 2089 proteins quantified in the whole tissue lysates, using a weighted correlation network analysis. This allowed to divided the sizeable proteomic data set into individual modules of less proteins, by grouping proteins in terms of the similarities between their expression patterns across all measured samples. From the 2089 proteins 70% were assigned to one of 10 modules based on their similarities in expression patterns (**Figure 8**). The resulting groups of proteins enabled a second functional annotation analysis, which showed both a similituted to the previous approach considering solely the DE proteins, as well as revealing additional mechanisms of interest. As such we showed the representation of aforementioned terms such as *cytoskeleton* and *ribosome* in three of the modules, with the addition of new terms such as *mitochondria* and *synapse* (**Figure 10**).

3. Results

Of special interest to the focus of this study in regards to synaptic dysfunction in PD, the module W03 showed a promising prominent representation of the synapse with a very high enrichment of terms related to it, such as *synaptic vesicle cycle*, *synapse organization*, *presynapse* and *postsynaptic specialization*. This module furthermore contained 14 of the 55 proteins found to be differentially abundant in PD, including amongst others GAP43, SYN1 and NPTX1, all proteins found more abundant in PD (**Figure 11**).

We further validated the findings of the altered abundance of proteins in the PD hippocampus in a mass spectrometry independent manner. Based on the functional annotation analyses and the known literature, NPTX1 was selected as a promising target of interest based on its representation of the synaptic compartment in our study, combined with its known involvement in neurodegenerative diseases such as AD. As such, we validated the increase of abundance of NPTX1 in PD via western blots, showing a significant increase compared to CTRs.

To further address the synaptic dysfunction in the PD hippocampus, we isolated synaptosomal fractions from a subset of the initially addressed cohort of human hippocampal samples, based on the feasibility of an adequate yield of protein quantities for subsequent proteomic studies. From the isolated synaptosomal fractions, we identified a total of 2413 unique proteins. Based on a limited number of available samples (PD = 6 and CTR = 4), we were not able to detect a differential protein abundance in PD using the eBayes function of the limma R package and correcting for multiple testing via BH. For further analyses we considered a less stringent approach, considering p-Values < 0.05 prior to BH correction as significant. With this consideration, we identified a total of 194 proteins differentially abundant in PD, with 101 more abundant in PD and 93 less abundant in PD (**Figure 21**).

In terms of similarities to the whole tissue lysate samples of the whole cohort, there was an overlap of 2009 proteins identified in both proteomic data sets, with the whole tissue lysate samples having 80 unique proteins and the synaptosomal fractions presenting 404 unique proteins. As for the DE proteins, three proteins were shared between both data sets: YWHAH, CORO1A and ATP6V1H (**Figure 19**).

Characterization of the DE proteins from the synaptosomal fraction showed similarities to the enriched terms we found for the whole tissue samples, overlapping in terms such as *localization*, *transport*, and *cytoskeletal protein binding* (**Table 11** to **Table 13**). Expanding the characterization of the synaptosomal fractions, the WGCNA analysis aimed at 10 modules to enable comparisons to the whole tissue samples, we detected a similar biological relevance based on the functional

annotation analysis of the modules, with *cellular localization* and *transport* being representative umbrella terms for several modules of both data sets (**Figure 25**).

Interestingly, we found the largest of the modules of the synaptosomal fraction to be almost identical to the synaptic module W03 from the whole tissue lysate samples, displaying a high enrichment of several terms related to the synaptic compartment. The S01 synaptic module comprised 23 DE proteins, amongst which were proteins like CPLX2, CAMK2A and NPTXR, the receptor of the protein of interest for our study, NPTX1 (**Figure 26**).

Finally we addressed the influence of the dysregulation of the abundance of NPTX1 in the hippocampal network, by artificially increasing NPTX1 levels in mouse hippocampal primary cell culuters. We showed morphological alterations of the synapse elicited by a chronic treatment of cultured cells with recombinant NPTX1 suministered via the culture medium. The treated cells showed a significant decrease in area compared to vehicle treated cells (37.7 vs. 39.73 a.u. respectively, $p= 0.01$). Furthermore the shape of treated cells became stubbier, with their major axis remaining similar to vehicle treated cells and the minor axis showing a significant increase (5.34 vs. 5.32 a.u, respectively, $p = 2.52 \cdot 10^{-5}$) (**Figure 30**).

Chapter 4: Discussion

The work presented in this thesis, characterized alterations present in the human hippocampus in the context of PD. In order to achieve this, the proteomic composition of post-mortem human samples of PD patients was analysed and compared to matched control subjects, identifying a broad range of proteins with differential abundancies in PD. Furthermore, we characterized the differentially abundant proteins in regard to their biological relevance, both for individual proteins and in the frame of the entire proteomic data retrieved from the hippocampal samples. The functional characterization provided a broad range of mechanisms affected by the differential abundance of individual proteins and provided a frame for the selection of a particular protein of interest. Based on our initial interest in synaptic dysfunction present in the hippocampus, we identified NPTX1 as a promising target protein showing increased abundancies in the hippocampus of PD. We further showed that addition of NPTX1 to primary hippocampal neuron cultures *in vitro* elicits morphological changes in the synapse, pointing towards a contribution to a synaptic pathology in the hippocampus.

4.1 Differences in the hippocampus of Parkinson's disease

In order to address the differences in the hippocampus of PD, we first collected tissue samples from fresh-frozen post-mortem human hippocampal samples as well as hippocampal synaptosomal fractions for a proteomic approach, gathering quantifiable data on protein expression levels (**Figure 2** and **Figure 17**).

The analysis of this specific brain area was based on several considerations. Firstly, the late-stage involvement of the hippocampus was hypothesized as a possible source of evidence of earlier pathomechanisms, considering a shorter time of degeneration up to the end-stage picture of the disease present in post-mortem samples. This hypothesis is in line with the temporal and spatial progression proposed for PD, where the pathology starts at the medulla oblongata and advances through the brain stem and basal ganglia to the neocortex (Braak et al., 2003). Considering the different stages at which distinct brain areas are thought to be affected in PD, the amount of damage accumulated over a given period of time varies between regions, with areas involved at earlier stages being exposed longer to insults and possibly accumulating more damage. As such, we considered, that the usage of post-mortem tissue, a sample representative of the end-stage of the disease, might present different ranges

of accumulated insult depending on the brain area assessed. In this regard, hippocampal post-mortem samples likely present earlier pathological alterations due to late-stage involvement of the hippocampus in the progression of PD, as compared to areas affected earlier in the disease, such as the frequently studied Substantia nigra, which was affected for a longer period until the time of death of the patient.

Furthermore, the impact that late-stage complications have on the quality of life of patients suffering from PD, where a vast majority experience cognitive decline and advance to develop dementia (Hely et al., 2008), further postulates the hippocampus as an important area to be further characterized in the context of PD.

Studies have shown that the PD hippocampus presents a higher density of LB in patients with dementia, as well as detecting a progressive atrophy of the hippocampus with the progression of the disease (Harding and Halliday, 2001; Hall et al., 2014, Weintraub et al., 2011; Mak et al, 2015), making it an interesting target for proteomic profiling, in order to characterize potential changes and gain insight into the mechanisms contributing to this atrophy.

Previous proteomic studies using post-mortem human samples frequently analyzed the midbrain in context of the prominent loss of dopaminergic neurons and the crucial implications for the progression of the disease. In line with this, a study assessing post-mortem nigral tissue (n= 5 PD and n= 8 CTRs) identified and quantified a total of 1795 proteins using high-throughput shotgun proteomics. From the established proteomic data set, 204 proteins were determined to present a significant alteration in expression levels in the PD samples (Licker et al., 2014). In comparison, a study addressing changes in protein levels, analysed the frontal cortex based in a cohort of 5 PD patients with LB located only in the brainstem, 5 PD patients with LB in the brainstem and limbic system and 5 PD patients with LB in the brainstem, limbic system and the frontal cortex, as well as 5 control patients. Proteins were detected with mass spectrometry, using isobaric tagging for relative and absolute quantification (iTRAQ). A total of 1864 proteins were quantified, which yielded 256 proteins showing significant changes in expression levels across the different PD groups. From these, a total of 33 DE proteins were found in all PD groups (Shi et al., 2008).

In this thesis, the proteomic profile of potential changes in protein abundance, was first assessed using whole tissue lysates of hippocampal post-mortem tissue. Samples were gathered from a cohort of 16 PD patients and 14 CTRs. Using a high-throughout label-free mass spectrometry approach based on a sequential window acquisition of all theoretical mass spectra (SWATH-MS),

4. Discussion

2089 unique proteins were identified across all whole tissue lysate samples. The usage of a label-independent technique such as SWATH, provides the advantage of a high throughput allowing a wider profiling of the proteome, however resulting in a highly complex MS/MS data set. Advances in data analysis have however enabled a complemented profiling utilizing a reference proteome for a precise detection of proteins, often similar in accuracy to targeted multiple reaction monitoring (MRM), however still presenting the advantage of a wider screening (Huang et al., 2015; Gillet et al., 2012).

While a proteomic analysis taking advantage of the label-free approach is highly efficient, limitations are still to be considered, for example the less reliable quantification of small proteins (<10kDa) (Zhu et al., 2010; Old et al., 2005), as well as the obstacles in correct solubilization of proteins during sample preparations and the subsequent representation of these proteins in the proteomic data set.

In a second proteomic approach, we aimed for an enrichment of proteins of the synaptic compartment, to complement the data obtained from the whole tissue lysates. In addition to characterizing the overall proteome of PD hippocampus, we had a special interest in addressing a potential synaptic dysfunction, which appears to play an important role not only in the midbrain (Chung et al., 2009; Schirinzi et al., 2016).

Due to the limited amount of tissue provided by the brain banks, we were restricted in the number of samples from which synaptosomal fractions could be successfully extracted. Targeting a total tissue mass of ~600mg for an ideal yield of proteins in the synaptosomal fractions, 6 PD patients and 4 CTR were found to be suitable for the isolation.

The isolation of synaptosomes is a widely used approach, based on a series of centrifugation steps which fractionate homogenized tissue samples into different subcellular fractions. Homogenization of the tissue in iso-osmotic buffer (sucrose) enables the detachment of the nerve terminal from the cell, which subsequently re-seal and often maintain pre- and postsynaptic morphology as well as functional characteristics (Whittaker et al., 1964; Gulyássi et al., 2020). The final retrieval of the isolated and enriched synaptosomal fractions, presents great potential for a proteomic profiling of synaptic proteins. The isolation of the synaptosomes presents however some challenges, particularly when addressing the isolation of a synaptosomal fraction from post-mortem human tissue.

Firstly, the desired removal of debris and nuclei as well as myelin and mitochondrial proteins, represents a significant loss of mass, with the yield in protein content of the synaptosomal fractions

being evidently significantly lower than the initial tissue mass. The restriction of available human tissue for the isolation of synaptosomes plays thus a critical factor when considering synaptosomal fraction isolation. In a study which isolated synaptosomes from post-mortem human cortex in context of AD, ~1g of tissue yielded sufficient synaptosomes suitable for consequent flow cytometry experiments (Postupna et al., 2014). Precise protocols have been adapted to enable the isolation of synaptosomal fractions from even smaller tissue amounts, with another study reporting the isolation of synaptosomes in tissue from human SN tissue, with sample masses in a range between 150mg-350mg (Plum et al., 2013).

The synaptosomal fraction isolation conducted for this thesis had ~600mg of starting material, from which sufficient protein was gathered for a subsequent proteomic profiling. A total of 2413 unique proteins were identified from the isolated synaptic fractions (**Figure 21B**). No significant differences in protein abundances between PD and CTRs were detectable in the DE analysis, which could be explained by the limited number of samples available for isolation. The high heterogeneity of samples retrieved from human tissue coupled with a small sampling size, likely played an important role in the comparison of protein abundances in the samples. This heterogeneity is especially evident in the CTRs, which is likely explained by the inherent variability of the individuals. In contrast to the PD group in which all patients most likely shared a very similar set of biological changes over several years, predominantly caused by the common denominator of PD, the CTR group shared no such condition, having in common solely the absence of a known neurodegeneration (**Figure 20**). Considering this, we analyzed the changes in the synaptosomal fraction with a less stringent approach, further assessing proteins based on p values of the Bayes-Empirical analysis prior to correction for multiple testing ($p < 0.05$). By this approach, we obtained a data set of 194 proteins, with almost equal amount with higher abundance (101) and lower abundance (93) in PD (**Figure 21B**).

Finally, for both the proteomic data sets obtained from whole tissue lysates as well as the synaptosomal fractions, it must be kept in mind that while post-mortem human tissue represents a unique opportunity to analyze neuropathology, it is inevitable to have deterioration in the samples in the period between the time of death of the patients and adequate storage. The quality of post-mortem human samples can be assessed via the post-mortem interval (PMI) (Stan et al., 2006; Blair et al., 2016). The PMI provides an estimate on the exposure time the samples had to factors such as temperature, moisture, pH and partial pressure of oxygen, which are widely recognized to influence the rate of decomposition (Clark et al., 1997). Several studies have shown feasible retrieval of intact nucleic acids and proteins in samples with PMIs surpassing 72h (Barton et al., 1993; Schramm et al.,

4. Discussion

1999; Yasojima et al., 2001), with caveats like phosphorylation in proteins, which has been shown to occur in less than a minute (Ahmed et al., 2011). Furthermore, variable vulnerability has been shown among proteins (Ferrer et al., 2007), with a higher vulnerability shown for synaptic proteins such as rab3a, rabphilin and alpha-synuclein (Ferrer et al., 2007) as well as syntaxin and PSD-95 (Siew et al., 2004).

In sum, our results show a quantifiable difference in the hippocampus of PD, with an altered abundance of several distinct proteins, which might represent the impact of PD on the hippocampus.

4.2 Biological relevance and biological processes impacted by dysregulation of hippocampal proteins in PD

In the 2089 unique proteins identified in the whole tissue lysate samples, we addressed changes in abundance by conducting a differential analysis. 55 proteins were differentially abundant in PD, with 37 being more abundant in PD and 18 presenting lower abundance in PD (**Figure 4**). Several of the DE proteins, had been previously described in other brain areas of PD, as well as in the context of neurodegeneration and dementia. Among the proteins evidencing a higher abundance in the hippocampus of PD, we identified a set of growth-associated proteins, brain acid soluble protein 1 (BASP1), myristoylated alanine-rich C-kinase substrate (MARCKS) and growth associated protein 43 (GAP43). Previous publications had described the involvement of GAP43 and BASP1 in the regulation of actin dynamics, mediating regenerative axonal growth as well as in synaptic vesicle cycling (Chung et al., 2020). In neurons, GAP43 and BASP1 can be found predominantly in axon terminals (Meiri et al., 1986; Widmer and Caroni, 1990), showing a downregulation after contributing to the establishment of the target connections (Chung et al., 2020), preserving however an elevated expression in regions of the adult brain implicated in learning and memory such as the neocortex and the hippocampus (Benowitz et al., 1988; Frey et al., 2000). Furthermore, in connection to synaptic vesicle cycling, GAP43 has been described to interact with the presynaptic vesicle fusion complex (Syntaxin, SNAP-25 and VAMP) (Haruta et al., 1997), while BASP1, a caspase-3 substrate (Han et al., 2013), has been described on synaptic vesicles (Yamamoto et al., 1997). These findings support a potential role in modulation of synaptic vesicle cycling and a consequent impact on neurotransmitter release and synaptic plasticity (Chung et al., 2020).

In addition, GAP43 has further been described in the context of PD, where mRNA levels were found to be lower in the SN of PD patients, suggesting a decreased regenerative response to the loss of dopaminergic neurons (Saal et al., 2017), in contrast to the elevated abundance we detected in the PD hippocampus, a possibly compensatory regenerative response to degeneration. A similar region-specific difference in dysregulation of GAP43 has also been shown in context of AD, where the frontal cortex shows decreased levels and the hippocampus presents increases (Davidsson et al., 1998; Bogdanovic et al., 2000; Rekart et al., 2004), while additionally levels of GAP43 in CSF are elevated, associated with tau and amyloid pathology (Sandelius et al., 2018).

Another set of proteins that was found to be more abundant in the hippocampus of PD are 14-3-3 protein isoforms YWHAH, YWHAQ and YWHAZ. The 14-3-3 proteins have been described to bind a vast number of proteins, among which are proteins associated to programmed cell death, transcriptional control of gene expression and structural and cytoskeletal proteins (Fu et al., 2000; Roberts, 2000; Van Hemert et al., 2001; Tzivion et al., 2001; Yaffe, 2002). General mechanisms of action for the 14-3-3 proteins include changes in the activity of bound ligands, altered association of bound ligands with other cellular components and changes in intracellular localization of the bound ligands (Yaffe, 2002). In PD, YWHAQ and YWHAZ had been previously found in LB of the SN of PD patients (Berg et al., 2003), while YWHAH was proven to strongly affect aSyn aggregation and kinetics (Plotegher et al., 2014). Moreover, YWHAH was one of the three proteins we found also dysregulated in the synaptosomal fraction, with a significant increase in abundance.

In addition to the individual proteins characterized as differentially abundant in the hippocampus of PD, we further characterized the PPI network of the DE proteins, coupled with a functional annotation analysis. The clustering of the PPI network showed the 14-3-3 isoforms at the nucleus of the biggest cluster, with strong interactions between 21 of the 55 DE proteins, while the second smaller cluster containing 13 proteins clustered around the growth associated proteins. The functional annotation analysis was highly representative of the clusters. Among the top enriched terms for *biological process*, several related to *localization*, with the majority of annotated proteins (19 proteins) present in the biggest cluster and 4 present in the smaller cluster. This result is in line with the known functions of the 14-3-3 isoforms, with high numbers of known ligands and a general mechanism of action mediating the change of localization of the bound ligands (Yaffe, 2002) (**Figure 6A; Figure 7A**).

Similarly, among the top terms enriched for *cellular compartment*, several are related to neuron projection and cytoskeleton, with the majority of annotated proteins corresponding to the

4. Discussion

cluster formed around growth associated proteins such as GAP43 and BASP1, once again in line with the known involvement of these proteins, further supporting the hypothesis of a compensatory mechanism being activated in the hippocampus in response to degeneration (**Figure 6A**; **Figure 7C**).

Widespread annotation of biological relevance was however observed in the highest term enriched for *biological processes*. The term cellular component organization or biogenesis annotated 32 of the proteins, nearly equally distributed amongst the two clusters and the non-clustering proteins. This broad annotation can most likely be explained by the variety of mechanisms described and encompassed in cellular component organization or biogenesis.

While cellular component organization or biogenesis encompasses multiple mechanisms, ribosomal proteins RPS16, RPS9 and RPL4 can be highlighted for their important role in ribosomal function and protein synthesis, mechanisms found to be relevant in neurodegenerative diseases such as PD and AD (Ding et al., 2005; Honda et al., 2005). In a study addressing protein synthesis alterations in PD, a region and stage-dependent dysregulation was shown for several ribosomal proteins, accompanied by an overall altered machinery for protein synthesis. In the substantia nigra, reduced expression of ribosomal rRNA was detected in the SN at Braak stages 3-4 and progressively decreasing in stages 5-6, pointing towards nucleolar stress, as well as a possible energy homeostasis preservation in acute stress situations. Furthermore, a correlation was established between the alteration of protein machinery and the presence of aSyn oligomeric species (Garcia-Esparcia et al., 2015). Our data show a similar dysregulation, with RPS16, RPS9 and RPL4 being less abundant in PD, suggesting a nucleolar stress in the hippocampus of PD. Ribosomal proteins RPS21 and RPL11 were also found to be less abundant in the synaptosomal fractions.

The division of the functional analysis into DE proteins with higher abundance and lower abundance in PD, further defined the main involvements annotated to the highly interacting DE protein clusters found in the undivided PPI network. The higher abundance proteins encompassed the majority of the proteins previously described in the main and the secondary clusters of the undivided PPI network, while the low abundance proteins, with only 17 proteins, present a smaller PPI network with less clustering (**Figure 6B-C**). In terms of functional annotation, the more abundant proteins still represent *biological processes* involved in *localization* as well as having top ranking terms such as *cytoskeleton* and *neuron projection for cellular compartments*.

Additional interesting terms surfacing through the division of the employed data set, are for example the involvement of *Proton-transport ATPase activity in molecular function*, annotating V-

type proton ATPase subunits B (ATP6V1B2) and H (ATP6V1H), which might indicate the involvement of a dysregulation of V-ATPase dependent lysosomal acidification, a mechanism known to be important in the clearance, signalling and energy metabolism process. In PD, the role of lysosomes in the elimination of misfolded proteins as well as damage mitochondria, positions lysosomal failure as a risk factor in aberrant toxic accumulation (Song et al., 2020).

In turn, the functional annotation of the proteins found in lower abundance shows multiple *biological processes* related to *translation*, annotating mainly the aforementioned ribosomal proteins RPS16, RPS9 and RPL4, suggesting that the lower abundant proteins are related to dysfunctional protein synthesis (**Figure 6B-C**).

Finally, we took advantage of the entire protein data set identified in the whole tissue lysates, as well as the data set of the synaptosomal fraction and rescaled the data set with both DE proteins and non-DE proteins, into sub-sets with smaller total protein numbers. This re-scaling of the considerably large proteomic data sets, conducted by grouping proteins with high similarity in protein expression patterns, yielded 10 modules of correlated proteins. Coupled with a functional annotation analysis, the individual modules of proteins with highly similar expression patterns, provided a scaffold of biological relevance to which DE proteins could be assigned, facilitating a more precise description of mechanisms impacted by the dysregulated abundances of individual DE proteins.

The functional annotation of the 55 DE proteins already hinted towards several mechanisms possibly represented by the dysregulation in abundance of diverse proteins in the hippocampus of PD including increased abundance of growth related proteins associated with a possible compensatory mechanism, increased chaperone-like protein abundance related to localization and transport as well as LB and aSyn aggregation and decreased ribosomal proteins and lysosome regulating V-type ATPases related to altered protein synthesis and lysosomal failure. The scaffold provided by the rescaled modules, further broadened the possibly implied mechanisms, mainly adding the involvement of the mitochondrion and synapse, while supporting the findings of cytoskeleton and ribosomal involvement (**Figure 25**).

The majority of DE proteins (17%) were assigned to the largest module, W01. The functional annotation of this module revealed a strong enrichment for mitochondrial transport in *biological processes* and several mitochondrial parts in terms of *cellular compartment*. In line with this, complex I subunit NADH dehydrogenase iron-sulfur protein 7 (NDUFS7) and mitochondrial Rho GTPase 1 (RHOT1) were found downregulated in the synaptosomal fractions. Mitochondrial dysfunction and

4. Discussion

oxidative stress are well known factors involved in PD (Schapira and Jenner 2011; Schapira, 2008; Bueler, 2009), with mitochondrial complex I activity shown to be reduced in the Substantia nigra in PD (Parker et al., 1989). Further studies of synaptosomes of PD samples, showed furthermore a significant reduction of several mitochondrial proteins involved in mitochondrial translation in the SNpc of PD patients (Plum et al., 2020).

The third largest module, module W03, with 14 DE proteins, was further identified as highly representative of the synaptic compartment, with YWHAZ, SYN1 and NPTX1 being the DE annotated to several of the functional terms such as *synaptic vesicle cycle*, *regulation of transsynaptic signalling* and *synapse organization* (**Figure 11**). This module was further complemented with the largest module detected for the synaptosomal fractions, S01, which shared a highly similar functional annotation, with a very high representation of the synaptic compartment, while further having the receptor of NPTX1, neuronal pentraxin receptor (NPTXR) as a DE protein (**Figure 26**).

In line with this, NPTX1 had been previously implicated in neuronal survival, synaptic pruning and synaptic plasticity, as well as mitochondrial transport and mitochondrial fragmentation (Clayton et al., 2012; Figueiro-Silva et al., 2015; Gyöffry et al. 2018), and has been shown to contribute to amyloid- β overexpression and amyloid- β evoked neuronal damage (Abad et al., 2006). In context of neurodegenerative diseases, while not having been previously described in connection to PD, it was proposed as a biomarker for AD, with a correlation between increased levels in CSF and progression in cognitive decline from mild cognitive impairment to early dementia (Ma et al., 2018). The dysregulation of NPTX1 abundance that we observed in the hippocampus of PD might thus be representative of a synaptic dysfunction, a mechanism having already been implicated as an important early occurrence in the midbrain of PD (Schirinzi et al., 2016).

Finally, we addressed the similitudes between our findings on the changes of protein abundances in the human PD hippocampus and the changes in an animal model of PD. To this end, we quantified protein expression levels in the hippocampus and the cerebellum of transgenic mice expressing the human A53T aSyn variant. In humans the Ala53Thr mutation is a rare mutation (Vaughan et al., 1998; Payami et al., 1998) causing a parkinsonian syndrome, which shows a very similar course to idiopathic PD. Patients with this mutation have however some variants to idiopathic PD, such as an earlier onset with a more rapid course, lower incidence of tremor and a high incidence of dementia (Golbe et al., 1996; Gasser, 1998; Bajaj et al., 1998).

The expression of the human aSyn mutation in mice induces synaptic deficits before the onset of motor dysfunction as well as presenting significant synaptic transmission deficits, with older mice exhibiting motor dysfunction accompanied by cognitive impairment such as spatial memory deficits (Paumier et al., 2013). Together, these characteristics suggested the A53T mouse model as an interesting model in terms of similitudes in synaptic dysfunction and changes to the hippocampus of the host organism. We found a very sparse overlap in terms of dysregulation of proteins in both proteomic data sets, with only SYN1 and NPTX1 being significantly altered in humans and mice alike, with SYN1 being dysregulated in both the hippocampus and the cerebellum of young (250 days old) and old (400 days old) animals, whereas NPTX1 was found dysregulated solely in the cerebellum of old animals (400 days).

The limited overlap of proteins found to be dysregulated might be due to the distribution of aSyn inclusions in the transgenic animals. It was shown, that while the PD mouse model shares many similarities with PD and DLB in the localization of pathological lesions, the broad spread of aSyn inclusions in somato-dendritic compartments excludes some brain areas, leading to less aSyn pathology in the hippocampus (Giasso et al., 2002). This is different to the findings of late-stage PD in humans, where an increased degeneration of the hippocampus has been linked to the severity of the LB pathology, as well as being correlated to dementia (Harding and Halliday, 2001; Apaydin et al., 2002; Arnold et al., 2013; Hall et al., 2014).

In sum, we were able to further characterize the differences detected in the PD hippocampus, identifying several mechanisms possibly affected by the altered abundance of individual proteins in the hippocampus of PD. We showed the potential involvement of mechanisms such as a compensatory mechanism with increased abundance of growth-related proteins, a mitochondrial dysfunction with special focus on a dysfunction of the complex I, as well as mitochondrial fragmentation, an altered protein synthesis with a lower abundance of several ribosomal proteins and a synaptic dysfunction with the dysregulation of proteins involved in synaptic vesicle cycles, synaptic plasticity and neuronal excitability as well as synaptic pruning.

4.3 Changes in synaptic morphology caused by modulation of NPTX1 in primary mouse cultures

Based on the different mechanisms identified by the functional annotation analyses of the DE proteins in human PD hippocampus, we focused on one protein of interest that was further analyzed. In line with our initial interest in synaptic dysfunction, we selected NPTX1 as our target protein because of its role in synaptic pathology in other neurodegenerative disorders and the limited knowledge on this protein in PD.

We assessed the impact of increased NPTX1 abundance by modelling increased NPTX1 levels in primary mouse hippocampal cultures and quantifying morphological changes in the synapse. It was previously shown in an experiment of oxygen glucose deprivation, that secreted NPTX1 present in the culture medium of cells overexpressing NPTX1, induced the same toxicity in WT when exposed to the conditioned medium containing secreted NPTX1. Furthermore, the chronic treatment of organotypic hippocampal slices with recombinant NPTX1 supplied via the culture medium showed an increase in paired-pulse ratio in CA3-CA1 hippocampal synapses, indicative of a decrease in glutamate release, in a study conducted in the context of AD (Cummings et al., 2017).

Following a similar approach, we increased the abundance of NPTX1 in cultured hippocampal neurons by the addition of recombinant NPTX1 and showed a significant change in synapse morphology, with synapses of NPTX1-treated cells showing significantly smaller areas, as well as presenting an overall stubbier form (**Figure 29**).

Dendritic spine loss has been previously shown to be induced by aSyn aggregates in presynaptic compartments, which correlated to a significant decrease in postsynaptic scaffolding proteins PSD95 and debrin (Schulz-Schaeffer, 2010). Furthermore, NPTX1 had been shown to negatively regulate synaptophysin as well as PSD95 expression levels, with a knockdown of NPTX1 using shRNA significantly increasing the proteins levels of synaptophysin and PSD95 in cortical neurons, while the overexpression showed a reduction of ~30% in protein abundance (Figueiro-Silva et al., 2015).

The morphological changes that we observed in context of increased NPTX1 in hippocampal synapses of cultured cells combined with the known involvement of NPTX1 in synaptic plasticity and pruning, underscore synaptic dysfunction as early mechanism in the PD hippocampus.

Chapter 5: Concluding remarks

The experiments conducted for this doctoral project, provided some novel perspectives on the involvement of the hippocampus in the progression of late-stage cognitive decline in PD. Recent advances in the handling of high-throughput proteomics data with novel algorithms, such as WGCNA, facilitated the identification of functionally relevant protein clusters and thus provided insights to the molecular events contributing to hippocampal degeneration. The use of human samples in this project provided both advantages as well as challenges. It enabled a direct characterization of pathological changes in the organism of interest, but also introduced complexity by analysing one single timepoint in a progressive pathology, particularly as this time point represents end-stage phenomena in post-mortem samples. However, the findings presented here might contribute to the identification of novel therapeutic targets for PD, deepening our understanding of the changes in the late-stage PD hippocampus.

By means of mass spectrometry, we identified 55 proteins with differential abundance in the post-mortem samples of the hippocampus of PD patients, some of which had previously been addressed in the midbrain of PD patients.

Increased abundance in the PD hippocampus was observed for proteins known to be involved in the modulation of cytoskeleton dynamics as well as growth cone modulation, while previous studies showed a significant decrease of these proteins in the nigrostriatal area, a finding, which might hint towards compensatory mechanism taking place in the hippocampus in response to the longer accumulated insult to the midbrain. Moreover, we found an increased abundance of chaperone proteins in the hippocampus, which had been previously found in LB in the SN of PD patients and which were shown to have strong effects on aSyn aggregation and kinetics, a finding in line with the known increase in LB burden in the hippocampus correlated to dementia in PD.

In addition, the differential abundance of proteins in the hippocampus of PD further implied an impact in transport and localization of proteins, supported by the observed dysregulation of chaperone proteins often involved in translocation and altered subcellular localization of ligand proteins. Furthermore, diminished abundances of a complex I subunit and an enzyme involved in mitochondrial transport were identified, hinting to potential mitochondrial dysfunction in the hippocampus of PD.

5. Concluding remarks

Moreover, the increased abundance of several ribosomal proteins, both 40S and 60S subunits, suggests an increase in demand of protein synthesis, a concept supporting a compensatory mechanism, which is also suggested by the increase in abundance of growth-related proteins in the PD hippocampus.

Together, the proteomic profiling of hippocampal samples of PD patients revealed several levels of dysregulation in the as a biomarker, with increases in abundance correlated to progression of mild cognitive impairment to early dementia.

Moreover, our study described morphological changes in synapses, resulting from an artificial increase of NPTX1 in hippocampal primary neuronal cultures, further supporting a role of NPTX1 in a synaptic pathology.

Together, our findings suggest NPTX1 as an interesting target protein to be further characterized for its role in synaptic degeneration in PD.

In sum, the findings gathered in this thesis, provide an additional perspective on the alterations present in the hippocampus of late-stage PD, identifying mechanisms underlying the progression of the disease. Among the described mechanisms, synaptic dysfunction in the hippocampus was addressed, identifying a specific protein of interest, NPTX1. Our findings thus provide new insight to synaptic alterations present in the hippocampus and may contribute to the identification of novel therapeutic strategies for PD, particularly for cognitive decline as a late-stage complication of the disease.

Chapter 6: Summary

The scientific, technological, and medical advances of the last decades have significantly improved the life quality and life expectancy for humans. However, with longer life spans, age-dependent neurodegenerative diseases such as Parkinson's disease have seen a rapid increase in prevalence worldwide, constantly growing alongside the increase of the elderly population. The resulting burden of PD on the patients suffering from it significantly increases as the disease progresses, with late stages frequently being accompanied by cognitive decline and dementia. The resulting impact on patients, loved ones and the healthcare system, make the late-stage complications of PD a serious challenge to be addressed.

To date, the exact molecular mechanism behind the PD pathology remain elusive and contribute to the lack of curative treatments. Available treatments focus on the mitigation of motor and non-motor symptoms, not being able to provide protection against the progressive neurodegeneration. In late stages, the accumulated insult leads in the vast majority of patients to cognitive decline and the development of dementia, a severe complication, for which there is currently no treatment available. Profiling the expression changes of proteins in the hippocampus of late-stage PD patients, might broaden our knowledge on the pathological events in place, increasing the odds to address the mechanisms involved in search for novel therapeutic strategies for late stage PD.

In this doctoral project, the alterations in the hippocampus elicited by PD were addressed by quantifying changes in protein expression levels of human hippocampal PD samples. Several proteins were found to be differentially abundant in PD, with a subset of proteins having been previously described either in the context of PD in the nigrostriatal area, or in diverse brain areas of other neurodegenerative diseases including Alzheimer's disease. Moreover, the characterization of our proteomic data provided insights to a wide range of biological processes possibly impacted by the differential abundance of individual proteins, including altered transport and localization, cytoskeletal modulation, apoptosis-related processes and synaptic modulation.

Furthermore, the characterization of our proteomic data set, via a network analysis, complemented with a background search of previously published literature, facilitated the identification of neuronal pentraxin 1 (NPTX1) as a promising target protein related to synaptic alterations in the hippocampal pathology of PD. In turn, modelling its extracellular increase in

6. Summary

primary mouse hippocampal cell cultures, showed a significant change in the morphology of synapses. Hippocampal neurons exposed to increased levels of NPTX1 showed synapses with significantly smaller areas and an overall rounder shape.

All in all, these findings suggest a novel role for NPTX1. Whereas NPTX1 had been previously described in context of other forms of dementia correlating increased expression levels to cognitive decline and was characterized in the modulation of synaptic proteins, synapse density and synaptic plasticity, to our knowledge this is the first description of NPTX1 in the context of a synaptic pathology in the hippocampus of PD patients. Further in-depth analyses of the underlying mechanisms involved in the insult to the hippocampus in PD, combined with a detailed characterisation of the dysregulation of NPTX1 and the consequent impact on the hippocampal pathology, may contribute to a better treatment of late-stage cognitive decline in PD, significantly improving the life quality of people suffering from Parkinson's disease.

7. References

A

- Abad, M.A., et al. (2006). Neuronal Pentraxin1 Contributes to the Neuronal Damage Evoked by Amyloid- β and Is Overexpressed in Dystrophic Neurites in Alzheimer's Brain. *J Neurosci* 26(49), 12735-12747.
- Abbott, R.D., et al. (2001). Frequency of bowel movements and the future risk of Parkinson's disease. *Neurology* 57(3), 456-462.
- Adcock, R.A., et al. (2006). Reward-motivated learning: mesolimbic activation precedes memory formation. *Neuron* 50, 507–17.
- Agid, Y. (1991). Parkinson's disease: pathophysiology. *The Lancet* 337, 1321-1324.
- Ahmed, S., et al. (2011). Data-driven modelling reconciles kinetics of ERK phosphorylation, localization, and activity states. *Mol Syst Biol* 10, 718.
- Akiyama, H. et al., (19991). Association of amyloid P component with complement proteins in neurologically diseased brain tissue. *Brain Res* 548, 349-352.
- Alafuzoff, I., et al. (2009). Staging/typing of Lewy body related α -synuclein pathology: a study of the BrainNet Europe Consortium. *Acta Neuropathol* 117, 635–652.
- Apaydin, H., et al. (2002). Parkinson disease neuropathology: later-developing dementia and loss of the levodopa response. *Arch Neurol* 59, 102–112.
- Appel-Cresswell, S., et al. (2013). Alpha-synuclein p.H50Q, a novel pathogenic mutation for Parkinson's disease. *Mov. Disord.* 28, 811–813.
- Arnold, S.E., et al. (2013). Comparative survey of the topographical distribution of signature molecular lesions in major neurodegenerative diseases. *J Comp Neurol* 521, 4339–4355.
- Aybeck, S., et al. (2009). Hippocampal atrophy predicts conversion to dementia after STN-DBS in Parkinson's disease. *Parkinsonism Relat Disord* 15, 521–524.

B

- Barton, A. J. L., et al. (1993). Pre- and postmortem influences on brain RNA. *J Neurochem* 61, 1– 11.
- Bartus, R.T., et al. (1982). The cholinergic hypothesis of geriatric memory dysfunction. *Science*. 217(4558), 408–414.
- Bajaj, N.P.S., et al. (1998). The genetics of Parkinson's disease and parkinsonian syndromes. *J Neurol* 245, 625-633.
- Beach, T.G., et al. (2010). Multi-organ distribution of phosphorylated alpha-synuclein histopathology in subjects with Lewy body disorders. *Acta Neuropathol* 119(6), 689-702.
- Benowitz, L.I., et al. (1988). Anatomical distribution of the growth-associated protein GAP-43/B-50 in the adult rat brain. *J Neurosci* 8(1), 339-352.
- Berg, D., et al. (2003). Specification of 14-3-3 proteins in Lewy bodies. *Annals Neurol* 54, 135.
- Blair, J.A., et al. (2016). Individual case analysis of postmortem interval time on brain tissue preservation. *PLoS One* 11, e0151615.
- Blauwendraat, C., et al. (2019). The genetic architecture of Parkinson's disease. *Lancet Neurol* 19, 170–178.
- Bogdanovic, N., et al. (2000). Growth-associated protein GAP-43 in the frontal cortex and

7. References

in the hippocampus in Alzheimer's disease: an immunohistochemical and quantitative study. *J Neural Transm* 107, 463–478.

- Boiten, W.A., et al. (2021). Pathologically Decreased CSF Levels of Synaptic Marker NPTX2 in DLB Are Correlated with Levels of Alpha-Synuclein and VGF. *Cells* 10, 38.
- Bueler, H. (2009). Impaired mitochondrial dynamics and function in the pathogenesis of Parkinson's disease. *Exp Neurol* 218, 235-246.
- Braak, H. et al. (2003). Staging of brain pathology related to sporadic Parkinson's disease. *Neurobiol Aging* 24, 194-211.
- Braak, H., et al. (2006). Gastric alpha-synuclein immunoreactive inclusions in Meissner's and Auerbach's plexuses in cases staged for Parkinson's disease-related brain pathology. *Neurosci Lett* 396(1), 67-72.
- Bredesen, D. E., et al. (2006). Cell death in the nervous system. *Nature*, 443(7113), 796–802.
- Brooks, D.J. (2007). Imaging non-dopaminergic function in Parkinson's disease. *Mol Imaging Biol* 9, 217–222.
- Burke, R.E. and O'Malley, K. (2013). Axon degeneration in Parkinson's disease. *Exp Neurol* 246, 72-83.
- Butler, P.J., et al. (1990). Pentraxin-chromatin interactions: serum amyloid P component specifically displaces H1-type histones and solubilizes native long chromatin. *J Exp Med* 172, 13-18.

C

- Calabresi, P., et al. (2013). New experimental and clinical links between the hippocampus and the dopaminergic system in Parkinson's disease. *Lancet Neurol* 12, 811-821.
- Caldi Gomes, L.A. (2019). Multi-omics analysis of human brain tissue and an animal model of Parkinson's Disease. (Doctoral dissertation, Georg August Universität Göttingen). Retrieved from: eDiss Dissertations at Georg-August Universität Göttingen.
- Cesca, F., et al. (2010). The synapsins: Key actors of synapse function and plasticity. *Progr Neurobiol* 91(4), 313-348.
- Chapuis, S., et al. (2005). Impact of the motor complications of Parkinson's disease on the quality of life. *Mov Dis* 20, 224-230.
- Charbonnier-Baupel, F., et al. (2015). Gene expression analyses identify narp contribution in the development of L-DOPA-induced Dyskinesia. *J Neurosci* 35, 96-111.
- Chaudhuri, K.R., et al. (2006). National Institute for clinical excellence. Non-motor symptoms of Parkinson's disease: diagnosis and management. *Lancet Neurol* 5(3), 235–245.
- Chaudhuri, K.R. and Schapira, A.H. (2009). Non-motor symptoms of Parkinson's disease: dopaminergic pathophysiology and treatment. *Lancet Neurol* 8, 464–474.
- Chin, L.S., et al. (1995). Impairment of axonal development and of synaptogenesis in hippocampal neurons of synapsin I-deficient mice. *Proc Natl Acad Sci USA* 92, 9230-9234.
- Cho, R.W., et al. (2008). mGluR1/5-dependent long-term depression requires the regulated ectodomain cleavage of neuronal pentraxin NPR by TACE. *Neuron* 57, 858-871.
- Chung, C.Y., et al. (2009). Dynamic changes in presynaptic and axonal transport proteins combined with striatal neuroinflammation precede dopaminergic neuronal loss in a rat model of AAV alpha-synucleinopathy. *J Neurosci* 29, 3365–3373.
- Chung, D., et al. (2020). GAP-43 and BASP1 in Axon Regeneration: Implications for the Treatment of Neurodegenerative Diseases. *Front. Cell Dev Biol* 8:567537.
- Clark, M.A., et al. (1997). Postmortem changes in soft tissues. *Forensic Taphonomy: The Postmortem Fate of Human Remains*, CRC Press, Boca Raton, Florida, 151-160.

- Clayton, K.B., et al. (2012). NP1 Regulates Neuronal Activity-Dependent Accumulation of BAX in Mitochondria and Mitochondrial Dynamics. *Neurobio Dis* 32(4), 1453-1466.
- Conolly, B.S. and Lang, A.E. (2014). Pharmacological Treatment of Parkinson Disease A Review. *JAMA* 311(16), 1670-1683.
- Cummings, D.M., et al. (2017). Neuronal and Peripheral Pentraxins Modify Glutamate Release and may Interact in Blood-Brain Barrier Failure. *Cerebr Cortex* 27(6), 3437-3448.

D

- Darby, R.R., et al. (2019). Network localization of heterogeneous neuroimaging findings. *Brain* 142, 70–79.
- Davidsson, P., et al. (1983). Neurochemical dissection of synaptic pathology in Alzheimer's disease. *Int Psychogeriatr* 10, 11–23.
- De Camilli, P., et al. (1983). Synapsin I (protein I), a nerve terminal-specific phosphoprotein. I. Its general distribution in synapses of the central and peripheral nervous system demonstrated by immunofluorescence in frozen and plastic sections. *J Cell Biol* 96, 1337-1354.
- De Lau, L.M.L and Breteler, M.M.B (2006). Epidemiology of Parkinson's disease. *Lancet Neurol* 5, 525-535.
- De Gregorio-Rocasolano, N., et al. (2001). Overexpression of neuronal pentraxin 1 is involved in neuronal cell death evoked by low K(+) in cerebellar granule cells. *J Biol Chem* 276, 796-803.
- Dexter, D.T. and Jenner, P. (2013). Parkinson disease: from pathology to molecular disease mechanisms. *Free Radi Bio and Med* 62, 132-144.
- Ding, Q., et al. (2005). Ribosome dysfunction is an early event in Alzheimer's disease. *J Neurosci* 25, 9171–9175.
- Diógenes, M.J., et al. (2012). Extracellular alpha-synuclein oligomers modulate synaptic transmission and impair LTP via NMDA-receptor activation. *J Neurosci* 32, 11750–11762.
- Dodds, D.C., et al. (1997). Neuronal pentraxin receptor, a novel putative integral membrane pentraxin that interacts with neuronal pentraxin 1 and 2 and taipoxin-associated calcium-binding protein. *J Biol Chem* 272, 21488-21494.
- Docherty, M.J. and Burn, D.J. (2010). Parkinson's disease dementia. *Curr Neurol Neurosci Rep* 10(4), 292–298.
- Dorsey, E.R., et al. (2018). The emerging evidence of The Parkinson pandemic. *J Parkin Dis* 8(s1), S3-S8.
- Downton, S.B. and McGrew, S.D. (1990). Rat serum P amyloid component. Analysis of cDNA sequence and gene expression. *Biochem* 270, 553-556.
- Du Clos, T.W. (1989). C-reactive protein interacts with the UI small nuclear ribonucleoprotein. *J Immunol* 143, 2553-2559.
- Du Clos, T.W. (1996). The interaction of C-reactive protein and serum amyloid P component with nuclear antigens. *Mol Biol Rep* 23, 253-260.
- Duits, F.H., et al. (2018). Synaptic proteins in CSF as potential novel biomarkers for prognosis in prodromal Alzheimer's disease. *Alz Res Therapy* 10, 5.

E

- Emre, M., et al. (2007). Clinical diagnostic criteria for dementia associated with Parkinson's disease. *Mov Disord* 22(12), 1689–1707.
- Exner, N., et al. (2012). Mitochondrial dysfunction in Parkinson's disease: molecular

7. References

mechanisms and pathophysiological consequences. *The EMBO Journal* *31*(14), 3038–3062.

F

- Ferrer, I., et al. (2007). Brain protein preservation largely depends on the postmortem storage temperature: implication for study of proteins in human neurologic diseases and management of brain banks: a BrainNet Europe Study. *J Neuropathol Exp Neurol* *66*, 35-46.
- Figueiro-Silva, J., et al. (2015). Neuronal Pentraxin 1 Negatively Regulates Excitatory Synapse Density and Synaptic Plasticity. *J Neurosci* *35*(14), 5504-5521.
- Fox, N.C., et al. (1996). Presymptomatic hippocampal atrophy in Alzheimer's disease. A longitudinal MRI study. *Brain* *119* (Pt 6), 2001–2007.
- Frank, M.J., et al. (2004). By carrot or by stick: cognitive reinforcement learning in parkinsonism. *Science* *306*, 1940-1943.
- Frey, D., et al. (2000). Shared and unique roles of CAP23 and GAP43 in actin regulation, neurite outgrowth, and anatomical plasticity. *Cell Biol* *149*(7), 1443-1454.
- Fu, H., et al. (2000). Document details - 14-3-3 Proteins: Structure, function, and regulation. *Annu Rev Pharmacol and Toxicol* *40*, 617-647.

G

- Garcia-Esparcia, P., et al. (2015). Altered machinery of protein synthesis region- and stage-dependent and is associated with α -synuclein oligomers in Parkinson's disease. *Act Neuropath Commu* *3*(1), 1-25.
- Garlanda, C., et al. (2005). Pentraxins at the crossroads between innate immunity, inflammation, matrix deposition, and female fertility. *Annu Rev Immunol* *23*, 337-366.
- Gasser, T. (1998). Genetics of Parkinson's disease. *Clin Genet* *54*, 259-265.
- GBD 2016 Neurology Collaborators (2019). Global, regional, and national burden of neurological disorders, 1990–2016: a systematic analysis for the global burden of disease study 2016. *Lancet Neurol* *18*(5), 459-480.
- Gerlach, M., et al. (1991). MPTP mechanisms of neurotoxicity and their implications for Parkinson's disease. *European J of Pharma: Mol Pharma* *208*(4), 273–286.
- Gewurz, H., et al. (1995). Structure and function of the pentraxins. *Curr Opin Immunol* *7*(1), 54-64.
- Giasson, B.I., et al. (2002) Neuronal α -Synucleinopathy with Severe Movement Disorder in Mice Expressing A53T Human α -Synuclein. *Neuron* *34*(4), 521-533.
- Gillet, L.C., et al. (2012). Targeted data extraction of the MS/MS spectra generated by data-independent acquisition: a new concept for consistent and accurate proteome analysis. *Mol Cell Proteom* *11*, O111.016717.
- Goetz, C.G. (2003). Treatment of advanced Parkinson's disease: an evidence-based analysis. *Adv Neurol* *91*, 213-228.
- Golbe, L., et al. (1996). Clinical genetic analysis of Parkinson's disease in the Contursi kindred. *Ann Neurol* *40*, 767-775.
- Gonera, E.G., et al. (1997). Symptoms and duration of the prodromal phase in Parkinson's disease. *Mov Dis* *12*(6), 871-876.
- Grace, A.A., et al. (2007). Regulation of firing of dopaminergic neurons and control of goal-directed behaviors. *Trends Neurosci* *30*, 220-227.
- Gulyássi, P., et al. (2020). Proteomic comparison of different synaptosome preparation procedures. *Amino Acids* *52*, 1529-1543.
- Gyöffry, B.A., et al. (2018). Local apoptotic-like mechanisms underlie complement-mediated synaptic pruning. *PNAS* *115*, 6303-6308.

H

- Halgin, R., et al. (1977). Levodopa, parkinsonism, and recent memory. *J Nerv Ment Dis* 164(4), 268–272.
- Hall, H., et al. (2014). Hippocampal Lewy pathology and cholinergic dysfunction are associated with dementia in Parkinson's disease. *Brain* 137, 2493–2508.
- Hammad, H. and Wagner, J.J. (2006). Dopamine-mediated disinhibition in the CA1 region of rat hippocampus via D3 receptor activation. *J Pharmacol Exp Ther* 316, 113–20.
- Han, H.Q. and Greengrad, P. (1994). Remodeling of cytoskeletal architecture of nonneuronal cells induced by synapsin. *Proc Natl Acad Sci USA* 91, 8557-8561.
- Han, M.H., et al. (2013). The novel caspase-3 substrate Gap43 is involved in AMPA receptor endocytosis and long-term depression. *Mol Cell Proteomics* 12(12), 3719-3731.
- Harding, A.J. and Halliday, G.M. (2001). Lewy body pathology in the diagnosis of dementia. *Acta Neuropathol* 102, 355–363.
- Haruta, T., et al. (1997). Ca²⁺-dependent interaction of the growth-associated protein GAP-43 with the synaptic core complex. *Biochem J* 325 (Pt 2), 455-463.
- Hely, M.A., et al. (2008). The Sydney multicenter study of Parkinson's disease: the inevitability of dementia at 20 years. *Mov Disord* 23(6), 837–844.
- Hicks, P.S., et al. (1992). Serum amyloid P component binds to histones and activates the classical complement pathway. *J Immunol* 149, 3689-3694.
- Hind, C.R., et al. (1984). Binding specificity of serum amyloid P component for the pyruvate acetal of galactose. *J Exp Med* 159, 1058-1069.
- Hirsch, E.C. and Hunot, S. (2009). Neuroinflammation in Parkinson's disease: a target for neuroprotection? *The Lancet Neurol* 8, 382-397.
- Honda, K., et al. (2005). Ribosomal RNA in Alzheimer disease is oxidized by bound redox-active iron. *J Biol Chem* 280, 20978–20986.
- Hossain, M.A., et al. (2004). Neuronal Pentraxin 1: A Novel Mediator of Hypoxic-Ischemic Injury in Neonatal Brain. *Neurobiol Dis* 24(17), 4187-4196.
- Huang, Q., et al. (2015). SWATH enables precise label-free quantification on proteome scale. *Proteomics* 15, 1215-1223.
- Hughes, C.S., et al. (2019). Single-pot, solid-phase-enhanced sample preparation for proteomics experiments. *Nature protocols* 14(1), 68.

I

- Irwin, D.J., et al. (2012). Neuropathologic substrates of Parkinson disease dementia. *Ann. Neurol* 72, 587-98.

•

J

- Jacobson, R.D., et al. (1986). A protein associated with axon growth, GAP-43, is widely distributed and developmentally regulated in rat CNS. *Neurosci* 6(6), 1843-1855.
- Janetzky, B., et al. (1994). Unaltered aconitase activity, but decreased complex I activity in substantia nigra pars compacta of patients with Parkinson's disease. *Neurosci Letters* 169(1-2), 126–128.
- Jankovic, J. (2008). Parkinson's disease: Clinical features and diagnosis. *J of Neurol, Neurosurg & Psychiatry* 79(4), 368–376.
- Johnson, M.E. et al. (2019). Triggers, Facilitators and Aggravators: Redefining Parkinson's Disease Pathogenesis. *Trends in Neurosci* 13, 15.

7. References

- Jones, D.H., et al. (1995). Isoforms of 14-3-3 protein can form homo- and heterodimers in vivo and in vitro: implications for function as adapter proteins. *FEBS Letters* 368(1), 55-58.

K

- Kalaria, R.N., et al. (1991) Widespread serum amyloid P immunoreactivity in cortical amyloid deposits and the neurofibrillary pathology of Alzheimer's disease and other degenerative disorders. *Neuropathol Appl Neurobiol* 17, 189-201.
- Kandel, E.R., et al. (2000). Principles of neural science. New York: Mc Graw-Hill, Health Professions Division.
- Katzenschlager, R. And Lees, A.J. (2004). Olfaction and Parkinson's syndromes: its role in differential diagnosis. *Curr Opin Neurol* 17(4), 417-423.
- Kehagia, A.A., et al. (2010). Neuropsychological and clinical heterogeneity of cognitive impairment and dementia in patients with Parkinson's disease. *Lancet Neurol* 9, 1200–1213.
- Kempster, P.A., et al. (2010). Relationships between age and late progression of Parkinson's disease: a clinic-pathological study. *Brain* 133, 1755-62.
- Ki, C.S., et al. (2007). The Ala53Thr mutation in the a-synuclein gene in a Korean family with Parkinson disease. *Clin. Genet.* 71, 471–473.
- Kim, M.J., et al. (2003). The heparan sulfate proteoglycan agrin modulates neurite outgrowth mediated by FGF-2. *J Neurobiol* 55(3), 261-277.
- Kirkpatrick, L. L., et al. (200). Biochemical interactions of the neuronal pentraxins. Neuronal pentraxin (NP) receptor binds to taipoxin and taipoxin-associated calcium binding protein 49 via NP1 and NP2. *J Biol Chem* 275, 17786-17792.
- Kitada, T., et al. (1998). Mutations in the parkin gene cause autosomal recessive juvenile parkinsonism. *Nature* 392(6676), 605–8.
- Kobayashi, K. and Suzuki, H. (2007). Dopamine selectively potentiates hippocampal mossy fiber to CA3 synaptic transmission. *Neuropharmacology* 52, 552–561.
- Koch, S.M. and Ullian, E.M. (2010). Neuronal pentraxins mediate silent synapse conversion in the developing visual system. *J Neurosci* 30, 5404-5414.
- Kövari, E., et al. (2003). Lewy body densities in the entorhinal and anterior cingulate cortex predict cognitive deficits in Parkinson's disease. *Acta Neuropathol* 106(1), 83–88.
- Krüger, R., et al. (1998). Ala30Pro mutation in the gene encoding alpha-synuclein in Parkinson's disease. *Nat. Genet.* 18, 106–108.

L

- Lachén-Montes, M., et al. (2018). Unveiling the olfactory proteostatic disarrangement in Parkinson's disease by proteome-wide profiling. *Neurobiol of Aging* 73, 123-134.
- Langfelder, P. and Horvath, S. (2008). WGCNA: an R package for weighted correlation network analysis. *BMC Bioinformatics* 9, 559.
- Lanskey, J.H., et al. (2018). Can neuroimaging predict dementia in Parkinson's disease? *Brain* 141, 2545–2560.
- Lázaro, D.F., et al. (2014). Systematic Comparison of the Effects of Alpha-synuclein Mutations on Its Oligomerization and Aggregation. *PLoS Genet* 10.
- Lee, S., et al. (2010). LRRK2 kinase regulates synaptic morphology through distinct substrates at the presynaptic and postsynaptic compartments of the Drosophila neuromuscular junction. *J Neurosci* 30, 16959–16969.
- Lees, A.J. (2007). Unresolved issues relating to the shaking palsy on the celebration of

- James Parkinson's 250th birthday. *Mov Dis*, 22 *Suppl 1*, S327–34.
- Lesage, S., et al. (2013). G51D α -synuclein mutation causes a novel Parkinsonian-pyramidal syndrome. *Ann. Neurol.* 73, 459–471.
 - Liao, Y., et al. (2019). WebGestalt 2019: gene set analysis toolkit with revamped UIs and APIs, *Nuclei Aci Res* 47, W199-W205.
 - Licker, V., et al. (2014). Proteomic analysis of human substantia nigra identifies novel candidates involved in Parkinson's disease pathogenesis. *Proteomics* 14(6), 784-94.
 - Lim, S.-Y., et al. (2009). Overview of the Extranigral Aspects of Parkinson Disease. *Arch Neurol* 66(2), 167-172.
 - Lisman, J.E. and Grace, A.A. (2005). The hippocampal-VTA loop: controlling the entry of information into long-term memory. *Neuron* 46, 703–713.
 - Lisman, J., et al. (2011). A neo-Hebbian framework for episodic memory; role of dopamine dependent late LTP. *Trends Neurosci* 34, 536–547.
 - Liu, A.K.L, et al. (2019). Hippocampal CA2 Lewy pathology is associated with cholinergic degeneration in Parkinson's disease with cognitive decline. *Acta Neuropathol Commun* 7, 61.
 - Loveless, R.W., et al. (1992). Human serum amyloid P is a multispecific adhesive protein whose ligands include 6-phosphorylated mannose and the 3-sulphated saccharides galactose, N-acetylgalactosamine and glucuronic acid. *EMBO J* 11, 813-819.
 - Lu, L., et al. (2005). Gene expression profiling of Lewy body-bearing neurons in Parkinson's disease. *Exp Neurol* 195, 27-39.

M

- Ma, Q., L., et al. (2018). Neuronal pentraxin 1: a synaptic-derived plasma biomarker in Alzheimer's disease. *Neurobiol of disea* 114, 120-128.
- Mak, E., et al. (2015). Baseline and longitudinal grey matter changes in newly diagnosed Parkinson's disease: ICICLE-PD study. *Brain* 138, 2974–2986.
- Mann, V. M., et al. (1994). Complex I, iron, and ferritin in Parkinson's disease substantia nigra. *Annals of Neurology* 36(6), 876–881.
- Marsden, C.D. (1994). Problems with long-term levodopa therapy for Parkinson's disease. *Clin Neuropharmacol* 17(Suppl 2), S32-S44.
- Maserejian, N., Vinkoor-Imler, L. and Dilley, A. (2020). Estimation of the 2020 Global Population of Parkinson's Disease (PD) [abstract]. *Mov Disord* 35(suppl 1).
- Matta, S., et al. (2012). LRRK2 controls an EndoA phosphorylation cycle in synaptic endocytosis. *Neuron* 75, 1008–1021.
- Mattila, P.M., et al. (2000). Alpha-synuclein-immunoreactive cortical Lewy bodies are associated with cognitive impairment in Parkinson's disease. *Acta Neuropathol* 100(3), 285–290.
- McNaught, K. S. P., et al. (2002). Impairment of the ubiquitin-proteasome system causes dopaminergic cell death and inclusion body formation in ventral mesencephalic cultures. *J of Neurochem* 81(2), 301–306.
- McNaught, K. S. P., et al. (2004). Systemic exposure to proteasome inhibitors causes a progressive model of Parkinson's disease. *Annals of Neurology* 56(1), 149–162.
- Meiri, K.F., et al. (1986). Growth-associated protein, GAP-43, a polypeptide that is induced when neurons extend axons, is a component of growth cones and corresponds to pp46, a

7. References

major polypeptide of a subcellular fraction enriched in growth cones. *Natl Acad Sci U S A* *83*(10), 3537-3541.

- Mihaescu, A.S., et al. (2018). Brain degeneration in Parkinson's disease patients with cognitive decline: a coordinate-based meta-analysis. *Brain Imaging Behav*.
- Moore, D. J., et al. (2003). Role for the ubiquitin-proteasome system in Parkinson's disease and other neurodegenerative brain amyloidoses. *Neuromolecular Medicine* *4*(1-2), 95–108.
- Moran, L.B., et al. (2008). Neuronal pentraxin II is highly upregulated in Parkinson's disease and a novel component of lewy bodies. *Acta Neuropathol* *115*, 471-478.

N

- Noland, T.D., et al. (1994). The sperm acrosomal matrix contains a novel member of the pentraxin family of calcium-dependent binding proteins. *J Biol Chem* *269*, 32607-32614.
- Noriyama, Y., et al. (2006). Dopamine profoundly suppresses excitatory transmission in neonatal rat hippocampus via phosphatidylinositol-linked D1-like receptor. *Neuroscience* *138*, 475–485.
- Noursadeghi, M., et al. (2000). Role of serum amyloid P component in bacterial infection: protection of the host or protection of the pathogen. *Proc Natl Acad Sci USA* *97*, 14584-14589.
- Nutt, J.G., et al. (1994). Effect of peripheral catechol-O-methyltransferase inhibition on the pharmacokinetics and pharmacodynamics of levodopa in parkinsonian patients. *Neurology* *44*(5), 913.

O

- Obeso, J. A., et al. (2000). Pathophysiology of the basal ganglia in Parkinson's disease. *Trends Neurosciences*, *23*(Box 1), 9–19.
- Olanow, C.W., et al. (2004). Lewy-body formation is an aggregates-related process: a hypothesis. *The Lancet Neurol* *3*, 496-503.
- Old, W.M., et al. (2005). Comparison of label-free methods for quantifying human proteins by shotgun proteomics. *Mol Cell Proteom* *4*, 1487-502.

P

- Perrett, C.W., et al. (1988). Characterisation of messenger RNA extracted post-mortem from the brains of schizophrenic, depressed and control subjects. *J Neurol Neurosurg Psychiatr* *51*, 325–331.
- Parkinson, J. (1817). *An Essay on the Shaking Palsy* (London).
- Pasanen, P., et al. (2014). A novel α -synuclein mutation A53E associated with atypical multiple system atrophy and Parkinson's disease-type pathology. *Neurobiol. Aging* *35*, 2180.e1-5.
- Paumier, K.L., et al. (2013). Behavioral Characterization of A53T Mice Reveals Early and Late Stage Deficits Related to Parkinson's Disease. *Plos One* *8*(8), e70274.
- Payami, H., et al. (1998). Genetic epidemiology of Parkinson's disease. *J Geriatr Psychiatry Neurol* *11*, 98-106.

- Pepys, M.B. and Butler, P.J. (1987). Serum amyloid P component is the major calcium-dependent specific DNA binding protein of the serum. *Biochem Biophys Res Commun* 148, 308-313.
 - Pepys, M.B. and Hirschfield, G.M. (2003). C-reactive protein: a critical update. *J Clin Invest* 111, 1805-1812.
 - Pepys, M.B. (2006). Amyloidosis. *Annu Rev Med* 57, 223-241.
 - Perry, E.K., et al. (1985). Cholinergic correlates of cognitive impairment in Parkinson's disease: comparisons with Alzheimer's disease. *J Neurol Neurosurg Psychiatry* 48(5), 413-421.
 - Plotegher, N., et al. (2014). The chaperone-like protein 14-3-3eta interacts with human alpha-synuclein aggregations intermediates rerouting the amyloidogenic pathway and reducing alpha-synuclein cellular toxicity. *Hum Mol Genet* 23(21), 5615-29.
 - Plowey, E.D and Chu, C.T. (2010). Synaptic dysfunction in genetic models of Parkinson's disease: A role for autophagy? *Neurobiol of Dis* 43, 60-67.
 - Plum, S., et al. (2013) Combined enrichment of neuromelanin granules and synaptosomes from human substantia nigra pars compacta tissue for proteomic analysis. *J Proteomics* 94, 202-206.
 - Plum, S., et al. (2020). Proteomic Characterization of Synaptosomes from Human Substantia Nigra indicates Altered Mitochondrial Translation in Parkinson's Disease. *Cells* 9, 2580.
 - Pessiglione, M., et al. (2006). Dopamine-dependent prediction errors underpin reward-seeking behaviour in humans. *Nature* 442, 1042-1045.
 - Postuma, R.B., et al. (2015). MDS clinical diagnostic criteria for Parkinson's disease. *Mov Disord* 30(12), 1591-1601.
 - Postupna, N.O., et al. (2014). Flow cytometry analysis of synaptosomes from post-mortem human brain reveals changes specific to Lewy body and Alzheimer's disease. *Labor Invest* 94, 1161-72.
 - Przedborski, S., et al. (1998). Experimental developments in movement disorders: update on proposed free radical mechanisms. *Current Opinion in Neurology* 11(4), 335-339.
 - Puschmann, A. (2013). Monogenic Parkinson's disease and parkinsonism: clinical phenotypes and frequencies of known mutations. *Parkinsonism Relat Disord* 19, 407-415.
- Q**
- Quadri, M., et al. (2018). LRP10 genetic variants in familial Parkinson's disease and dementia with Lewy bodies: a genome-wide linkage and sequencing study. *Lancet Neurol* 17, 597-608.
- R**
- Rahim, A., et al. (2012). Critical role of neuronal pentraxin 1 in mitochondrial-mediated hypoxic-ischemic neuronal injury. *Neurobiol Dis* 50, 59-68.
 - Rassouli, M., et al. (1992). Derivation of the amino acid sequence of rat C-reactive protein from cDNA cloning with additional studies on the nature of this dimeric component. *J Biol Chem*, 267, 2947-2954.
 - Rekart, J.L., et al. (2004). Subfield-specific increase in brain growth protein in postmortem hippocampus of Alzheimer's patients. *Neurosci* 126, 579-584.
 - Roberts, M.R. (2000). Document details - Regulatory 14-3-3 protein-protein interactions in plant cells. *Curr Op Plant Biol* 3(5), 400-405.

7. References

S

- Saal, K.A., et al. (2017). Altered Expression of Growth Associated Protein-43 and Rho Kinase in Human Patients with Parkinson's Disease. *Brain Patho* 27(1), 13-25.
- Sandelius, Å., et al. (2018). Elevated CSF GAP-43 is Alzheimer's disease specific and associated with tau and amyloid pathology. *Alzheim and Dement* 15(1), 55-64.
- Schapira, A.H., et al. (1990). Mitochondrial Complex I Deficiency in Parkinson's Disease. *J of Neurochem* 54, 823–827.
- Schapira, A.H., et al. (2006). Novel pharmacological targets for the treatment of Parkinson's disease. *Nat Rev Drug Discov* 5, 845–854.
- Schapira, A.H. (2008). Mitochondria in the aetiology and pathogenesis of Parkinson's disease. *Mov Disord* 26, 1049-1055.
- Schapira, A.H. and Jenner, P. (2011). Etiology and pathogenesis of Parkinson's disease. *Mov Dis* 26(6), 1049-1055.
- Schaukowitz, K., et al. (2017). An Intrinsic Transcriptional Program Underlying Synaptic Scaling during Activity Suppression. *Cell Rep* 18, 1512-1526.
- Schenck, C.H., et al. (1996). Delayed emergence of a parkinsonian disorder in 38% of 29 older men initially diagnosed with idiopathic rapid eye movement sleep behaviour disorder. *Neurology* 46(2), 388-393.
- Schenck, C.H., et al. (2002). REM sleep behavior disorder: clinical, developmental, and neuroscience perspectives 16 years after its formal identification in SLEEP. *Sleep* 25(2), 120-138.
- Schirinzi, T., et al. (2016). Early Synaptic Dysfunction in Parkinson's Disease: Insights From Animal Models. *Mov Disord* 31, 802-813.
- Schrag, A., et al. (2007). Rate of clinical progression in Parkinson's disease. A prospective study. *Mov Dis* 22, 938-945.
- Schramm, M., et al. (1999) Stability of RNA transcripts in post-mortem psychiatric brains. *J Neural Transm* 106, 329– 335.
- Schulz-Schaeffer, W.J. (2010). The synaptic pathology of α -synuclein aggregation in dementia with Lewy bodies, Parkinson's disease and Parkinson's disease dementia. *Acta neuropathologica* 120(2), 131-143.
- Seeley, W.W., et al. (2009). Neurodegenerative diseases target large-scale human brain networks. *Neuron* 62, 42–52.
- Selikhova, M., et al. (2009). A clinic-pathological study of subtypes in Parkinson's disease. *Brain* 132, 2947-57.
- Sharma, K., et al. (2015). Cell type-and brain region-resolved mouse brain proteome. *Nature Neuroscience* 18, 1819-1831.
- Shi, M., et al. (2008). Mortalin: A Protein Associated With Progression of Parkinson Disease? *Jour Neuropa Exp Neurol* 67(2), 117-124.
- Shohamy, D. and Adcock, R.A. (2010). Dopamine and adaptive memory. *Trends Cogn Sci* 14, 464–472.
- Sia, G.M., et al. (2007). Interaction of the N-terminal domain of the AMPA receptor GluR4 subunit with the neuronal pentraxin NP1 mediates GluR4 synaptic recruitment. *Neuron* 55, 87-102.
- Sidhu, A., et al. (2004). The Role of α -Synuclein in Both Neuroprotection and Neurodegeneration. *Annals of the New York Academ of Scienc* 1035(1), 250–270.

- Siew, L.K., et al. (2004). Measurement of pre- and post-synaptic proteins in cerebral cortex: effects of post-mortem delay. *J Neurosci Methods* 139, 153–159.
- Singleton, A. and Hardy, J. (2016). The evolution of genetics: Alzheimer's and Parkinson's Diseases. *Neuron* 90, 1154–1163.
- Singleton, A. and Hardy, J. (2019). Progress in the genetic analysis of Parkinson's disease. *Hum Mol Genet* 28, R215–R218.
- Skovronsky, D.M., et al. (2006). NEURODEGENERATIVE DISEASES: New Concepts of Pathogenesis and Their Therapeutic Implications. *Ann Rev of Pathol: Mech of Dis*, 1(1), 151–170.
- Smith, Y., et al. (2012). Parkinson's Disease Therapeutics: New Developments and Challenges Since the Introduction of Levodopa. *Neuropsychopharm* 37(1), 213–246.
- Song, Q., et al. (2020). The emerging roles of vacuolar-type ATPase-dependent Lysosomal acidification in neurodegenerative diseases. *Transl Neurodegen* 9, 1–14.
- Spillantini, G. M., et al. (1997). Alpha-Synuclein in Lewy bodies. *Nature*, 839–840.
- Sudhaman, S., et al. (2016). Evidence of mutations in RIC3 acetylcholine receptor chaperone as a novel cause of autosomal-dominant Parkinson's disease with non-motor phenotypes. *J Med Genet* 53, 559–566.
- Stan, A.D., et al. (2006) Human postmortem tissue: what quality markers matter? *Brain Res* 1123, 1–11.
- Svenningsson, P., et al. (2012). Cognitive impairment in patients with Parkinson's disease: diagnosis, biomarkers, and treatment. *Lancet Neurol* 11, 697–707.
- Szalai, A.J., et al. (1999). C-reactive protein: structural biology and host defence function. *Clin Chem lab Med* 37, 265–270.
- Szalai, P. (2000). The antimicrobial activity of C-reactive protein. *Microbes Infect* 4, 201–205.
- Szklarczyk, D., et al. (2019). STRING v11: protein–protein association networks with increased coverage, supporting functional discovery in genome-wide experimental datasets. *Nucleic Acids Research* 47, D607–D613.

T

- Tan, E.K., et al. (2000). Polymorphism of NACP-Rep1 in Parkinson's disease: an etiologic link with essential tremor? *Neurology* 54, 1195–1198.
- Tennet, G.A., et al. (1995). Serum amyloid P component prevents proteolysis of the amyloid fibrils of Alzheimer disease and systemic amyloidosis. *Proc Natl Acad Sci USA* 92, 4299–4303.
- Thatipamula, S. And Hossain, M.A. (2014). Critical role of extracellularly secreted neuronal pentraxin 1 in ischemic neuronal death. *BMC Neurosci* 15, 133.
- Tillett, W.S. and Francis, T. Jr. (1930). Serological reactions in pneumonia with a non protein somatic fraction of pneumococcus. *J Exp Med* 52, 561–585.
- Tolosa, E., et al. (2006). The diagnosis of Parkinson's disease. *Lancet Neurol* 5, 75–86.
- Tolosa, E. And Pont-Sunyer, C. (2011). Progress in defining the premotor phase of Parkinson's disease. *J of Neurol Scienc* 310, 4–8.
- Tönges, L., et al. (2012). Inhibition of rho kinase enhances survival of dopaminergic neurons and attenuates axonal loss in a mouse model of Parkinson's disease. *Brain* 135, 3355–3370.

7. References

- Tretiakoff, C. (1919). Contributions à l'étude de l'anatomie pathologique du locus niger de Soemmering avec quelques déductions relatives à la pathogénie des troubles de tonus musculaire et de la maladie de Parkinson. Thèse de Paris.
- Tsui, C.C, et al. (1996). Narp, a novel member of the pentraxin family, promotes neurite outgrowth and is dynamically regulated by neuronal activity. *J Neurosci* 16, 2463-2478.
- Tzivion, G., et al. (2001). Document details - 14-3-3 Proteins; bringing new definitions to scaffolding. *Oncogene* 20(44), 6331-6338.

V

- Van Hemert, M.J., et al. (2001). 14-3-3 Proteins: Key regulators of cell division, signalling and apoptosis. *BioEssays* 23(10), 936-946.
- Vaughan, J.R., et al. (1998). Sequencing of the alpha-synuclein gene in a large series of cases of familial Parkinson's disease fails to reveal any further mutations: the European Consortium on Genetic Susceptibility in Parkinson's Disease (GSPD). *Hum Mol Genet* 7, 751-753.
- Voon, V., et al. (2009). Chronic dopaminergic stimulation in Parkinson's disease: from dyskinesias to impulse control disorders. *Lancet Neurol* 8, 1140–1149.
- Voon, V., et al. (2011.1) Dopamine agonists and risk: impulse control disorders in Parkinson's disease. *Brain* 134, 1438-1446.
- Voon, V., et al. (2011.2). Impulse control disorders in Parkinson's disease: recent advances. *Curr Opin Neurol* 24, 324-330.

W

- Walker, M.D., et al. (2014). Behavioral deficits and striatal DA signaling in LRRK2 p.G2019S transgenic rats: a multimodal investigation including PET neuroimaging. *J Parkinsons Dis* 4, 483–498.
- Wang, Y., et al. (2011). Reversed-phase chromatography with multiple fraction concatenation strategy for proteome profiling of human MCF10A cells. *Proteomics* 11, 2019-2026.
- Wang, Z., et al. (2020). The Basic Characteristics of the Pentraxin Family and Their Functions in Tumor Progression. *Front Immunol* 11, 1757.
- Weil, R.S., et al. (2019). Neuroimaging in Parkinson's disease dementia: connecting the dots. *Brain Comm* 1(1), fcz006.
- Weintraub, D., et al. (2011). Neurodegeneration across stages of cognitive decline in Parkinson disease. *Arch Neurol* 68, 1562–1568.
- Weintraub, D., et al. (2012). Alzheimer's disease pattern of brain atrophy predicts cognitive decline in Parkinson's disease. *Brain* 135, 170–180.
- Whittaker, V.P., et al. (1964). The separation of synaptic vesicles from nerve-ending particles ('synaptosomes'). *Biochem J* 90(2), 293–303.
- Widmer, F. and Caroni, P. (1990). Identification, localization, and primary structure of CAP-23, a particle-bound cytosolic protein of early development. *J Cell Biol* 111(6 Pt 2), 3035-3047.
- Wittmann, B.C., et al. (2005). Reward-related fMRI activation of dopaminergic midbrain is associated with enhanced hippocampus-dependent long-term memory formation. *Neuron* 45, 459–456.

Y

- Yaffe, M.B. (2002). How do 14-3-3 proteins work? – Gatekeeper phosphorylation and the molecular anvil hypothesis. *FEBS Letters* 513(1), 53-57.
- Yamamoto, Y., et al. (1997). Biochemical evidence for the presence of NAP-22, a novel acidic calmodulin binding protein, in the synaptic vesicles of rat brain. *Neurosci Lett* 224(2), 127-130.
- Yasojima, K., et al. (2001) High stability of mRNAs post-mortem and protocols for their assessment by RT-PCR. *Brain Res Prot* 8, 212– 218.
- Ying, S.C., et al. (1992). Human serum amyloid P component (SAP) binds and activates the classical complement pathway via collagen-like region of C1q. *FASEB J* 6, (Abstr).

Z

- Zarranz, J.J., et al. (2004). The New Mutation, E46K, of α -Synuclein Causes Parkinson and Lewy Body Dementia. *Ann. Neurol.* 55, 164–173.
- Zhu, W., et al. (2010). Mass spectrometry-based label-free quantitative proteomics. *J Biomed Biotechnol* 2010:840518.

8. Acknowledgments

First of all I would like to thank Prof. Dr. Paul Lingor for the opportunity he gave me to work at his lab. During the course of my PhD I was able to learn a lot, not only on the subject of neuroscience and Parkinson's disease, but overall on being a scientist and a group member. This is an experience I am very grateful for. I would also like to thank Prof. Dr. Mathias Bähr, for having me as part of his group.

Furthermore, I would like to thank my thesis advisory committee members Prof. Dr. Paul Lingor, Prof. Dr. Silvio Rizzoli and Prof. Dr. Tiago Outeiro. I am specially grateful for the support and opportunity to discuss different angles of my work, always being extremely kind in answering questions and offering assistance. I would also like to thank the members of my extended examination board Prof. Dr. Carolin Wichmann, Prof. Dr. Christine Stadelmann-Nessler and Prof. Dr. André Fischer, for the time they kindly offered, agreeing to attend my thesis defense and assessing my work.

Moreover, I would like to thank my collaboration partners Prof. Dr. Henning Urlaub, Dr. Christof Lenz and Prof. Dr. Stefan Bonn for their assistance in key aspects of the work. A special thanks goes out to Ivan Silbern, for the kind and friendly disposition he always had. It was an absolute joy working with you, even on such a challenging task as the isolation of the synaptosomal fractions.

Similarly, I would like to thank my colleagues for the constant support, even during the challenging times of a complete relocation of the lab. Thank you Dr. Lars Tatenhorst for all the support on both technical as well as organizational topics. Dr. Lucas Caldi has my utmost respect and gratitude for being such a nice human being. The degree of friendly disposition you always have towards anybody in need of help is commendable. I am very thankful for your help. I am also very happy to have shared part of my time at the lab with Dr. Karina Joppe. You were always a very gentle person with whom I enjoyed very much talking about all the hardships and obstacles that come with finishing a PhD. A very special thanks goes to Vivian Dambeck. I am sincerely not sure if the work presented here would have been the same without your continuous assistance. Your help and support, both on the technical as well as the personal side, were invaluable and I am very happy and lucky to have had you as a colleague.

These last years would also not have been the same without the lovely company of Mary Xylaki, Magdalena Redondo and Lujane Slitin. You are the best and sharing an office with you was great. I didn't just get to know three amazing scientists but was also fortunate to gain three beautiful women as cherished friends. Your support during the really tough times made the difference. Thank you girls!

In terms of support, I am eternally grateful to my love Dr. Sebastian Stein. I am extremely lucky to not only have a partner that is my rock in any situation, but who is such a great scientist and physicist, that he often understood my work and challenges better than I could. I can't think of any other person I would have wanted at my side to go through this challenging experience. Thank you for always shining the ray of calm positivity on my storms. You believed I could, so I did.

Finalmente quisiera darle las gracias a mi familia, sin la cual no sería la persona que soy hoy. Gracias mamá, por siempre haber querido lo mejor para mí. Tu dedicación y tenacidad para impulsarme fueron parte de la razón por la cual hoy he logrado este capítulo de mi vida. Gracias papá por haber hecho posible el que pudiese dedicarme de tiempo completo a educarme. Gracias hermanita. Los últimos años han sido los mejores de mi vida y la mayoría de mis memorias más preciadas las he compartido contigo. Estoy orgullosa de ser tu hermana! Awrr awrr fiiuuu.

